U.S. Department
of Transportation

Federal Highway
Administration

Advances in Weigh-in-Motion Using Pattern Recognition and Prediction of Fatigue Life of Highway Bridges

Volume I: Final Report

FOREWORD

This report will be of interest to bridge design, maintenance, and inspection engineers, particularly those concerned with the evaluation of fatigue life of existing steel bridges and the survey of truck traffic on the highway system.

Four steel girder bridges were instrumented to obtain strain data at fatigue critical details, and at sections of maximum strain to compute the gross vehicle weight (GVW) of trucks crossing the bridges. Two were simple spans, and two continuous spans.

A comparative study of three of the four alternatives suggested by AASHTO showed that the fatigue life computed with direct measurements of the stress ranges were greater than those computed with the simplified approaches.

An innovative approach to the analysis of strain data collected with the WIM+R system is presented. It involves three pattern recognition techniques. Those numerical techniques may be applied to model the underlying processes of the measured data in other problems.

This Volume I report is being distributed to provide a minimum of one copy to each regional office, division office and State highway agency. Direct distribution is being made to the division offices. Volume II is a data report that is not being distributed but will be available from the National Technical Information Service, 5285 Port Royal Road, Springfield, Virginia 22161.

Thomas J. Ptak
Director, Office of Engineering and
Highway Operations Research and Development

NOTICE

1. Report No. FHWA-RD-92-046	2. EB93-123594	3. Recipient's Catalog No.

4. Title and Subtitle	5. Report Date
ADVANCES IN WEIGH-IN-MOTION USING PATTERN RECOGNITION AND PREDICTION OF FATIGUE LIFE OF HIGHWAY BRIDGES: Vol. I Final Report	September 1992
	6. Performing Organization Code

7. Author(s) Nicolas Gagarine and Pedro Albrecht	8. Performing Organization Report No. GRF89-09

9. Performing Organization Name and Address University of Maryland Department of Civil Engineering College Park, MD 20705	10. Work Unit No. (TRAIS) 2D1a1022
	11. Contract or Grant No. DTFH61-89-P-40005

12. Sponsoring Agency Name and Address Office of Engineering & Highway Operations R&D Federal Highway Administration 6300 Georgetown Pike McLean, VA 22101-2296	13. Type of Report and Period Covered Final Report June 1989 - September 1991
	14. Sponsoring Agency Code

16. Abstract
The two main objectives of the present study were to: (1) demonstrate the advantages of using the Weigh-in-Motion and Response (WIM+R) system to evaluate the fatigue life of existing bridges and (2) introduce pattern recognition methods in the analysis of WIM+R data. Four steel girder bridges were instrumented to obtain strain data at fatigue critical details, and at sections of maximum strain to compute the gross vehicle weight (GVW) of each truck. Two were simple spans, and two continuous spans. A comparative study of three of the four alternatives suggested by AASHTO showed that the fatigue life computed with direct measurements of the stress ranges were greater than those computed with the simplified approaches. The effect of secondary cycles was negligible for the four bridges. The damage equivalent secondary cycle factor for fatigue was defined. The applicability of three pattern recognition methods for WIM+R was investigated. The dynamic time warping, hidden Markov model, and feed forward neural network methods can classify trucks with the measured strain patterns alone. This new approach in the analysis of the data would remove the need to lay tapeswitches on the pavement, facilitating the field operations during a bridge test. An improved WIM+R system could be used to survey the truck traffic while monitoring fatigue critical details.

This volume is the first in a series of two. The other volume is:

Vol. II FHWA-RD-92-045 Data Report

17. Key Words Bridge, steel, fatigue, weigh-in-motion, pattern recognition, structural response	18. Distribution Statement No restrictions. This document is available to the public through the National Technical Information Service, Springfield, Virginia 22161

19. Security Classif. (of this report) Unclassified	20. Security Classif. (of this page) Unclassified	21. No. of Pages 101	22. Price

Form DOT F 1700.7 (8-72)   Reproduction of completed page authorized

SI* (MODERN METRIC) CONVERSION FACTORS

APPROXIMATE CONVERSIONS TO SI UNITS

Symbol	When You Know	Multiply By	To Find	Symbol
LENGTH				
in	inches	25.4	millimeters	mm
ft	feet	0.305	meters	m
yd	yards	0.914	meters	m
mi	miles	1.61	kilometers	km
AREA				
in²	square inches	645.2	millimeters squared	mm²
ft²	square feet	0.093	meters squared	m²
yd²	square yards	0.836	meters squared	m²
ac	acres	0.405	hectares	ha
mi²	square miles	2.59	kilometers squared	km²
VOLUME				
fl oz	fluid ounces	29.57	milliliters	ml
gal	gallons	3.785	liters	l
ft³	cubic feet	0.028	meters cubed	m³
yd³	cubic yards	0.765	meters cubed	m³

NOTE: Volumes greater than 1000 l shall be shown in m³.

Symbol	When You Know	Multiply By	To Find	Symbol
MASS				
oz	ounces	28.35	grams	g
lb	pounds	0.454	kilograms	kg
T	short tons (2000 lb)	0.907	megagrams	Mg
TEMPERATURE (exact)				
°F	Fahrenheit temperature	5(F-32)/9 or (F-32)/1.8	Celcius temperature	°C
ILLUMINATION				
fc	foot-candles	10.76	lux	l
fl	foot-Lamberts	3.426	candela/m²	cd/m²
FORCE and PRESSURE or STRESS				
lbf	poundforce	4.45	newtons	N
psi	poundforce per square inch	6.89	kilopascals	kPa

APPROXIMATE CONVERSIONS FROM SI UNITS

Symbol	When You Know	Multiply By	To Find	Symbol
LENGTH				
mm	millimeters	0.039	inches	in
m	meters	3.28	feet	ft
m	meters	1.09	yards	yd
km	kilometers	0.621	miles	mi
AREA				
mm²	millimeters squared	0.0016	square inches	in²
m²	meters squared	10.764	square feet	ft²
m²	meters squared	1.195	square yards	ac
ha	hectares	2.47	acres	mi²
km²	kilometers squared	0.386	square miles	
VOLUME				
ml	milliliters	0.034	fluid ounces	fl oz
l	liters	0.264	gallons	gal
m³	meters cubed	35.71	cubic feet	ft³
m³	meters cubed	1.307	cubic yards	yd³
MASS				
g	grams	0.035	ounces	oz
kg	kilograms	2.202	pounds	lb
Mg	megagrams	1.103	short tons (2000 lb)	T
TEMPERATURE (exact)				
°C	Celcius temperature	1.8C + 32	Fahrenheit temperature	°F
ILLUMINATION				
lx	lux	0.0929	foot-candles	fc
cd/m²	candela/m²	0.2919	foot-Lamberts	fl
FORCE and PRESSURE or STRESS				
N	newtons	0.225	poundforce	lbf
kPa	kilopascals	0.145	poundforce per square inch	psi

* SI is the symbol for the International System of Units

ii

TABLE OF CONTENTS

TABLE OF CONTENTS (Continued)

LIST OF FIGURES

LIST OF FIGURES (Continued)

LIST OF FIGURES (Continued)

LIST OF FIGURES (Continued)

LIST OF TABLES

LIST OF ABBREVIATIONS

AASHTO = American Association of State Highway and Transportation Officials

ADTT = Average Daily Truck Traffic

AISI = American Iron and Steel Institute

DOS = Disk Operating System

DTW = Dynamic Time Warping

FEM = Finite Element Method

FFN = Feed Forward Neural Network

FFT = Fast Fourier Transform

FHWA = Federal Highway Administration

GVW = Gross Vehicle Weight

HMM = Hidden Markov Model

IT = Influence Track

NCHRP = National Cooperative Highway Research Program

RAM = Random Access Memory

WIM = Weigh-In-Motion

WIM+R = Weigh-In-Motion and Response

INTRODUCTION

Problem

The current assumptions on truck loading and simplified analysis methods lead to inaccuracies in the prediction of bridge behavior. This is clear from the following three observations. First, the HS20 truck and lane loads introduced in 1941 do not represent the majority of the present truck traffic circulating on the highway system. Since then, weight and frequency of occurrence of trucks have increased significantly. Also, the U.S. Congress has raised the maximum gross vehicle weight (GVW) to 355 kN (80 kip). Many states design bridges for HS20 truck loading of 320-kN (72 kip) GVW, because this loading still produces stresses higher than the heavier trucks which in reality have axles more widely spaced. Other states, such as Maryland, design bridges for HS25 truck loading, increasing the safety margin for GVW's within the legal limit. The problem of service stresses exceeding design stresses is caused by trucks with GVW's much greater than the 355-kN (80 kip) limit, sometimes twice this legal limit. These trucks exceed the legal limit either illegally, or with permits or, in some states, under "grand-father laws".

Second, steel bridges on major highways are designed for fatigue using an average daily truck traffic of ADTT = 2,500 and either 2,000,000 cycles of HS20 truck loading on multiple lanes or over 2,000,000 cycles of HS20 truck loading on a single lane. In reality, these bridges should be designed for 0.7(HS20) = HS14 fatigue truck loading on a single lane according to Albrecht,[1] or 54/72(HS20) = HS15 fatigue truck loading according to the Guide Specifications for Fatigue Design of Steel Bridges, which include the effect of overload trucks.[2] Main members should be designed for the actual number of trucks crossing the bridge when possible, as recommended by the Guide[2], and not the fictitious values of 100,000, 500,000, 2,000,000, or over 2,000,000 cycles. The current AASHTO guide specifications are therefore much more rational in their approach.

Third, three-dimensional, multi-girder bridges are analyzed under the Standard Specifications for Highway Bridges,[3] assuming that: (1) each girder is modeled as a two-dimensional beam acting separately from all other beams, (2) the fraction of the wheel loads resisted by each beam is calculated with empirical formulas for distribution factors, and (3) composite beams act with an effective width of the deck that is also calculated with empirical formulas. Such a simplified model cannot accurately predict the behavior of three-dimensional bridge structures. In general, the AASHTO 2-D formulas result in conservative answers.

As a result, the design methods recommended in the specifications of the American Association of State Highway and Transportation Officials (AASHTO) can lead to large differences between the calculated and measured responses of bridges. The following selected examples from recent studies illustrate the effects of these differences on loading, and static and fatigue strength behaviors of bridges:

o   Loading of Highway Bridges

The GVW data recorded in two Weigh-In-Motion (WIM) studies funded by the
Federal Highway Administration (FHWA) have shown that many trucks weigh
more than 355 kN (80 kip), the legal weight limit. For example, Snyder et al.
reported that 4.1 percent of the trucks at all sites and 5.8 percent at the Interstate
sites weighed more than 355 kN (80 kip).[4] The corresponding number from the
study by Daniels et al. was 7.6 percent for two bridges in Pennsylvania. The
number of trucks weighing more than 534 kN (120 kip) were 0.13 percent in the
former and 0.32 percent in the latter study. The heavy trucks are of particular
interest because they damage bridges most.[5]

o   Strength Behavior of FHWA-AISI Model Bridge

For HS20 truck loading on three lanes of the three-girder, two-span, prototype
bridge of the FHWA-AISI study, the maximum positive moment calculated under
the AASHTO specifications was 46 percent higher than those calculated with the
finite element method (FEM).[6] The maximum negative moment was 56 percent
higher. On the other hand, moments calculated with the distribution factors for
slab-on-girder bridges developed in a just completed National Cooperative High-
way Research Program (NCHRP) study were 24 and 21 percent lower than those
calculated with the FEM.[7] The former results are too conservative, the latter too
unsafe. The NCHRP study does recommend 3-D analysis, also providing 2-D
formulas for distribution factors, for use in simple bridges. Those formulas
model the distribution factors obtained with finite element models of steel-girder
bridges, varying the number and spacing of girders, and other parameters.

In contrast, the moments determined from the experiment and those calculated
with the FEM correlated very well, within 10 percent.[6] Both sets of results
showed that the exterior girder controlled the design, whereas the AASHTO
method incorrectly predicted that the interior girder would control the design.
The aforecited observations apply equally to HS20 lane loading.

The lack of accuracy of the AASHTO and NCHRP distribution factors point out
the limited validity of single-girder idealization of highway bridges. Therefore,
there is need to model steel-girder bridge in 3-D, as both AASHTO and NCHRP
recommend for all but the simplest cases.

o   Fatigue Behavior of FHWA-AISI Model Bridge

For HS-20 truck loading on one lane, the stress range from live load moment
calculated with the AASHTO specifications was 95 percent higher at mid-span
and 113 percent higher over the pier than those calculated with the FEM.[6]

On the other hand, the experimentally determined stress ranges due to truck loading on one lane correlated within 10 percent of those calculated with the FEM.

Fatigue life is inversely proportional to the third power of stress range. Since the AASHTO stress ranges were approximately twice the value of the finite element stress ranges, the former would lead to predictions of life $2^3 = 8$ times shorter than the latter.

o Fatigue Behavior of Two Pennsylvania Bridges

For HS-20 truck loading on one lane of two five-girder steel bridges in Pennsylvania, the AASHTO stress ranges were 150 and 300 percent higher than the finite element stress ranges, depending on whether the truck was located near the curb or near the centerline of the bridge.[5] Such conservatism results in extreme underestimates of fatigue life, by factors of $2.5^3 = 15$ and $4^3 = 64$, respectively.

In the same study, Daniels et al. also showed that stress range was not proportional to GVW, however no attempt was made to predict the relationship between the two values.[5] Lacking such response data, designers and researchers alike continue to assume that the proportionality holds. The relationship between load and response will be investigated in the present study to more accurately predict the fatigue life of steel bridges.

o Fatigue Behavior of 40 Bridges in Nine States

Shaaban and Albrecht collected and analyzed 190 stress range histograms that previous investigators had recorded between 1965 and 1973 on 40 bridges in nine states. They also analyzed all bridges for fatigue, using HS20 truck loading. They found that the maximum measured stress ranges for category A and B details located near or at midspan were about 60 percent of the values calculated with the AASHTO analysis method. The differences were much smaller for category E and E' details which were located closer to the supports than to midspan.[8] Such additional fatigue capacity may be avoided if fatigue is the controling design factor.

In summary, truck loading of highway bridges significantly differs from HS20 truck loading. Such discrepancy is attenuated with the introduction of the HS15 fatigue truck in the Guide.[2] Also, the AASHTO simplified method (2-D) poorly predicts the response of multi-girder steel bridges to truck loading with the assumptions that each girder acts separately from the remainder of the structure and resists part of the load determined with empirical equations. However, AASHTO does suggest 3-D analysis as an alternative.

The actual truck weights and the response of highway bridges to these trucks can be measured with the FHWA's Weigh-In-Motion and Response system (WIM+R). The present

r

3

study combines this capability with more accurate analysis methods to improve the prediction of the actual behavior of highway bridges.

Parameters

The application of the WIM+R system to the study of multi-girder highway bridges involved the following parameters that are conveniently categorized in terms of load, response, and bridge geometry as follows:

o   Load: GVW, axle weights, and axle spacings.

o   Response: Stress range, strain rate, impact factor, distribution factor, position of neutral axis, and effective deck width.

o   Geometry: Support conditions (right versus skewed support), aspect ratio (ratio of span length to deck width), number of girders, and alignment (straight versus curved girders).

The three load parameters--GVW, axle weights, and axle spacings--are essential in relating the load to the response of the bridge. These data were recorded with the WIM+R system. In a further improvement to the WIM+R system, the load parameters for trucks of similar types were determined from analysis of strain response data with pattern recognition methods. Such an improvement would eliminate the need to lay tapeswitches across the traffic lanes at the entrance of the bridge.

Of the response parameters, stress range is the most important for fatigue design. Daniels et al. reported plots of stress range versus GVW data, but they did not predict the response of the bridge to each truck nor did they correlate the calculated and measured stress ranges.[5] Such work had a high priority in this study.

The impact factor is the other important response parameter for fatigue design. Lai determined the effect of several variables on the bridge response with a dynamic model of the vehicle and bridge; he found that the most important variable was the initial vehicle deflection caused by the roughness of the approach slab and bridge deck and/or abrupt level changes at joints and pot holes. Such deflection affects the dynamic response of a bridge more than the spring constant of the vehicle, the residual vibrations of the bridge from previous truck crossings, and the damping ratio.[9]

The AASHTO formula for impact factor is a function of span length only. It sets an upper limit of 30 percent. The dynamic load allowance (impact factor) in the Ontario code is a function of the first flexural frequency. Its value is 0.2 for frequencies up to 1-Hz, increases linearly to 0.4 at 2.5 Hz, remains at a constant value of 0.4 between 2.5 and 4.5 Hz, decreases linearly to 0.25 at 6.0 Hz, and then remains at a constant of 0.25 for frequencies higher than 6.0 Hz.[10] The AASHTO and Ontario formulas for impact factor differ greatly. For example, the difference in the maximum values of 0.30 and 0.40 affects the

4

calculated fatigue life by a factor of $(1.30/1.40)^3 = 0.80$, or 20 percent of the life. The impact factor to be measured in the present study included all parameters relevant to the specific bridges.

The three remaining response parameters--distribution factor, position of neutral axis, and effective deck width--are needed only if the bridge is analyzed with the simplified approach suggested by AASHTO. They are an outgrowth of the days of hand calculations. When a bridge is analyzed with the FEM, these three parameters become an output from the analysis rather than being a required input to the analysis. Since empirical formulas for distribution factors and effective deck width are not needed in advanced analysis methods, these response parameters were not investigated.

The four geometry parameters listed above--support conditions, aspect ratio, number of girders, and alignment--help characterize the types of multi-girder bridges. WIM+R data was collected on four bridges with different aspect ratios, skews, and structural systems.

Based on the above description of the problems in bridge analysis and design as well as the parameters for which the WIM+R system can provide important data, this work focused on the stress range response of multi-girder bridges to single truck loading. The measured response includes the effects of impact factor and vibration-induced secondary cycles. As was stated previously, the difference between measured and calculated responses was computed for single truck loading, a loading condition which governs the fatigue design of bridges.

Objectives

This study can be broken into three parts. The first part was a WIM study. The data collected with the existing WIM+R system was analysed with 3-D influence surfaces. The second part is a response study. The author performed a comparative analysis of the alternatives specified in the AASHTO Guide for fatigue evaluation of existing steel bridges. The third part was a pattern recognition study. The measured strain records form patterns which are unique for a given truck. Three existing pattern recognition techniques were adapted to solve the bridge WIM problem.

The specific objectives of this study were to:

1.   Obtain a representative sample of truck traffic on four steel girder bridges with the existing WIM+R system and compute its corresponding GVW histogram.

2.   Determine 3-D influence surfaces for the static stress at each transducer from strain data collected as the test truck crosses the bridge at regular traffic speed and compare them to those obtained with the finite element method. This eliminates the need for traffic control and the safety hazards to the driving public associated with a test truck traveling at crawling speed across the bridge.

3. For a select number of bridges, demonstrate that the fatigue life predicted with WIM+R data is much longer than that calculated with the AASHTO simplified methods.

4. Evaluate the effect of the secondary cycles and impact factor on the remaining fatigue life of bridges with the measured data.

5. Develop a method of evaluating fatigue life of existing bridges from WIM data, Compare the predicted life with those obtained from stress ranges calculated with finite element and AASHTO simplified analysis methods.

6. Determine the number of axles and axle spacings directly from transducer data. This eliminates the need for laying tapeswitches across the approach lanes, a hazardous operation. Evaluate the use of three different pattern recognition methods for that purpose: dynamic time warping, hidden Markov method, and feed-forward networks.

BACKGROUND ON DEVELOPMENT OF WIM+R SYSTEM

The present study used the WIM+R system which is described in detail in six reports. These include a system's overview,[11] training guide,[12] user's guide,[13] description of hardware,[14] software reference,[15] and an executive summary.[16]

Four major studies have contributed to the evolution of the FHWA's bridge WIM+R system. In the first study, Moses and Kriss developed the prototype of the bridge WIM system, with the objectives of determining axle and GVW of trucks.[17] The system was limited to trucks traveling in one lane. As a truck approached the bridge, an operator pressed a button on a keypad to start data acquisition with the computer. The data were stored on tape for later analysis. The operator also counted visually the number of axles of each truck and manually recorded the data.

In the second study, Moses and Ghosn extended the capabilities of the bridge WIM system to weighing trucks in two lanes. They modified the software so that it would recognize the axles belonging to the same truck and would calculate axle weights and GVW immediately after a truck crossing.[18]

In the third study, Snyder et al. added the following features to the WIM system:[4]

O Automatic recognition of truck axle configuration based on tapeswitch times and spacing classification, thus eliminating the need for an observer except under high ADTT. Data are collected automatically for truck traffic in one lane. A keypad is needed to monitor two lanes simultaneously.

O Reduction of data acquisition time by about a factor of ten.

o Calculation of axle weights and GVW's in less than one second after the truck crossed the weigh span.

o Modernization of hardware, including reduction in size and increase in flexibility and performance.

With this improved WIM system, Snyder et al. calculated GVW's, axle weights, and axle spacings of 27,513 trucks crossing 33 bridges in Arkansas, Texas, California, Illinois, Georgia, New York, and Ohio. The study showed that the WIM system could record unbiased and continuous data.

The ideal "bridge for scale" has a short and simple span, steel girders, and little or no skew. Twenty-three of the 33 bridges chosen by Snyder et al. satisfied these criteria. Six were skewed 30 degrees or more, and four were continuous and/or reinforced concrete structures. Low ADTT and short spans increase the probability that only one truck crosses the bridge at a time. Therefore, a higher percentage of trucks from the traffic stream are weighed and classified. With short spans, the strain record has distinct peaks which correspond to the individual axles. The accuracy of calculating axle weights increases. It is easier to install portable transducers on steel girders than on concrete structures. The analysis of the data is more complicated if a bridge is skewed.

Snyder et al. reported problems with the acquisition and numerical analysis of data from the following four bridges: a plate girder bridge, 25.6 m (84 ft) long, of simple span; a reinforced concrete bridge with continuous spans; a prestressed concrete box girder bridge, 25.3 m (83 ft) long, of continuous spans; and a deep plate girder bridge, 27.4 m (90 ft) long, of continuous spans.[4]

Snyder et al. found that GVW's can be calculated more accurately than axle weights. The resulting GVW's can be used for unbiased planning studies, pavement and bridge loads, and economic studies. In their opinion, the results are sufficiently accurate for use in enforcing weight limits. The 356 kN (80 kip) legal weight limit was exceeded by 4.1 percent of the trucks on all bridges and 5.8 percent on interstate bridges. Also 69 percent of the trucks on all bridges drove faster than 88 km/h (55 mi/h), 18 percent faster than 98 km/h (61 mi/h), and 7 percent faster than 103 km/h (64 mi/h).[4]

In the fourth study, Daniels et al. added ten channels to the existing six so that structural response data could be acquired along with WIM data. The random access memory of the DEC MINC computer was expanded to 256 kb. Figure 1 shows a typical set-up of the instrumentation on a bridge and figure 2 illustrates the format of measured strain data. During a single truck event, a portion of the free vibrations are recorded after the forced vibrations. The WIM computations only use the first part of the data. The system was called Weigh-In-Motion and Response (WIM+R). Daniels et al. instrumented three simple span steel girder bridges and one simple span prestressed I-girder bridge, all in Pennsylvania. They determined GVW's, axle weights, and axle spacings of 19,402 trucks. They then calculated the maximum stress, stress range, strain rate, and load distribution for

each of the four bridges. For one or two truck events, the measured strains were compared with those obtained from 2-D single girder analysis and 3-D finite element analysis results.[5]

The basic principle used in WIM calculations with a 2-D idealization of the bridge is that the internal moment must be equal to the external moment at a given section. The internal moment is expressed in terms of measured strain and the external moment in terms of the loads, with the use of an influence line. Moses and Kriss first described the computations for single truck events.[17] The flow of calculations involves the following seven steps:

- Calculate **truck velocity** from tapeswitch times.
- Calculate **axle spacings** from tapeswitch times, knowing the velocity.
- Calculate **axle positions** on the bridge at each strain scan, knowing the velocity and axle spacings.
- Express the **external moment** in terms of axle weights and calculated influence line coefficients, knowing the axle positions at each scan. Figure 3 illustrates the use of an influence line to determine the external moment.
- Express the **internal moment** in terms of strain data and cross-sectional properties of girders. Figure 4 shows an example of measured strain during a single truck event in the right lane.
- For a test truck of known axle weights and spacings, solve the moment equilibrium equation for the "system" **calibration factor**.
- Knowing the calibration factor, solve the moment equilibrium equation for the **axle weights** of other trucks crossing the bridge.

The author included a description of this method and variants to it proposed by other researchers in the companion report. The available data acquisition software restricted the computation of axle weights for single truck events.

FIELD EXPERIMENTS

Four steel girder bridges were tested in the Washington area under this study. Three were located in Virginia, on Interstate Route I-66. The fourth bridge was in Maryland, on Interstate Route I-70. On average, WIM data was collected at each site for a week. In this report, the discussion focuses on the southbound I-70 over route 340 bridge. The results for the other bridges are available in the full report.

Westbound I-66 over Bull Run Bridge

Structure

1. Span length : 17.1 m (56.25 ft) first of three equal simple spans.
2. Roadway 13.4 m (44 ft) with two 3.66 m (12.0 ft) traffic lanes, and a 3.66 m (12.0 ft) emergency lane.
3. Non-composite construction; rolled beam with cover plates.

4. Six girders spaced 2.44 m (8.0 ft) apart.
5. Reinforced concrete slab.
6. Skew: 5 degrees.

Instrumentation

Three sets of transducers located on lines parallel to the abutments and piers as follows:
1. Transducers 1 to 6: at mid-span on bottom flange, used for WIM calculations.
2. Transducers 7 to 11: 20.3 cm (8 in) away from end of cover plate at entrance of bridge, bottom flange.
3. Transducers 12 to 16: 20.3 cm (8 in) away from end of cover plate at exit of bridge, bottom flange. (Transducer 16 was defective)

Tapeswitches installed in both lanes of traffic.
A total of 3080 truck events were recorded during four days.

Eastbound I-66 over Route 55 Bridge

Structure

1. Span length : 44.2 m (145.0 ft) simple span
2. Roadway 13.4 m (44 ft) wide with two 3.66 m (12.0 ft) traffic lanes, and a 3.35 m (11.0 ft) emergency lane.
3. Composite construction; deep plate girder.
4. Five girders spaced 2.90 m (9.5 ft) apart.
5. Reinforced concrete slab.
6. Skew: 35 degrees.
7. Cross-frames and cross-bracings.

Instrumentation

1. Nine transducers for weigh-in-motion at mid-span on the bottom flange. Two lines:
   o Transducers 1 to 5 perpendicular to the direction of traffic on bottom flange.
   o Transducers 3 and 7 to 10 parallel to abutment line on bottom flange.
2. Transducer 6 on top flange of center girder, at mid span.
3. Transducers 11 to 16 on both sides of web of interior girders, at mid-span, 10.2 cm (4 in) away from gusset plates, 17.8 cm (7 in) above flange.

Tapeswitches installed in both lanes of traffic.
A total of 1574 truck events were recorded during seven days.

Southbound I-70 over Route 340 Bridge

Figures 5 thru 7 are the plan view, cross-sectional and girder details for the I-70 over route 340 bridge, respectively. On the plan view, the location of the transducers is indicated. Also, the position of the axles in each lane is showm on the cross-section.

Structure

1.	Span length : 29.7-29.7 m (97.4-97.4 ft) continuous spans
2.	Roadway 12.8 m (42.0 ft) wide with two 3.66 m (12.0 ft) traffic lanes, and a 3.05 m (10.0 ft) emergency lane.
3.	Non-composite construction; rolled beam with partial cover plate on the bottom flange at mid-spans, on both top and bottom flanges at the center pier.
4.	Six girders spaced 2.22 m (7.28 ft) apart.
5.	Reinforced concrete slab.
6.	Skew: 9 degrees.
7.	Cross-frames.

Instrumentation

Three sets of transducers located on lines parallel to the abutment and pier as follows:

1.	Transducers 1 to 6: at mid-span on bottom flange, used for WIM calculations.
2.	Transducers 7 to 11: at 0.66L on bottom flange, 20.13 cm (8 in) away from end of cover plate.
3.	Transducers 13 to 16: at 0.87L on top flange, 20.13 cm (8 in) away from end of cover plate.

Tapeswitches installed in both lanes of traffic.
A total of 1760 truck events were recorded during three days.

Eastbound I-66 over Route 7100 Bridge

Structure

1.	Span length : 25.0-25.0 m (82.0-82.0 ft) continuous spans
2.	Roadway 17.0 m (55.8 ft) wide with two 3.66 m (12.0 ft) traffic lanes, a 3.66 m (12.0 ft) auxiliary lane, and a 3.66 m (12.0 ft) emergency lane.
3.	Composite construction; plate girder with field splice.
4.	Seven girders spaced 2.54 m (8.33 ft) apart.
5.	Reinforced concrete slab.
6.	no skew.

Instrumentation

Three sets of transducers located on lines parallel to the abutment and pier as follows:

1. Transducers 1 to 6 and 11: at 0.42L on bottom flange, used for WIM calculations.
2. Transducers 7 to 10: at 0.99L on bottom flange, 25.4 cm (10 in) away from bearing stiffener at center pier.
3. Transducers 13 to 16: at 0.99L on top flange, 25.4 cm (10 in) away from bearing stiffener at center pier.

Tapeswitches installed in both lanes of traffic, not in the auxiliary lane.
A total of 2090 truck events were recorded during four days.

WEIGH-IN-MOTION STUDY

A method of computing axle weights with 3-D FEM influence surfaces was introduced in the present study. Figure 8 shows, as an example, the influence surface for the bottom stress at 0.4L, in the longitudinal direction on the center girder of the I-66 over route 7100 bridge. In the proposed method, the measured stress is directly equated to the stress calculated as a product of the axle weights and their corresponding ordinates on a 3-D stress influence surface, at selected transducers.

In order to estimate the live load stresses with the influence surfaces, only the ordinates on the wheel paths were needed. These lines of ordinates were called influence tracks. An influence track for the stress at each transducer due to a unit axle load assumed travelling in the center of each lane was needed for the WIM computations. Figures 9 and 11 are the FEM influence tracks for the I-70 over route 340 bridge. With a system which can measure the actual lateral position of the truck in the lane, a complete surface would be used. The WIM+R system did not have such capability.

In addition, measured influence tracks were obtained from an analysis of the measured data during test truck events. The method by Goble et al. of computing the coefficients of the influence tracks with measured data requires the test truck to travel at low speed around 8 km/h (5 mi/h) to avoid the dynamic magnification of the measured stress.[19,20] In the present study, the test trucks traveled at normal traffic speed around 88 km/h (55 mi/h). A new method was developed to take in account the dynamic magnification of the stress. Figures 10 and 12 are the measured influence tracks corresponding to those shown in figures 9 and 11.

Finally, a method of optimizing the distribution of the GVW to the axles was developed and evaluated with the test truck events, for the 2-D and 3-D WIM methods. In this method, the position of the truck is shifted to minimize the error in weight distribution. The optimization for unknown trucks would depend on knowledge of GVW distribution obtained from survey studies on trucks.

The GVW's and axle weights were computed for single truck events, using the strain measured at transducers installed near the section of maximum moment, in the positive

moment region. Once the weights are computed, the static response of the strain record can be reconstructed with the influence tracks. Figures 13 and 14 show the superposition of the measured and reconstructed records side by side for the six transducers at 0.5L, for a right and left lane event respectively. The reconstructed data goes through the measured data as expected. The results are summarized with tables of average axle weights and spacings (table 1) for the different classes of trucks (figure 15), GVW histograms (figure 16), and probability density functions.

STRUCTURAL RESPONSE STUDY

Stress Ranges

The stress ranges at all instrumented locations were computed from the recorded data. A stress range is calculated as the difference between the maximum and minimum stresses measured during a truck event. Each stress range corresponds to one cycle of loading. For each truck event, at each channel, the primary static and dynamic cycles and the secondary cycles were computed.

The static response was approximated in two ways: first, by averaging the values at consecutive peak and valley points on the strain record, and second, by filtering the dynamic oscillations using FFT. To determine the cut-off frequency for the filtering process, the natural frequencies of each bridge were obtained from a finite element modal analysis. Those were superimposed on a spectrogram of the measured data shown in figure 17. The dashed line is the spectrogram obtained from FFT of the original measured data and the vertical lines are the FEM natural frequencies.

The first peak on the spectrogram represents the terms in the Fourier transforms which are believed to constitute the static response. The second peak is near the first natural frequency. The transforms at frequencies greater than 2.0 Hz represent the dynamic response of the bridge in its natural modes. Conceivably, some of the static response may have been removed during the filtering process. However, it would not be a significant amount. Leaping ahead, this filtering process is also used in pattern recognition. The filtered stresses shown in figure 28 qualitatively compare well to the FEM stresses in figure 29. Figure 18 graphically summarizes the FFT filter method.

For illustrative purposes, the first five modal shapes of the bridge deck are shown in figure 19. The first and fourth are bending modes; the second, third, and fifth modes are torsional modes. The bridge vibrates mostly in the first bending mode and to a lesser degree in the fourth bending mode. This confirms the findings with WIM data by Lai that the torsional modes seldom are excited.[9]

The secondary cycles are counted using the rainflow method.[21] The stress history can be pictured as a mountain range. The obstacles are removed from the path of the rain flowing from the highest peak. The primary dynamic cycle and the secondary cycles were

lumped as one. The stress range which would cause the same damage as all individual stress ranges is equal to:

$$f_{ri,tot} = \left[f_{ri,dyn} + \sum_j n_{ij} f_{rij,sec}^m \right]^{\frac{1}{m}} \tag{1}$$

where

$f_{ri,dyn}$ = stress range corresponding to primary dynamic cycle
$f_{ri,tot}$ = stress range corresponding to primary dynamic plus secondary cycles
$f_{rij,sec}$ = stress range corresponding to secondary cycles
n_{ij} = number of occurrence of secondary stress range j
m = slope of S-N curve (= 3)

Figure 20 shows the measured stress range histograms for the primary static cycles, primary dynamic cycles, and primary dynamic plus secondary cycles obtained at the transducer on girder three, near the cover plate end, the critical fatigue detail for the I-70 over route 340 bridge. For each stress range histogram, an equivalent stress range is computed so that it produces the same fatigue damage as all stress ranges:

$$f_{re} = \left[\frac{\sum_i n_i f_{ri}^m}{\sum_i n_i} \right]^{\frac{1}{m}} \tag{2}$$

where

f_{re} = equivalent stress range

Table 2 lists the computed equivalent stress ranges for all histograms. Five values were computed. The first three are primary static stresses computed from FEM, averaging peaks and valleys, and FFT filtering of the WIM data. The fourth value was determined from the maximum and minimum WIM readings. Finally, the fifth includes the effect of secondary cycles. The equivalent stress ranges for primary static cycles obtained by the peak and valley and FFT filtering methods are similar while the value obtained from FEM is larger. Also, including the secondary cycles slightly increases the equivalent stress range above the value of the primary dynamic cycle.

Evaluation of Fatigue Life

The fatigue life of the four bridges was estimated according to the AASHTO guide specifications.[22] There are four alternatives suggested in the specifications, all four based on the evaluation of equivalent stress ranges at critical fatigue details: (1) field measurement of individual stress ranges; (2) use of GVW's from a nearby weigh station; (3) use of GVW's computed with WIM data; or (4) use of HS15 fatigue truck. For the latter three alternatives, equivalent stress ranges are computed with 2-D or 3-D analyses. Reliability factors are assigned to each option so that, theoretically, the resulting stress ranges are equal. The

13

fatigue life of each bridge was computed for all but the second alternative. The effect of impact and secondary cycles were quantified by introducing damage equivalent impact and secondary cycle factors for fatigue. The damage equivalent impact factor for fatigue, originally proposed by Seifert, quantifies the effect on fatigue life resulting from the dynamic magnification of stress:[23]

$$I_e = \frac{f_{re,dyn}}{f_{re,sta}} - 1 \tag{3}$$

The AASHTO specifications suggest a range of impact factors between 1.1 and 1.3. Similarly, the damage equivalent secondary cycle factor for fatigue quantifies the effect of secondary cycles on fatigue life. It is equal to:

$$S_e = \frac{f_{re,tot} - f_{re,dyn}}{f_{re,sta}} \tag{4}$$

There is no mention of the effect of secondary cycles on fatigue life in the current AASHTO specifications. Estimates of those factors were computed from the measured data.

Computations of the fatigue life of the I-70 over route 340 bridge with the alternatives one, three, and four are summarized in table 3. In alternative one, the fatigue life is computed for the equivalent stress ranges corresponding to the primary dynamic cycle and primary dynamic plus secondary cycles. In the other two alternatives, the stress ranges from both the 2-D and 3-D analyses were computed with the equivalent GVW's.

The specifications state that the fatigue life is infinite if the equivalent stress range multiplied by the reliability factor is less than the limiting stress range for the detail. Otherwise, the following equation is used to compute an estimate of the fatigue life:

$$Y = \frac{fK(10^6)}{T_a C (R_s f_{re})^3} \tag{5}$$

where
R_s = reliability factor
f_{re} = equivalent stress range
T_a = estimated lifetime average daily truck volume in the right lane
C = stress cycles per truck passage $= 1$ for bridges longer than 12.2 m (40 ft)
K = detail constant
f = 1.0 for safe life, 2.0 for mean life
Y = fatigue life in years

To compare the alternatives, the fatigue lives are computed in the present study with equation 3 even if the limiting stress is not exceeded. Several terms in equation 3 represent the mean S-N line for constant amplitude:

$$N = \frac{10^b}{f_r^{\ m}} \qquad (6)$$

where

f_r	= stress range
m	= slope of S-N curve
b	= intercept of S-N curve
N	= mean number of cycles to failure

The allowable S-N line is obtained by shifting the intercept by two standard deviations, 2s, on the log of life. The number of cycles is:

$$N = 365\ T_a CY \qquad (7)$$

Finally, the detail constant is:

$$K = \frac{10^b}{2(365 \times 10^6)} \quad \text{for mean life}$$

$$K = \frac{10^{b-2s}}{1(365 \times 10^6)} \quad \text{for safe life} \qquad (8)$$

Figure 21 illustrates the fatigue life calculations for the I-70 over route 340 bridge. The primary dynamic stress range histogram is scaled so that the total number of cycles of equivalent stress range ($N = 1.20 \times 10^7$) is equal to the safe fatigue life. The safe and mean S-N lines are shown. The equivalent stress range for the primary dynamic stress range histogram is multiplied by the AASHTO reliability factor R_a. The number of cycles of safe life is found to be 1.20×10^7, the ordinate at the intersection of the S-N line and the horizontal line at the equivalent stress range.

In table 3, the equivalent stress ranges, reliability factors, and estimates of fatigue lives for the I-70 over route 340 bridge are listed for the first, third, and fourth alternatives. The measured equivalent stress range (22.77 MPa (3.30 Ksi)) is smaller than those calculated with the 2-D and 3-D analyses (28.76 MPa (4.17 Ksi) and 28.49 MPa (4.13 Ksi), respectively). The reliability factors increase their difference. For the measured, 2-D, and 3-D analyses, the reliability factors are 1.15, 1.28, and 1.23 respectively. The computed fatigue lives range from 29 to 7 years, decreasing with the accuracy of the data and analysis methods. The fatigue lives computed with alternatives three and four are shorter than that obtained with the field measurements. The I-70 bridge was opened to traffic in 1967 and is now 25 years old. According to alternatives 3 and 4, the bridge has exceeded the safe life as listed in table 1. It also exceeded the mean life, which by equation 3 is f = 2 times the safe life. Yet, no cracks have been found to date at the cover plate ends.

Alternatives 3 and 4 give excessively conservative estimates of the fatigue life. Since the results from 2-D and 3-D analyses are similar, the discussion focuses on the FEM option.

Alternative 3 gives a shorter life because: (1) stress ranges calculated with the 3-D FEM for a $GVW_e = 264$ kN are 28.5 MPa / 22.8 MPa = 1.25 times the measured stress ranges, and (2) the reliability factor is 1.23 / 1.15 = 1.07 times the one for alternative 1. The ratio of fatigue life estimates is $(1.25 \times 1.07)^3 = 2.39$, which is the same as the ratio of 29.7 years / 12.5 years = 2.38.

Similarly, alternative 4 gives a shorter life because: (1) stress ranges calculated with the 3-D FEM for a $GVW_e = 240$ kN are 25.9 MPa / 22.8 MPa = 1.14 times the measured stress ranges, (2) the reliability factor is 1.30 / 1.15 = 1.13 times the one for alternative 1, and (3) the assumed ADTT is 2,900 / 1,850 = 1.57 times the estimated ADTT in alternatives 1 and 3. The ratio of fatigue life estimates is $(1.14 \times 1.13)^3 \times 1.57 = 3.35$, the same as 29.7 years / 8.9 years = 3.34.

The Standard Specifications for Highway Bridges assigns all cover plate end details to category E, for which the detail constant is K = 2.9.[3] It gives no credit for end details of higher fatigue strength. The transverse end welds on the cover plate of the I-70 over route 340 bridge were builtup in several passes. The weld and the cover plate were then ground to a 3:1 slope. Yamada and Albrecht have shown that this treatment increases the fatigue strength from category E to C, meaning a corresponding increase in the detail constant to K = 12.0.[24] According to equation 3, the fatigue life is increased in proportion by a factor of 12.0/2.9 = 4.1. This factor is not large enough to raise the fatigue life estimated with alternatives 3 and 4 to the 75-year service life that AASHTO recommends.[2] However, the I-70 over route 340 bridge is found to have an adequate service life if the higher detail constant is used with the measured stress ranges of alternative 1.

The last three alternatives assume that the stress ranges are proportional to the GVW's, by calculating the stress range for a truck with an equivalent GVW and considering it as an equivalent stress range. To verify this assumption, correlation coefficients were computed between WIM GVW's and WIM stress ranges. For each bridge, the axle weights of each truck obtained from WIM were placed on the FEM influence tracks to estimate the stress ranges. Correlation coefficients were also computed between FEM and WIM stress ranges. Figures 22 and 23 are comparison plots illustrating the two relationships discussed above.

Distribution Coefficients

The distribution coefficients at the lines of WIM transducers were computed for traffic traveling in each lane. Figures 24 and 25 are the distribution of results for all trucks. Those are used with pattern recognition to identify the lane traveled by the trucks.

PATTERN RECOGNITION STUDY

Three new approaches to WIM are presented. All three involve pattern recognition methods which remove further use of tapeswitches on the roadway needed in the traditional methods to determine the lane traveled, axle configuration, and velocity of the trucks. The tapeswitches are slowly torn off and destroyed by the traffic when the pavement becomes wet due to rain. The test plan was considerably affected by this problem. It is not feasible to collect continuous data for WIM over a few days with a portable system which requires tapeswitches on the pavement if there is a chance of precipitation on the bridge. Such capability would allow a fatigue evaluation of existing bridges with field measurements as discussed in the structural response study. The applicability of the three methods was investiged in this study.

The first two methods, Dynamic Time Warping (DTW)[25] and Hidden Markov Models (HMM),[26,27] have been popular pattern recognition methods for the past twenty years. They have been used for example in speech recognition for which data is similar to the measured strain data because they are both taken continuously at equal time increments.[26] The Third method, Feed Forward Neural Network (FFN)[28] with back-propagation learning algo-rithm,[29,30] is the standard method emerging from the field of parallel distributed processing which has been in expansion for the past six years. It was the first time that these pattern recognition methods was used for the study of bridge behavior with field measurements.

The velocity and axle spacings obtained from tapeswitch data in the conventional method are determined by considering the stress pattern alone in the pattern recognition methods. Three questions arise: (1) if data is collected without tapeswitches, can data pertinent to the truck passage be isolated?; (2) can the lane on which the truck is traveling be determined?; and (3) can the velocity, GVW, axles weights and spacings of the truck be obtained from the strain data? The answer to the first question is yes. The channels are balanced at zero when no trucks are on the bridge. The beginning of the strain pattern is when the data deviates from the zero reference. The end of the pattern is found when the data returns to and remains at the zero reference. The answer to the second question is yes. In the case of the four tested bridges, the calculated distribution coefficients with strain data clearly show a distinction between the two lanes of traffic. Therefore, the calculated distribution coefficients can be used to determine the traveled lane. To answer the third question, the three pattern recognition methods were implemented. In order to recognize patterns in the stress data, there must be some existing data, either simulated or previously measured, which in form resembles the new data.

Since this was a pilot study, the set of patterns was limited to ten single truck events, which were selected randomly. Those were recorded on I-66 over Bull Run bridge, a short simple span. Since the lane traveled is easily determined with distribution coefficients, the ten selected truck events traveled in lane 1. If the methods work for one lane, the solutions should be applicable for the other lanes because the principles are the same. During the field tests, a visual description of each truck was made by the keypad operator. An event for ten

17

different types of trucks was randomly chosen. Figure 26 shows the ten patterns. Tables 4 and 5 contain the descriptive information for them.

For WIM, the library of known patterns was created by applying the axle configuration for the different classes of trucks to FEM influence tracks. Each constructed pattern begins and ends with the values of stress when the truck is at the entrance and exit of the bridge, respectively.

In all three cases, the solution process requires a transformation of the measured stress before the pattern is put through the recognition process. As part of the transformation, the dynamic stress amplification is removed with the DFT filtering method.

Dynamic Time Warping Model

The DTW method is non-parametric, therefore simpler to understand and implement than the other two. It was considered for WIM because it operates on patterns which are represented by sequences of points taken at equal time increments, which is the case of the measured data. The DTW method uses a library of known patterns to recognize a new pattern. The new sequence is compared to each known sequence, one at a time. The first and last points of the two sequences are matched automatically. The intermediary points are matched by a mapping function subjected to a set of constraints. A distance between the two patterns estimated by a metric function is minimized using a dynamic programming algorithm:

$$D(R_q^N,R_p^M)=\min_\phi \int_0^T \rho(\phi(R_q),R_p)^t g(t,\phi(R_q),\phi'(R_q))\,dt \qquad (9)$$

where

R_q^N	=	new pattern q of size N
R_p^M	=	known pattern p of size M
R_q	=	discrete value of new pattern q at time t
R_p	=	discrete value of known pattern at time t
$\phi()$	=	any function that maps natural time scale of pattern q monotonically onto that of pattern p.
$\rho()^t$	=	metric function used to calculate pointwise distance between patterns p and q at time t
$g()$	=	boundary function preventing mapping function from causing too abrupt, too non-linear a change in time scale.
$D()$	=	minimum cumulative distance between patterns p and q.

Figure 27 is a flowchart of the DTW method for WIM. First, the measured stress pattern is prepared. The size of the measured pattern varies with the speed and length of the truck. Its N values must represent the entire travel of the truck on the span. The measured stress pattern is compared to each contructed pattern. The two inner loops determine the

best mapping at each data point. The dynamic programming method minimizes the cumulative distance. The comparison process is interrupted if the increasing cumulative distance exceeds the current best overall cumulative distance. A detailed description of the application of the DTW method for WIM is available in appendix A. It includes an illustrative example of the comparison of two patterns. The reference numbers of the constructed patterns which are closest to the measured pattern are output. The truck which corresponds to the measured pattern is found to have the same axle configuration as the identified constructed patterns. With the addition of the size of the measured sequence, and the sampling rate, the velocity is computed using equation 16.

Figure 28 shows the ten measured stress patterns, transformed for DTW. The constructed patterns are shown in figure 29. Those patterns are also used in the other two methods. Their sample size M is determined by the smallest and largest sizes of the measured records. Those are obtained by entering the extreme conditions in equation 16.

Table 6 is the matrix of distances between the ten measured records and the ten constructed records. For example, the minimum cumulative distance between the first measured and the third constructed patterns is 98. On the right end side of the matrix, the best match for each measured pattern is given. All ten records were properly recognized. For patterns 1 through 10, the minimum distances are 19, 16, 40, 32, 84, 65, 36, 56, 52, and 142, respectively. The closest distances to the minimum are 33, 26, 123, 83, 165, 275, 89, 150, 105, and 298, respectively or 1.73, 1.62, 3.07, 3.59, 1.96, 4.23, 2.47, 2.68, 2.01, and 2.10 times the minimum distance.

Hidden Markov Model

The HMM method is based a probabilistic model of the observed process. The measured patterns are assumed to be a sequence of simple or primitive patterns, which are observed at different states of the process. The underlying process is assumed to be Markovian, i.e. that its value at any time depends only on a finite interval of its immediate history. The HMM's are trained to recognize different classes of patterns. The type of HMM, which is applicable to time varying data, is the left to right model. Figure 30 is a sketch of such a model.

A set of class-conditional density functions is chosen a priori for the primitive patterns. Figure 31 is a flowchart of the HMM method for WIM. The patterns are partitioned into the primitive patterns using a decision rule. The primitive patterns are refined using the K-means algorithm. They are used to create an HMM by defining likelihood functions associated with the doubly stochastic models for each class of pattern. For each HMM, two matrices of probabilities are the product of a training with the expectation-modification algorithm. Once the HMM's are trained, the maximum likelihood of having the same sequence of observations as the constructed patterns for each measured pattern is computed using the Viterbi algorithm:

$$\phi_t(j) = \max_{1 \le i \le N} \left\{ \phi_{t-1}(i) a_{ij} b_j(O_t) \right\}, \ \forall \ 1 \le t \le T$$

$$\psi_t(i_t) = \psi_{t-1}(i_{t-1}) \otimes q_{i_t}$$

(10)

where

a_{ij}	=	probability of transiting from state q_i at t to state q_j at t+1
$b_j(O_t)$	=	b_{jk} or probability of seeing primitive pattern ωk at state j during observation at time t
		$(1 \le k \le M)$
q_{it}	=	most likely state at time t
N	=	number of possible states
M	=	number of primitive patterns
T	=	number of discrete data points
$\phi_t(j)$	=	likelihood of being at state q_j at time t
$\psi_t(i_t)$	=	most likely partial state sequence of length t ending at state where likelihood of being at that state at time t is maximum (it = argmax$\{\phi_{t-1}(j)\}$)
$\otimes$	=	concatenate

A detailed description of the algorithms discussed above is available in appendix B. For WIM, the primitive patterns are a set of values for the slope of the stress. The states are described by the positions of the axles relative to the entrance and exit of the bridge and the position of the WIM transducers. Figures 32 and 33 illustrate the transformation of the measured data. The moment at mid-span due to an HS20 truck is computed for all positions of the truck with a 2-D influence line. The slope of the moment changes when an axle either enters or exits the bridge, or when it passes over the position of the WIM transducers. The states of the process are described by the position of the axles relative to those three locations. The observations at each state are the magnitude of the slopes which in the case of the 2-D moment remain constant. With FEM or measured stresses (3-D), the slopes vary slightly. The probabilities of transition show that measured data may indicate that there is a 50% chance of no change in state or a 50% chance of moving to the next state. At each state, the corresponding observation is given a probability of 0.6. The neighboring primitive patterns are assigned a probability of 0.2 to account for the possible small variations in slope.

Figures 34 and 35 are the transformed data for the measured and constructed patterns. Table 7 is the matrix of likelihoods between the ten measured and constructed stress patterns. The results show that 9 out of 10 patterns were properly identified. The third measured pattern is incorrectly matched with the fourth constructed pattern. The primitive patterns chosen as the slope of the stress vary with the amount of dynamic stress amplification. The proper recognition is dependent on the proper sequence of observations of primitive patterns at a proper sequence of states. The solution process is more sensitive to the variations in stress than in the DTW method. In this case, the FEM patterns would only serve as a starting block. As more data is measured, the probabilities of the HMM's representing each

class of truck would be modified with the Expectation-Modification algorithm which is described in appendix B.

The maximum likelihoods for patterns 1 thru 10 are 0.361, 0.362, 0.368, 0.366, 0.368, 0.358, 0.375, 0.357, 0.393, and 0.323. The closest likelihoods to the maximum are 0.346, 0.361, 0.363, 0.353, 0.366, 0.338, 0.337, 0.354, 0.369, and 0.289, respectively, or 0.96, 0.99, 0.98, 0.96, 0.99, 0.94, 0.90, 0.99, 0.94, and 0.89 times the maximum.

Both the DTW and HMM methods perform an optimization with a dynamic programming algorithm and both are classifiers. The transformation of the measured data for DTW is less computationally intensive than that for HMM. With the new hardware available, and an efficient data structure such as a hash table to access the constructed pattern rapidly, the DTW method is a better candidate for WIM than its homologue the HMM method. However, the HMM method has the advantage of allowing adaptive pattern recognition. The more data is read, the more accurate the probabilities of the models become.

Artificial Neural Network Model

Artificial Neural networks are used for pattern recognition. The FFN with sigmoidal activation function and the back-propagation training algorithm are the standard methods used. A neural network loosely models the nervous system of the brain. It is composed of a large number of identical units called cells which perform simple operations in parallel. Figure 36 is a graphical representation of a simple fully connected and layered feed forward neural network models.

The network, in this case, comprises three groups of cells: input, hidden, and output cells. The architecture is arbitrary. The number of hidden layers and hidden cells is empirically chosen. Each cell is assigned a value. The values of the various cells of a simple FFN are related as follows:

$$x_i = X_{pi} \ , \forall \ 1 \le i \le m$$

$$net_i = (\sum_{j=1}^{i-1} w_{ij} x_j) - \theta_j \ , \forall \ m+1 \le i \le N+n$$

(11)

$$x_i = s(net_i) \ , \forall \ m+1 \le i \le N+n$$

$$\hat{Y}_{pi} = x_{i+N} \ , \forall \ 1 \le i \le n$$

where
- m = number of input cells
- N = number of hidden and input cells
- N-m = number of hidden cells
- n = number of output cells
- x_i = value of cell i after activation

21

net_i = value of cell i before activation
$s()$ = activation function
w_{ij} = weight between cells i and j (j < i)
θ_i = bias of cell i
N+n = total number of cells
X_p = set of m input values for pattern p
Y_p = set of n target values for pattern p
$\hat{Y}_p$ = set of n calculated output values for pattern p

The activation level at the hidden and output cells varies between zero and one. There are three common types of activation functions shown in figure 37: a hard limiter which suddenly changes from zero to one; a threshold logic which goes from zero to one at a constant slope; and a sigmoid which varies from zero to one with horizontal asymptotes at zero and one. For a layered FFN, equation 11 is slightly modified to show the removal of some connections:

$$x_i = X_{pi} \; , \; \forall \; 1 \le i \le m$$

$$net_i = (\sum_{j=1}^{m} w_{ij}x_j) - \theta_j \; , \; \forall \; m+1 \le i \le m+N_1$$

$$net_i = (\sum_{j=m+1}^{m+N_1} w_{ij}x_j) - \theta_j \; , \; \forall \; m+N_1+1 \le i \le N \tag{12}$$

$$x_i = s(net_i) \; , \; \forall \; m+1 \le i \le N+n$$

$$\hat{Y}_{pi} = x_{i+N} \; , \; \forall \; 1 \le i \le n$$

where
N_1 = number of hidden cells in first layer
$N-m-N_1$ = number of hidden cells in second layer

A neural network has to be trained to recognize T known patterns. The values of the output are dependent on the values of the weights and biases which are empirically set, initially. An error function is used to determine how far off the estimates are from the target values. It is equal to the sum of the squares of the errors in output:

$$E_p = \sum_{i=1}^{n} \frac{1}{2}(\hat{Y}_{pi} - Y_{pi})^2$$

$$= \sum_{i=1}^{n} \frac{1}{2}(x_{i+N} - Y_{pi})^2 \tag{13}$$

The initial weights and biases are randomly chosen. Their values are usually very small. The weights and biases are adjusted using the back-propagation algorithm to minimize this error:[29,30]

$$w_{ij}^{new} = w_{ij}^{current} - \eta \frac{\partial^+ E_t}{\partial w_{ij}} + \alpha (w_{ij}^{current} - w_{ij}^{previous}) \qquad (14)$$

and,

$$\theta_i^{new} = \theta_i^{current} - \eta \frac{\partial^+ E_t}{\partial \theta_i} + \alpha (\theta_i^{current} - \theta_i^{previous}) \qquad (15)$$

where

α, η = learning rates.

A correction to the weights and biases is computed for each pattern. The back-propagation implies that all adjustments must accumulated for all patterns, and then applied to the values after each learning iteration. This study followed the recommendation made by Werbos to adjust the values after the computation for each pattern.[30] A detailed description of the evaluation of the ordered partial derivatives is included in appendix C. In the full report, the reverse process of WIM, of computing the moment knowing the axle configuration, was selected to illustrate FFN's.

For WIM, the FFN was trained as a classifier. The ten constructed patterns have 91 consecutive and equally spaced stress values. Ten output cells are computed for each pattern. The values of the target output are 1 for one cell and 0 for the other nine. Each output cell corresponds to one class of truck. If the value of an output is close to 1, the truck represented by the input is found to belong to the class assigned to that cell.

With 91 input, 0 hidden, and 10 output cells, the error function converges as shown in figure 38. The values of the output cells converge towards the target values with 100 percent success. The largest error in output for any training pattern is less than 5 percent after 40,000 learning iterations (Figure 46 shows the flowchart of the learning process). The initial values of the weights, biases, and learning rates are empirically set, initially. The error functions converged after a few reductions in the learning rate. Each output level was assigned a different learning rate.

Table 8 lists the outputs for the ten constructed patterns after the learning process. All output values in the diagonal are above 0.9 and all others are below 0.1. This shows that the learning process has converged for the ten FEM produced patterns.

Figure 39 is the flowchart of the FFN method for WIM. The learning process is performed once, unless additional patterns are added to the training set. The FFN operates by entering the input values. The output is obtained directly. Table 9 lists the outputs obtained by entering the the measured stress patterns into the classification FFN. All ten

patterns were properly recognized. The classification is distinct for all but pattern 8. The value of output cell 8 is 0.999. The next largest output is 0.980 from cell 5. The FFN did not converge towards a complete solution of the problem. The remedy for this problem might be to increase the number of training patterns. However, in doing so, the converge during the learning process is slowed. More training patterns would require more hidden cells which numbers are chosen empirically since there are no theories available to do so. Moreover, convergence is not guaranteed.

An FFN for WIM could be defined to directly output the lane traveled, the velocity, axle weights, and spacings of the truck. Figure 40 shows a conceptual sketch of such a neural network.

CONCLUSIONS AND RECOMMENDATIONS

Summary

Four Highway steel girder bridges were instrumented with the WIM+R system to determine their service loads and to measure stress ranges at fatigue critical details. The four bridges were the:

o   I-66 over Bull Run bridge, a short simple span with a small skew
o   I-66 over route 55 bridge, a long simple span with a large skew
o   I-70 over route 340 bridge, a typical two-span continuous bridge with rolled sections and a non-composite deck.
o   I-66 over route 7100 bridge, also a two-span continuous bridge with comparable spans and one more lane of traffic, with plate girders designed to be composite with the concrete deck.

Influence tracks for the stress at the location of each transducer were generated with a finite element analysis of each bridge. Those served two purposes: (1) the WIM calculations were performed with the influence tracks, and (2) once the axle weights of a truck were computed, they were positioned on the influence tracks in order to obtain the static stress range. A modal analysis produced the natural frequencies of each bridge.

Part of the test plan involved recording the stresses during the crossing of a test truck at normal traffic speed. With the complete information about the bridge and loading for those few truck events, the influence track was computed from the strain data.

The previous WIM process was described in detail to better understand its limitations. Previous studies have shown that GVW's could be estimated accurately with the WIM+R system. However, the distribution of the GVW to the individual axles of a truck was not generally satisfactory. Shifting the position of the truck was found to improve the estimates of axle weights. The shift was determined for the test truck only since its axle weights are

known. The optimum shift in position of the axles was calculated with the Newton-Cotes polynomial interpolation and Newton-Raphson iteration.

For each truck event, the dynamic stress ranges were computed as the maximum stress minus the minimum stress at each transducer. A spectrogram obtained with a fast Fourier transformation of the measured data, combined with the natural frequencies from the FEM modal analysis, were used to determine the cut-off frequency needed to filter out the dynamic amplification of the stress. As a result of this process, the primary static stress range was extracted from the measured data. A second estimate of the static stress range was computed by averaging the stresses at consecutive peaks and valleys. Also, the stress ranges corresponding to the secondary cycles were determined with the rainflow method.

Once the axle weights and the stress ranges were computed from the measured data, the correlation coefficients between the FEM stress ranges and the WIM stress ranges and the correlation coefficients between the WIM stress ranges and the WIM GVW's were computed.

The WIM GVW's and WIM stress ranges of all truck events were presented as histograms. This was done for all transducers on the four bridges. The equivalent stress ranges and equivalent GVW's were computed and the safe fatigue life of the four bridges were computed with the alternative methods recommended in the AASHTO fatigue guide.

Finally, established pattern recognition methods in the field of speech recognition were implemented for WIM. The purpose of this effort was to find a way of determining axle configuration without having to install tapeswitches on the roadway, as conventional bridge WIM systems require. Three different methods were implemented: dynamic time warping, hidden Markov models, and a feed forward neural network. It is the first time that these pattern recognition methods have been used for the study of bridge behavior with field measurements.

Conclusions and Recommendations

All five objectives stated in the introduction were met. Other problems encountered during the research study were also solved. The conclusions and recommendations of this study are:

Weigh-In-Motion Study:

o   The conventional WIM analysis with tapeswitches was improved in two ways:

> o   FEM influence tracks, which more closely represent the true three dimensional behavior of the bridge, were used instead of 2-D influence lines. Available pre- and post-processors simplify FEM analysis and should therefore replace 2-D analysis.

o   The optimization method of distributing the GVW to the individual axles proved successful with the test truck data. Further implementation of this method should be done for various truck types. This would require more data collection with test trucks of different axle configurations.

o   The 3-D influence tracks for the stress at each transducer can be determined from strain data collected at regular traffic speed with the test truck. In comparison to FEM influence tracks, the results were good for all but the short span of the I-66 over Bull Run bridge. This procedure should be considered as an alternate to the FEM method and to the approach suggested by Goble with test data collected at crawling speed.[19]

Response Study:

o   The GVW's and stress ranges were found to be linearly dependent at a 95 percent level of confidence, therefore the assumption of proportionality between GVW's and stress ranges made in the AASHTO guide specifications is statistically correct.[2]

o   The FEM and WIM stress ranges were also found to be linearly dependent at a 95 percent confidence level. However, the FEM tends to overestimates the magnitude of the stress ranges by about 10 to 20 percent.

o   The conclusions from the comparative study of alternatives 1, 3, and 4 described in the AASHTO guide specifications are:[2]

    o   The average GVW_c for the four instrumented bridges $(222+250+264+243)/4$ = 245 kN (55 kip) is only 2 percent higher than the GVW = 240 kN (54 kip) of the HS15 fatigue truck.

    o   For the four bridges, the fatigue life resulting from alternative 1 is greater than those obtained with alternatives 3 and 4 with 2-D analysis.

    o   If FEM is used instead of 2-D analysis, the computed lives are less conservative. In the case of the I-66 over Bull Run bridge, the fatigue life is slightly overestimated without any serious consequences since the bridge is found to have a fatigue life six times greater than the 75-year service life suggested by AASHTO.

    o   The secondary vibration cycles did not significantly decrease the estimated fatigue lives of the four bridges.

o   The Standard Specifications for Highway Bridges assigns all cover plate end details to category E.[3] Some credit should be given to end details of higher fatigue strength. This would considerably affect the findings for the I-70 over route 340 bridge.

26

Raising the fatigue strength of the end welded and ground cover plate from E to C quadruples the fatigue life.

o The fatigue life of a bridge, which was designed before the AASHTO guide specifications[2] were adopted, should be first with alternative 4 of the Guide Specifications for Fatigue Evaluation of Existing Steel Bridges giving a conservative estimate.[22] If the safe life is found to be shorter than the desired service life, the fatigue analysis described as alternative 1 should be performed with stress ranges directly measured with the WIM+R system at the fatigue critical details.

Pattern Recognition Study:

o The axle configuration can be determined from the stress pattern measured during the truck event. The results obtained for the I-66 over Bull Run bridge are promising. Ten different patterns were used for illustration purposes. In all three methods (DTW, HMM, and FFN), the measured data was filtered with FFT method, and the training patterns were constructed with finite element influence tracks.

o The back-propagation method was successful in training the fully connected simple classification FFN with sigmoids as activation functions. No transformation of the data is needed in addition to the FFT filter. Contrary to the other two proposed methods, the FFN can directly compute the axle weights, axle spacings and truck velocity. A study should be conducted to determine the number of training patterns required to obtain the proper output for most situations measured with the WIM system, knowing that both the velocity and axle spacings are required. Furthermore, the size of the training set would depend on the ability of the neural network to interpolate between training "points." For that purpose, a Gaussian-based network may be superior to the traditional sigmoidal network with back-propagation learning algorithm.[31] A Gaussian-based FFN resulted in a faster learning stage for WIM and promising results during a follow-up study on this research.[32]

A complete description of the study is presented in Gagarine.[33]

APPENDIX A. DYNAMIC TIME WARPING

The dynamic time warping method for WIM is described in detail. The records q and p, and the five functions d, D, g, ϕ, and ρ are defined for WIM. Each record consists of a set of discrete stress data for one or more transducers. The number of consecutive scans during the presence of the truck on a span is equal to:

$$N = \frac{(L+L_t)r}{v} \tag{16}$$

where
L = span length

L_t = length of truck
r = sampling rate
v = velocity of truck
Sequences of discrete stress readings for each transducer c are formed for records p and q:

$$R_q^N = \left[R_{qc}^{n\Delta t} \right]_{m=1}^N = \left[\sigma_{ic} \right]_{i=1}^N \tag{17}$$

$$R_p^M = \left[R_{pc}^{m\Delta t} \right]_{m=1}^M = \left[\sigma_{kc}^* \right]_{k=1}^M$$

where

Δt = time increment
$R_{qc}^{n\Delta t}$ = n-th element of sequence of measured record q
$R_{pc}^{m\Delta t}$ = m-th element of sequence of constructed record
       p
σ_{ic} = i-th stress reading at transducer c
σ_{kc}^* = k-th predicted stress at transducer c

A dual nomenclature is introduced in equation A-2. The n-th element of the sequence of record q, $R_{qc}^{n\Delta t}$ is equal to the i-th stress reading, σ_{ic}, at time $n\Delta t$.

Each constructed record R_p^M is composed of stress σ_{kc} computed with FEM influence tracks, and truck configurations obtained from WIM data and other sources such as weigh stations. The records are constructed as shown in figure 3. The mapping function ϕ matches measured and predicted stresses. The resulting sequence of measured stress is:

$$\phi(R_q^N) = R_q^M$$

$$= \left[R_{qc}^{m\Delta t} \right]_{m=1}^M = \left[\sigma_{jc} \right]_{j=1}^M \tag{18}$$

The distance at time $t = m\Delta t$ is equal to:

$$\rho(\phi(R_{qc}^{n\Delta t}), R_{pc}^{m\Delta t}) = \rho(\phi(\sigma_{ic}), \sigma_{kc}^*) \tag{19}$$

$$= \rho(\sigma_{jc}, \sigma_{kc}^*)$$

The first and last points of the two sequences are matched. Therefore $\phi(\sigma_{1c}) = \sigma_{1c}$ and $\phi(\sigma_{Nc}) = \sigma_{Mc}$. These two equalities imply that σ_{1c} and σ_{Nc} are compared to σ_{1c}^* and σ_{Mc}^*, respectively. If one transducer is used, the metric function is taken as:

$$\rho(\sigma_{jc}, \sigma_{kc}^*) = \left(\sigma_{jc} - \sigma_{kc}^* \right)^2 \tag{20}$$

If Nc transducers are used, linear prediction coefficients (LPC) (weight factors) can be applied to the stresses so that the effect of some transducers outputs are emphasized. The metric function can be taken as the logarithm of the ratio of prediction residuals as shown in the Itakura method:

28

$$\rho(\{\sigma_j\},\{\sigma_k^*\}) = \log \left[\frac{\{a_j\}^T[\sigma_j]\{a_j\}}{\{a_k\}^T[\sigma_k^*]\{a_k\}} \right] \geq 0$$

$$\text{where} \quad \{\sigma_j\} = \begin{Bmatrix} \sigma_{j1} \\ \sigma_{j2} \\ . \\ \sigma_{jN_c} \end{Bmatrix}, [\sigma_j] = \begin{bmatrix} \sigma_{j1} & 0 & . & 0 \\ 0 & \sigma_{j2} & . & 0 \\ . & . & . & . \\ 0 & 0 & . & \sigma_{jN_c} \end{bmatrix}, \{a_j\} = \begin{Bmatrix} a_{j1} \\ a_{j2} \\ . \\ a_{jN_c} \end{Bmatrix} \qquad (21)$$

similarly for $\{\sigma_k^*\}, [\sigma_k^*]$, and $\{a_k\}$

A simpler metric function for multi-dimensions is the sum of the differences squared:

$$\rho(\{\sigma_j\},\{\sigma_k^*\}) = \sum_{c=1}^{N_c} \left[\sigma_{jc} - \sigma_{kc}^* \right]^2 \qquad (22)$$

In this function, all transducer outputs are weighed equally.

The case of one dimension is used in the explanation of the boundary function. The variables in the boundary function g are the time, the value of the slope and ordinate of the mapping function at that time. Three global constraints are imposed on the slope of the mapping function:

$$g(n\Delta t,\phi(\sigma_{ic}),\phi'(\sigma_{ic})) = \begin{bmatrix} \infty, & \text{if } \phi'(\sigma_{ic}) < \dfrac{1}{2} \\ 1, & \text{if } \dfrac{1}{2} \leq \phi'(\sigma_{ic}) \leq 2 \\ \infty, & \text{if } \phi'(\sigma_{ic}) > 2 \end{bmatrix} \qquad (23)$$

The slope is computed with the counters of two consecutive stresses. Figure 41 shows the global boundaries. The horizontal axis is the sequence of measured stresses (from 1 to N). The vertical axis is the sequence of constructed stresses (from 1 to M). Two boundaries originate from each end point: their slopes are 1/2 and 2, the extreme imposed by the above boundary conditions. Any point inside the four boundaries are permissible comparisons. In order to make a comparison, there must be some area within the four boundaries. It is the case only if M/2 < N < 2M. This restriction sets the criteria for the selection of the size of the constructed patterns.

The mapping function is subjected to three local constraints:

$$g(n\Delta t,\phi(\sigma_{ic}),\phi'(\sigma_{ic})) = \begin{bmatrix} \infty, \text{ if } \phi(\sigma_{i-1c}) = \phi(\sigma_{ic}) \\ \qquad\qquad = \phi(\sigma_{i-2c}) \\ 1, \text{otherwise} \\ \\ 1, \text{if } 0 \le \phi(\sigma_{ic}) - \phi(\sigma_{i-1c}) \le 2 \\ \infty, \text{otherwise} \end{bmatrix} \qquad (24)$$

These conditions prevent the comparison of three consecutive measured stresses to the same predicted value. Figure 41 shows which situations are permitted by the local constraints within the global boundaries. The first two constraints allow the comparison of two consecutive measured stresses to the same predicted value but not three. The next two constraints allow at most one predicted value to be skipped. Also, the comparison has to go forward in time. It is not possible to go back to a previously matched predicted stresses.

The cumulative distance function D for one dimension (for one transducer c) is equal to:

$$D(R_q^N, R_p^M) = \min_\phi \sum_{i=0}^{M-1} \rho(\phi(\sigma_{ic}), \sigma_{kc}^*) \, g(t, \phi(\sigma_{ic}), \phi'(\sigma_{ic})) \qquad (25)$$

In order to further describe the minimization process of D with dynamic programming, the notation is simplified:

$$D(N-1, M-1) = D(R_q^N, R_p^M)$$

$$d(i,k) = \rho(\phi(\sigma_{ic}), \sigma_{kc}^*) \qquad (26)$$

$$g(i,k) = g(n\Delta t, \phi(\sigma_{ic}), \phi'(\sigma_{ic}))$$

Equation 26 becomes:

$$D(N,M) = \min_\phi \sum_{i=1}^{M} d(i,k) \, g(i,k) \qquad (27)$$

The dynamic programming method is a recurrence. The cumulative distance of the first i points the sequence R_q^N mapped on the k points of sequence R_p^M defined as:

$$D(i,k) = d(i,k)\,g(i,k) + \min \begin{Bmatrix} D(i-1,k)\,g(i-1,k) \\ D(i-1,k-1) \\ D(i-1,k-2) \end{Bmatrix} \qquad (28)$$

An illustrative example for one transducer is shown with N=18 and M=12. Figure 42 shows the value of the individual distances within the global boundaries. The ordinates are the counters of the measured sequence and the abscissa are the counters of the constructed sequence. The stress values are plotted next to the counters. Figure 43 is the best cumulative distances obtained with dynamic programming for all the comparison within the

30

global boundaries. Figure 44 is the plot of the critical path obtained by backtracking from the last point. Also shown with dashed lines are the paths which would have resulted in a larger overall cumulative distance. The cumulative distance is shown at each measured stress in table 10.

APPENDIX B. HIDDEN MARKOV MODEL

The hidden Markov models method for WIM is described in detail. The measured patterns are assumed to be a sequence of simple or primitive patterns, which are observed at differents states of the measured process. The underlying process must a sequence of N states q_1, q_2, ..., q_N. The observable process is a sequence of T observations O_1, O_2, ... ,O_T of the primitive patterns.

For WIM, the primitive patterns are values of the slope of the stress. The states are described by the positions of the axles relative to the entrance and exit of the bridge and the location of the WIM transducers.

Primitive Patterns

The primitive patterns are identified using the following decision rule:

$$\sigma_t' \in \omega_k \text{ iff } \delta(\sigma_t', \omega_k) \geq \delta(\sigma_t', \omega_j), \forall \ 1 \leq j,k \leq M \qquad (29)$$

where

$$\sigma_t' \quad = \quad \text{change in slope of strain function at time t}$$
$$\omega_k \quad = \quad \text{k-th primitive pattern}$$
$$M \quad = \quad \text{number of primitive patterns}$$
$$\delta() \quad = \quad \text{distance between point and primitive pattern}$$

The distance between a discrete point and a primitive pattern is calculated by using a metric:

$$\delta(y,\omega) = \min_{x \in \omega}[\rho(x,y)] \qquad (30)$$

where
$$\rho() \quad = \quad \text{metric function}$$

The metric function is equal to the absolute value of the minimum difference between the new value and a point of the primitive pattern.

K-Means Algorithm

The training patterns are partitioned into primitive patterns. The K-means algorithm optimizes the partition process by modify the basic prototypes of each primitive pattern. It is an iterative method. First, the values of the prototypes of each primitive pattern are selected arbitrarily. Each training value is classified:

31

$$\sigma_t' \in \omega_k \text{ iff } \rho(\sigma_t',\sigma'^k) \ge \rho(\sigma_t',\sigma'^j), \quad \forall \ 1 \le j,k \le M \qquad (31)$$

where

σ'^j = prototype value of j-th primitive pattern

After all training values are classified, the prototype values are modified. They are taken as the average of the training values classified in their primitive patterns:

$$\sigma'^k = \frac{1}{m_k} \sum_{j=1}^{m_k} \sigma'_j \qquad (32)$$

The iterations are stopped when the change in the prototype values is less than a preset value θ.

Likelihood Functions

The likelihood $\mathcal{L}(O/A,B)$ of sequence O of observations for the HMM specified by probability matrices A and B for all state sequences is defined as:

$$\mathcal{L}(O/A,B) = \sum_{Q_T} \prod_{t=1}^{T} a_{ij} \ b_j(O_t) \qquad (33)$$

$$= \mathcal{L}(O/\lambda)$$

where

A	=	state transition matrix
	=	$[a_{ij}]_{N \times N}$ where a_{ij} = pr[q_j at t/q_i at t-1]
a_{ij}	=	probability of transiting from state q_i at t-1 to state q_j at t
B	=	Observation probability matrix
	=	$[b_{jk}]_{M \times N}$ where b_{jk} = pr[ω_k at t/q_j at t]
$b_j(O_t)$	=	b_{jk} or probability of seeing primitive pattern ωk at state q_j during observation at time t
T	=	number of discrete data points
Q_T	=	number of state sequences
λ	=	HMM defined by matrices A and B

Note that the following equations on probabilities must remain true:

$$a_{ij} \geq 0, \ \forall \ 1 \leq i,j \leq N$$

$$\sum_{j=1}^{N} a_{ij} = 1, \ \forall \ 1 \leq i \leq N$$

$$b_{jk} \geq 0, \ \forall \ 1 \leq j \leq N, \ \forall \ 1 \leq k \leq M \tag{34}$$

$$\sum_{k=1}^{M} b_{jk} = 1, \ \forall \ 1 \leq j \leq N$$

The likelihood of O for the HMM specified by A and B is equal to the sum of the likelihoods of all possible state sequences. The likelihood of a particular state sequence is equal to:

$$\mathcal{L}(Q_i/A,B) = \prod_{t=1}^{T} a_{ij} \ b_j(O_t) \tag{35}$$

To reduce the computational effort from N^T to N^2T in evaluating the likelihood functions, a forward and backward partial likelihood functions are used. The likelihood of having observed O_1, O_2, ... ,O_t and ending up at state q_j at t for HMM $\lambda(A,B)$ is equal to:

$$\alpha_t(j) = \sum_{i=1}^{N} \alpha_{t-1}(i) a_{ij} b_j(O_t) \tag{36}$$

The likelihood of observing O_{t+1}, O_{t+2}, ..., O_T, starting at time t at state q_i is equal to:

$$\beta_t(i) = \sum_{j=1}^{N} a_{ij} b_j(O_{t+1}) \beta_{t+1}(j) \tag{37}$$

then:

$$\mathcal{L}(O/\lambda) = \sum_{i=1}^{N} \sum_{j=1}^{N} \alpha_t(i) a_{ij} b_j(O_{t+1}) \beta_{t+1}(j), \forall 1 \leq t \leq T-1$$

$$\tag{38}$$

$$\mathcal{L}(O/\lambda) = \sum_{i=1}^{N} \alpha_T(i)$$

Expectation-Modification Algorithm

The probability matrices A and B can be modified to take in account the results accumulated. For a state transition probability a_{ij}, a new estimate can be computed. It is equal to the number of transitions from qi to qj divided by the expected number of transitions out of qi conditional on O and $\lambda(A,B)$:

33

$$a_{ij}^{new} = \frac{\displaystyle\sum_{t=1}^{T-1} \alpha_{t-1}(i) a_{ij} b_j(O_t) \beta_t(j)}{\displaystyle\sum_{t=1}^{T-1} \alpha_t(i) \beta_t(i)}, \quad \forall \; 1 \leq i,j \leq N \tag{39}$$

For the observation probability b_{jk}, a new estimate is equal to the ratio of the expected number of occurrence of the k-th primitive pattern in state q_j divided by the number of occurrence of state q_j:

$$b_{jk}^{new} = \frac{\displaystyle\sum_{\substack{t \ni O_t = \omega_k}} \alpha_t(j) \beta_t(j)}{\displaystyle\sum_{t=1}^{T} \alpha_t(j) \beta_t(j)}, \quad \forall \; 1 \leq j \leq N, \; 1 \leq k \leq M \tag{40}$$

The number of occurrences are kept in counters until the probabilities are modified.

Viterbi Algorithm

The most likely state sequence is obtained by using dynamic programming to maximize cumulatively the likelihood function of being at a state:

$$\phi_t(j) = \max_{1 \leq i \leq N} \{\phi_{t-1}(i) a_{ij} b_j(O_t)\}, \quad \forall \; 1 \leq t \leq T \tag{41}$$

$$\psi_t(i_t) = \psi_{t-1}(i_{t-1}) \otimes q_{i_t}$$

where

$(1 \leq k \leq M)$

q_{i_t} = most likely state at time t
N = number of possible states
$\phi_t(j)$ = likelihood of being at state q_j at time t
$\psi_t(i_t)$ = most likely partial state sequence of length t ending at state where likelihood of being at that state at time t is maximum (it = argmax$\{\phi_{t-1}(j)\}$)
$\otimes$ = concatenate

The initial conditions are:

$$\phi_0(1)=1 \; , \; \phi_0(i)=0, \; \forall \; 2 \leq i \leq N$$
$$\psi_0(1)=q_1 \; , \; \psi_0(i)=\infty, \; \forall \; 2 \leq i \leq N \tag{42}$$

The results of the dynamic programming can be shown graphically the same way as for DTW. In the case of the left to right algorithm, the constraints prevent any transition from a higher state to a lower state.

APPENDIX C. ARTIFICIAL NEURAL NETWORK

The back-propagation learning algorithm is also known as the generalized delta rule. It is the standard method of training sigmoidal networks.

Both the input and target values for T training patterns are available. Initially, the weights and biases are empirically set to small values. The input values are submitted to the network. An estimate of the output values is computed with the initial weights and biases. An error function is used to determine how far off the estimates are. It is equal to the sum of the squares of the errors in output:

$$E_p = \sum_{i=1}^{n} \frac{1}{2}(\hat{Y}_{pi} - Y_{pi})^2$$

$$= \sum_{i=1}^{n} \frac{1}{2}(x_{I+N} - Y_{pi})^2$$

(43)

The weights and biases are modified using a steepest descent algorithm so that, for all T patterns, the error is minimized:

$$w_{ij}^{new} = w_{ij}^{current} - \eta \frac{\partial^+ E_t}{\partial w_{ij}} + \alpha (w_{ij}^{current} - w_{ij}^{previous})$$

(44)

and,

$$\theta_i^{new} = \theta_i^{current} - \eta \frac{\partial^+ E_t}{\partial \theta_i} + \alpha (\theta_i^{current} - \theta_i^{previous})$$

(45)

where

α, η = learning rates.

The second terms are the slope terms. The third terms are the momentum terms which take in consideration changes from the previous iteration.

The partial derivatives in the second term of the previous two equations are evaluated using the chain rule for partial derivatives. For the weights:

$$\frac{\partial^+ E_t}{\partial w_{ij}} = \frac{\partial^+ E_t}{\partial x_i} \frac{\partial x_i}{\partial w_{ij}}$$

(46)

The two partial derivatives in equation 46 are evaluated separately. The second term reduces to:

$$\frac{\partial x_i}{\partial w_{ij}} = \frac{\partial [s(net_i)]}{\partial w_{ij}} = \frac{\partial [s(net_i)]}{\partial net_i} \frac{\partial net_i}{\partial w_{ij}} = s'(net_i)x_j$$

(47)

The first term is an ordered partial derivative. The chain rule for ordered partial derivatives is applied to it:

$$\frac{\partial^+ E_t}{\partial x_i} = \frac{\partial E_t}{\partial x_i} + \sum_{l>i} \frac{\partial^+ E_t}{\partial x_l} \frac{\partial x_l}{\partial x_i} \tag{48}$$

where

$$\frac{\partial x_l}{\partial x_i} = \frac{\partial[s(net_l)]}{\partial x_i} = \frac{\partial[s(net_l)]}{\partial net_l} \frac{\partial net_l}{\partial x_i} = s'(net_l)w_{li} \tag{49}$$

and

$$\frac{\partial E_t}{\partial x_i} = x_i - Y_{\pi - N} = \hat{Y}_{\pi - N} - Y_{\pi - N} \ , \ \forall \ N+1 \le i \le N+n \tag{50}$$

$$\frac{\partial E_t}{\partial x_i} = 0 \ , \ \forall \ 1 \le i \le N$$

The computation starts at the last output cell and proceeds in descending order until it reaches the first hidden cell. Substituting the evaluated partial derivatives into the original equation 46:

$$\frac{\partial^+ E_t}{\partial w_{ij}} = \left[x_i - Y_{pi-N} + \sum_{l>i} \frac{\partial^+ E_t}{\partial x_l} s'(net_l)w_{li} \right] s'(net_i)x_j$$
$$, \ \forall \ N+1 \le i \le N+n, j < i$$

$$\frac{\partial^+ E_t}{\partial w_{ij}} = \left[\sum_{l>i} \frac{\partial^+ E_t}{\partial x_l} s'(net_l)w_{li} \right] s'(net_i)x_j \tag{51}$$

$$, \ \forall \ 1 \le i \le N, j < i$$

For the biases:

$$\frac{\partial^+ E_t}{\partial \theta_i} = \frac{\partial^+ E_t}{\partial x_i} \frac{\partial x_i}{\partial \theta_i} \tag{52}$$

The first term is already evaluated. The second term reduces to:

$$\frac{\partial x_i}{\partial \theta_i} = \frac{\partial[s(net_i)]}{\partial \theta_i} = \frac{\partial[s(net_i)]}{\partial net_i} \frac{\partial net_i}{\partial \theta_i} \tag{53}$$

$$= s'(net_i)(-1)$$

36

Substituting the evaluated partial derivatives into equation 52:

$$\frac{\partial^+ E_t}{\partial w_{ij}} = \left[x_i - Y_{pi-N} + \sum_{l>i} \frac{\partial^+ E_t}{\partial x_l} s'(net_l) w_{li} \right] s'(net_j)(-1)$$

$$, \ \forall \ N+1 \le i \le N+n, j < i$$

$$\frac{\partial^+ E_t}{\partial w_{ij}} = \left[\sum_{l>i} \frac{\partial^+ E_t}{\partial x_l} s'(net_l) w_{li} \right] s'(net_j)(-1) \tag{54}$$

$$, \ \forall \ 1 \le i \le N, j < i$$

After the computation for each training pattern, the weights and biases are updated. Figure 46 is a flowchart of the learning process. The weights and biases are modified after each training pattern. An alternative would be to add the adjustments for all training patterns and modify the weights and biases after each learning iteration. If after a preset number of iterations the errors do not reduce, the learning rates and/or the initial values of the weights and biases need be changed, or the number of hidden cells need be increased. The learning iterations are stopped when the errors are less than a preset threshold.

REFERENCES

1. Albrecht, P. (1983). "S-N Fatigue Reliability Analysis of Highway Bridges." *Probabilistic Fracture Mechanics and Fatigue Methods: Applications for Structural Design and Maintenance.* ASTM STP 798, American Society for Testing and Materials, pp. 184-204.

2. *Guide Specifications for Fatigue Design of Steel Bridges* (1989). American Association of State Highway and Transportation Officials, Washington, D.C.

3. *Standard Specifications for Highway Bridges* (1989). American Association of State Highway and Transportation Officials, Washington, D.C.

4. Snyder, R.E., Likins, G.E., and Moses, F. (1985). "Loading Spectrum Experienced by Bridge Structures in the United States." Report *FHWA/RD-85/012*, Federal Highway Administration, McLean, Virginia.

5. Daniels, J.H., Wilson, J.W., Yen, B.T., Lai, L.Y., and Abbaszadeh, R. (1987). "Weigh-In-Motion and Response Study of Four Inservice Bridges." Report *FHWA/RD-86/045*, Federal Highway Administration, McLean, Virginia.

6. Elnahal, M.K., Albrecht, P., and Cayes, L.R. (1989). "Influence Surfaces and Distribution Factors for Reactions and Moments in Two-Span Continuous Composite Steel Girder Bridge." Federal Highway Administration, McLean, Virginia.

7. Nutt, R.V., Zokaie, T. and Schamber, R. A. (1987). "Distribution of Wheel Loads on Highway Bridges." Report *NCHRP 12-26*, Transportation Research Board, National Research Council, Washington, D.C..

8. Shaaban, H. and Albrecht, P. (1985). "Collection and Analysis of Stress Range Histograms Recorded on Highway Bridges." Civil Engineering Report, University of Maryland, College Park.

9. Lai, L.Y. (1988). "Traffic Induced Stress Range Cycles in Bridge Main Members." Ph.D. Dissertation, Lehigh University, Bethlehem, Pennsylvania.

10. *Ontario Highway Bridge Design Code* (1983). Ministry of Transportation, Downsview, Ontario, Canada.

11. Daniels, J.H., Wilson, J.W., Lai, L.Y., Abbaszadeh, R., and Yen, B.T. (1986a). "Weigh-In-Motion and Response System Overview." Report *FHWA/RD-86/046*, Federal Highway Administration, McLean, Virginia.

12. Wilson, J.W., Daniels, J.H., and Abbaszadeh, R. (1986a). "Weigh-In-Motion and Response Training Guide." Report *FHWA/RD-86/047*, Federal Highway Administration, McLean, Virginia.

13. Wilson, J.W., Abbaszadeh, R., Lai, L.Y., and Daniels, J.H. (1986b). "Weigh-In-Motion and Response User's Guide." Report *FHWA/RD-86/048*, Federal Highway Administration, McLean, Virginia.

14. Wilson, J.W., Daniels, J.H., Lai, L.Y., and Abbaszadeh, R. (1986c). "Weigh-In-Motion and Response Hardware." Report *FHWA/RD-86/049*, Federal Highway Administration, McLean, Virginia.

15. Wilson, J.W., Lai, L.Y., Abbaszadeh, R., and Daniels, J.H. (1986d). "Weigh-In-Motion and Response Software Reference Manual." Report *FHWA/RD-86/050*, Federal Highway Administration, McLean, Virginia.

16. Daniels, J.H., Wilson, J.W., Lai, L.Y., Abbaszadeh, R., and Yen, B.T. (1986b). "Weigh-In-Motion and Response Study of Four In-Service Bridges: Executive Summary." Report *FHWA/RD-86/065*, Federal Highway Administration, McLean, Virginia.

17. Moses, F. and Kriss M. (1978). "Weigh-In-Motion Instrumentation." Report *FHWA/Rd-78/81*, Federal Highway Administration, McLean, Virginia.

18. Moses, F. and Ghosn, M. (1983). "Instrumentation for Weighing Trucks-In-Motion for Highway Bridge Loads." Report *FHWA/OH-83/001*, Federal Highway Administration, McLean, Virginia.

19. Goble, G.G., Schulz, J.X., Commander, B.C., Burgess, C.U., Dow, J.O., and Frangopol, D.M. (1991a). "Load Prediction and Structural Response: Volume I. Draft of Final Report.", Federal Highway Administration, McLean, Virginia.

20. Goble, G.G., Schulz, J.X., Commander, B.C., Burgess, C.U., Dow, J.O., and Frangopol, D.M. (1991b). "Load Prediction and Structural Response: Volume II. Draft of Final Report.", Federal Highway Administration, McLean, Virginia.

21. Fuchs, H.O. and Stephens, R.I. (1980). *Metal Fatigue in Engineering*. John Wiley & Sons, New-York, New-York, pp. 196-203.

22. *Guide Specifications for Fatigue Evaluation of Existing Steel Bridges* (1989). American Association of State Highway and Transportation Officials, Washington, D.C.

23. Seifert, P. (1990). " Fatigue Loading and Design for Road Bridges." Ph.D. Dissertation, Technische Hochschule Darmstadt, Germany.

24. Yamada, K. and Albrecht, P. (1977). "Fatigue Behavior of Two Flange Details." Journal of the Structural Division, ASCE, Vol. 103, No. ST4, pp. 781-791.

25. Sankoff D. and Kruskal J.B. (1983). *Time Warps, String Edits, and Macromolecules: The Theory and Practice of Sequence Comparison*. Addison-Wesley Publishing Company, Inc., London, England.

26. Levinson, S.E. (1985). "Structural Methods in Automatic Speech Recognition." Proceedings of the IEEE, Vol. 73, No. 11, pp. 1625-1650.

27. Poritz, A.B. (1988). "Hidden Markov Models: A Guided Tour." Institute for Defense Analyses, Communications Research Division, Princeton, New-Jersey.

28. Lippmann, R.P. (1987). "An Introduction to Computing with Neural Nets." IEEE ASSP Magazine, April, pp. 4-22.

29. Rumelhart, D.E., McClellan, J.L., and PDP Research Group (1986). *Parallel Distributed Processing - Explorations in the Microstructures of Cognition Volume 1: Foundations*. The MIT Press, Cambridge, Massassuchetts.

30. Werbos, P.J. (1990). "Backpropagation Through Time: What it does and How to Do It." Proceedings of the IEEE, Vol. 78, No. 10, pp. 1550-1560.

31. Flood, I. (1991). "A Gaussian-Based FeedForward Network Architecture and Complementary Training Algorithm." Proceedings of the International Joint Conference on Neural Network Computing, Singapore.

32. Gagarine, N., Flood, I., and Albrecht, P. (1992). "Weighing trucks in motion using Gaussian-Based Neural Network," International Joint Conference on Neural Networks, Baltimore.

33. Gagarine, N. "Advances in Weigh-In-Motion with Pattern Recognition and Prediction of Fatigue Life of Highway Bridges." Ph.D. Dissertation, University of Maryland, College Park, Maryland.
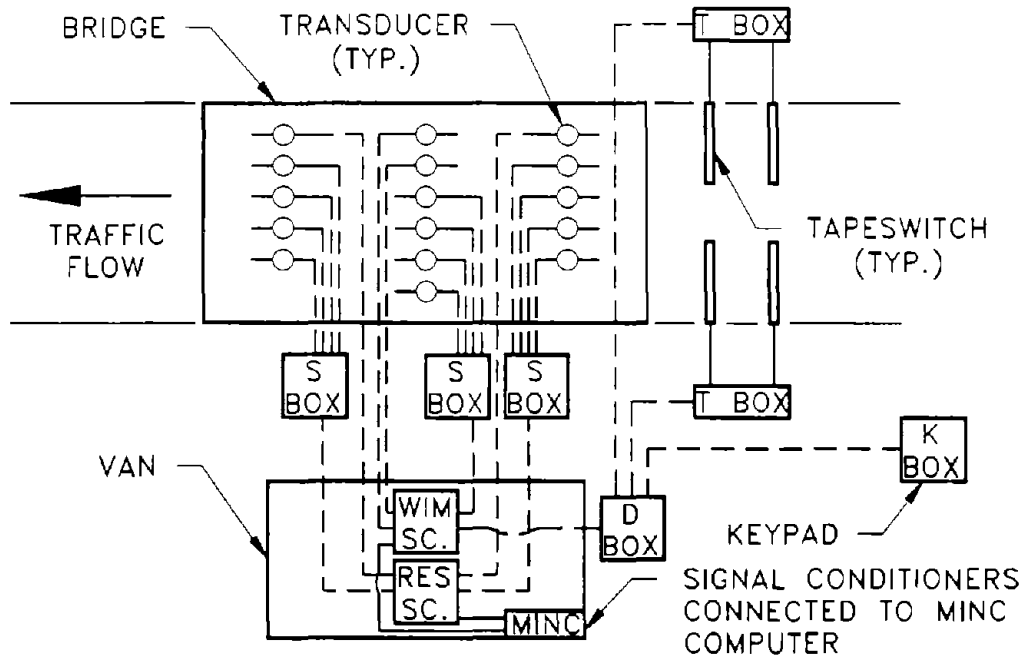
Figure 1. Set-up of WIM+R system.
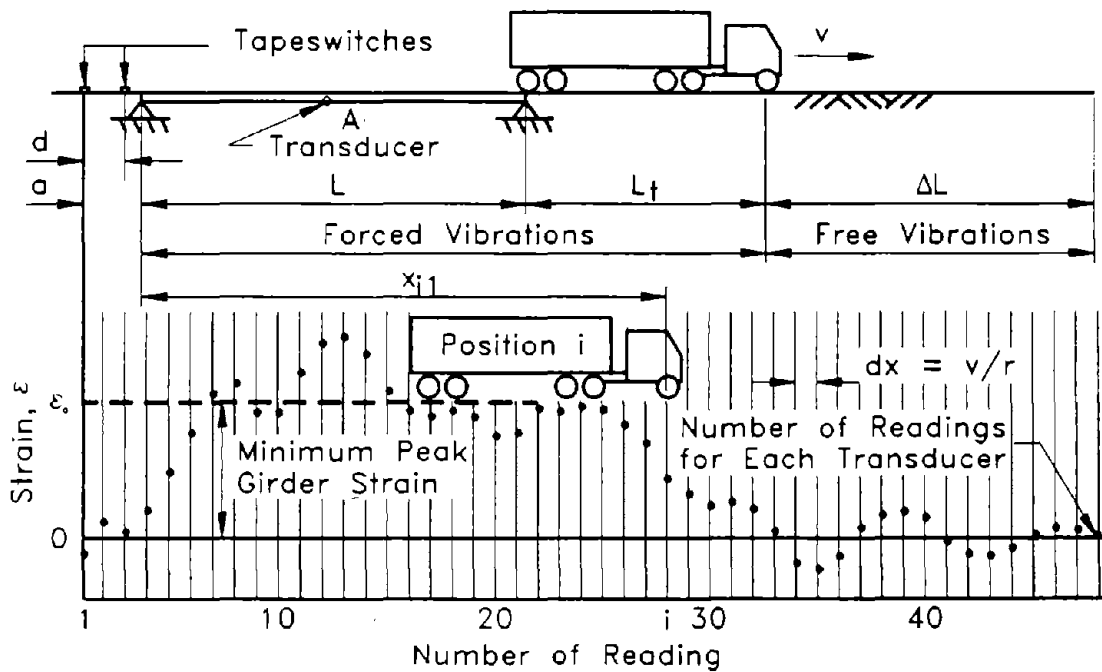
Figure 2. Graphical representation of data collection.

BRIDGE AND LOADING:
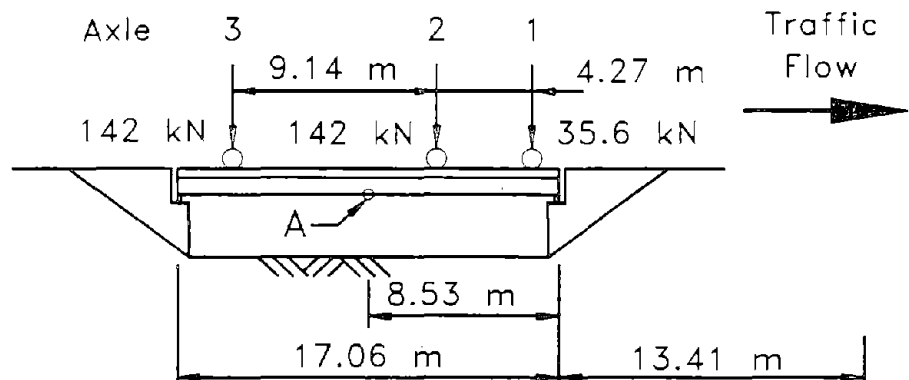
INFLUENCE LINE FOR MOMENT AT POINT "A":
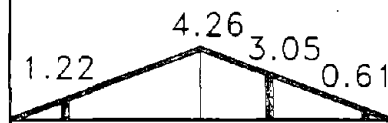
MOMENT AT "A" PLOTTED AT POSITION OF AXLE 1:
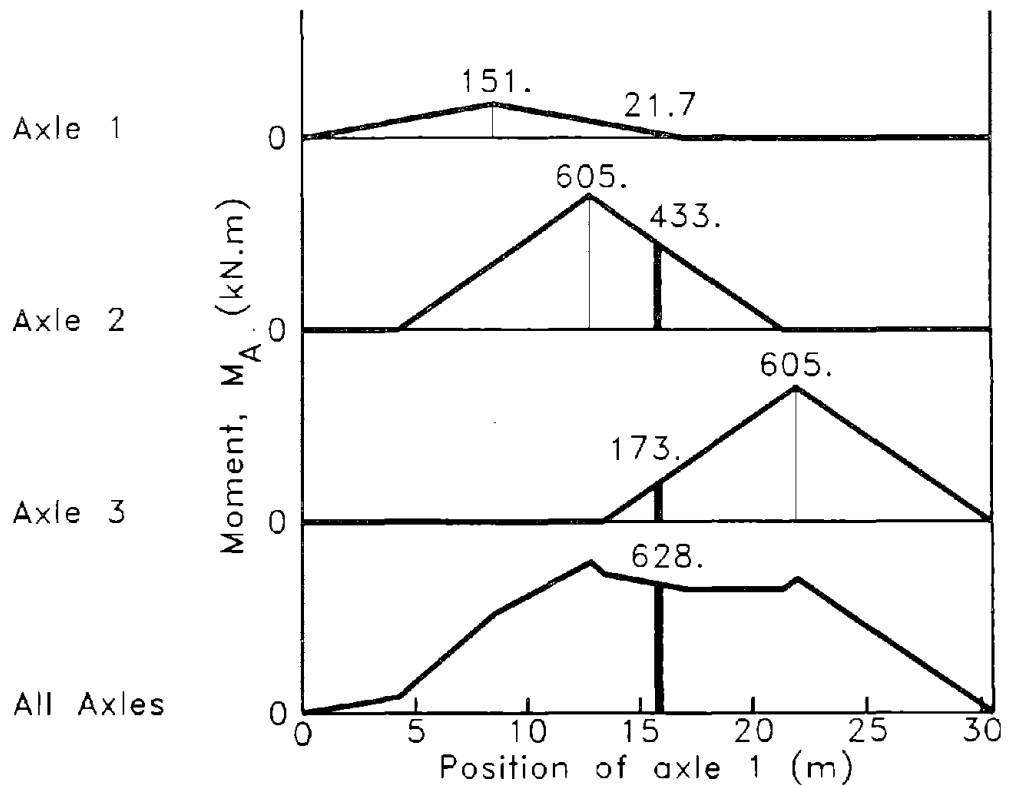
Figure 3. Use of influence line to construct plot of moment vs. position of axle 1 for one truck event. (Example: HS-20)

42
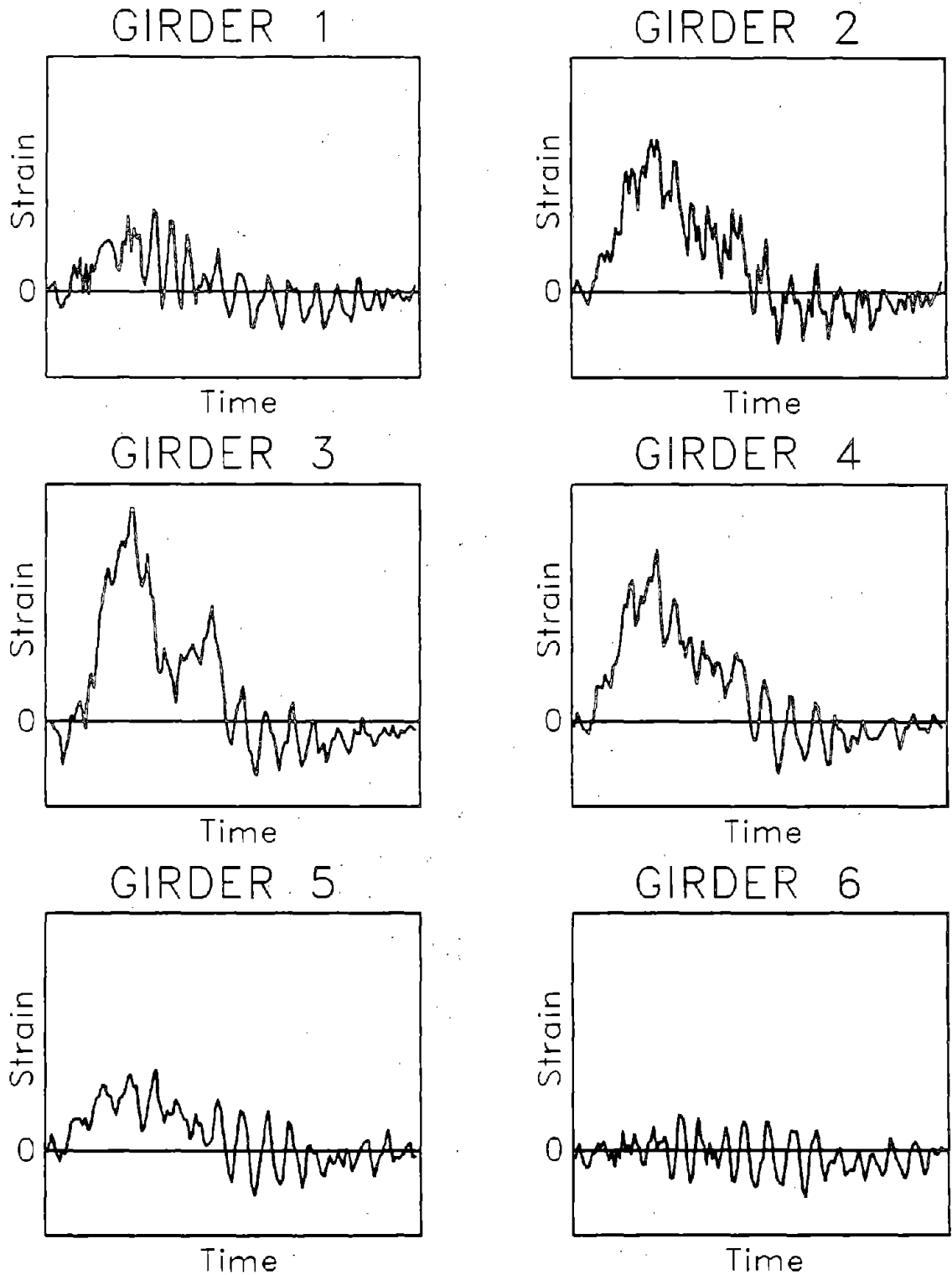
Figure 4. Example of strain output from transducer at mid-point of six girders of simple span bridge. (westbound I-66 over Bull Run)
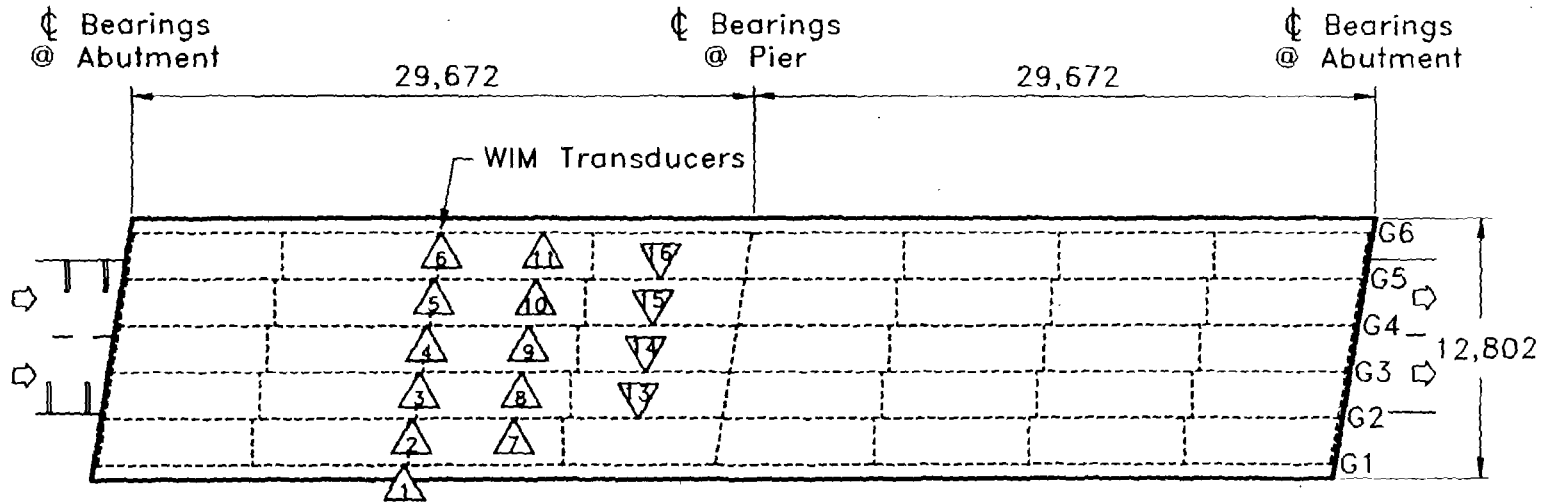
Figure 5. Plan view of instrumented span of southbound I-70 over route 340 bridge.
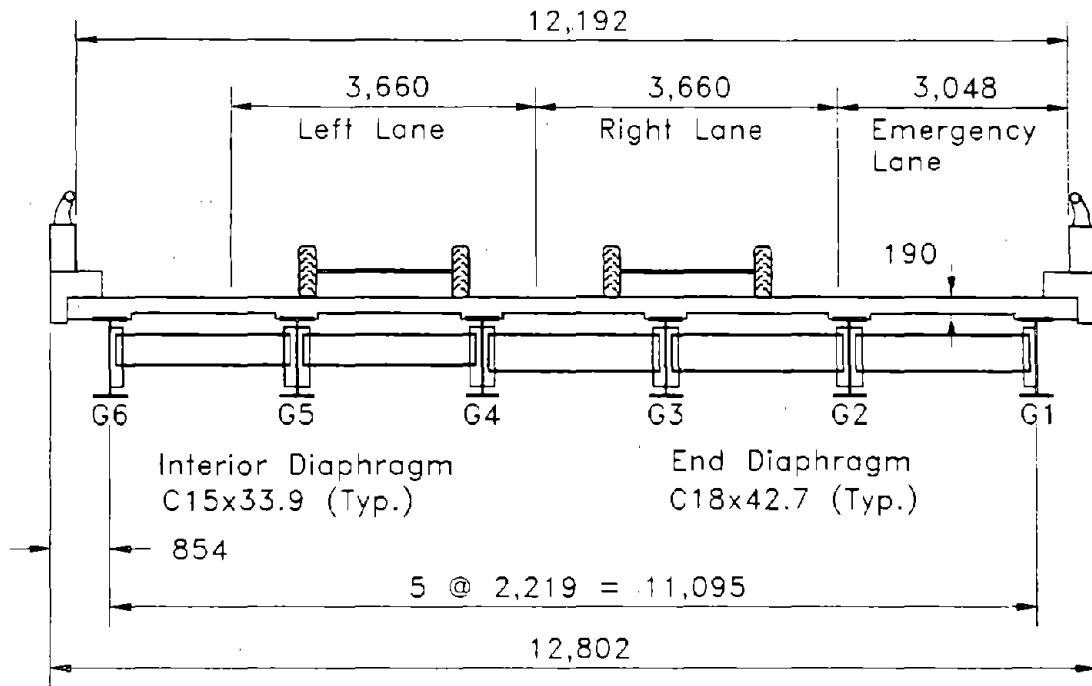
Figure 6. Cross-section of I-70 over route 340 bridge.
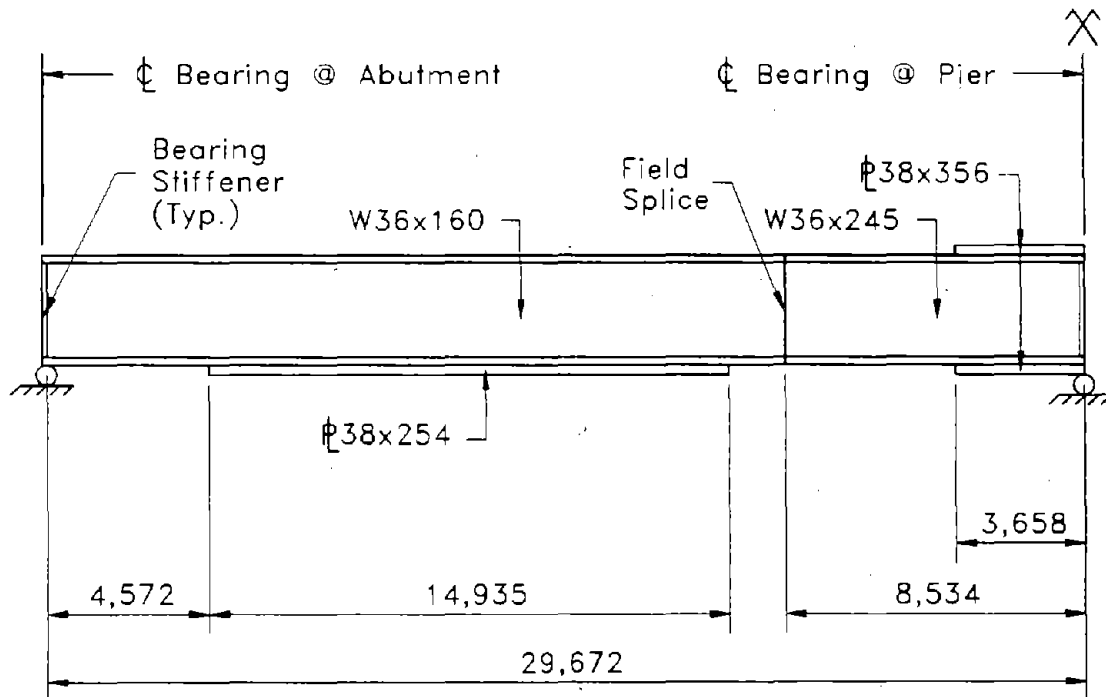
Figure 7. Girder detail of I-70 over route 340 bridge.

45
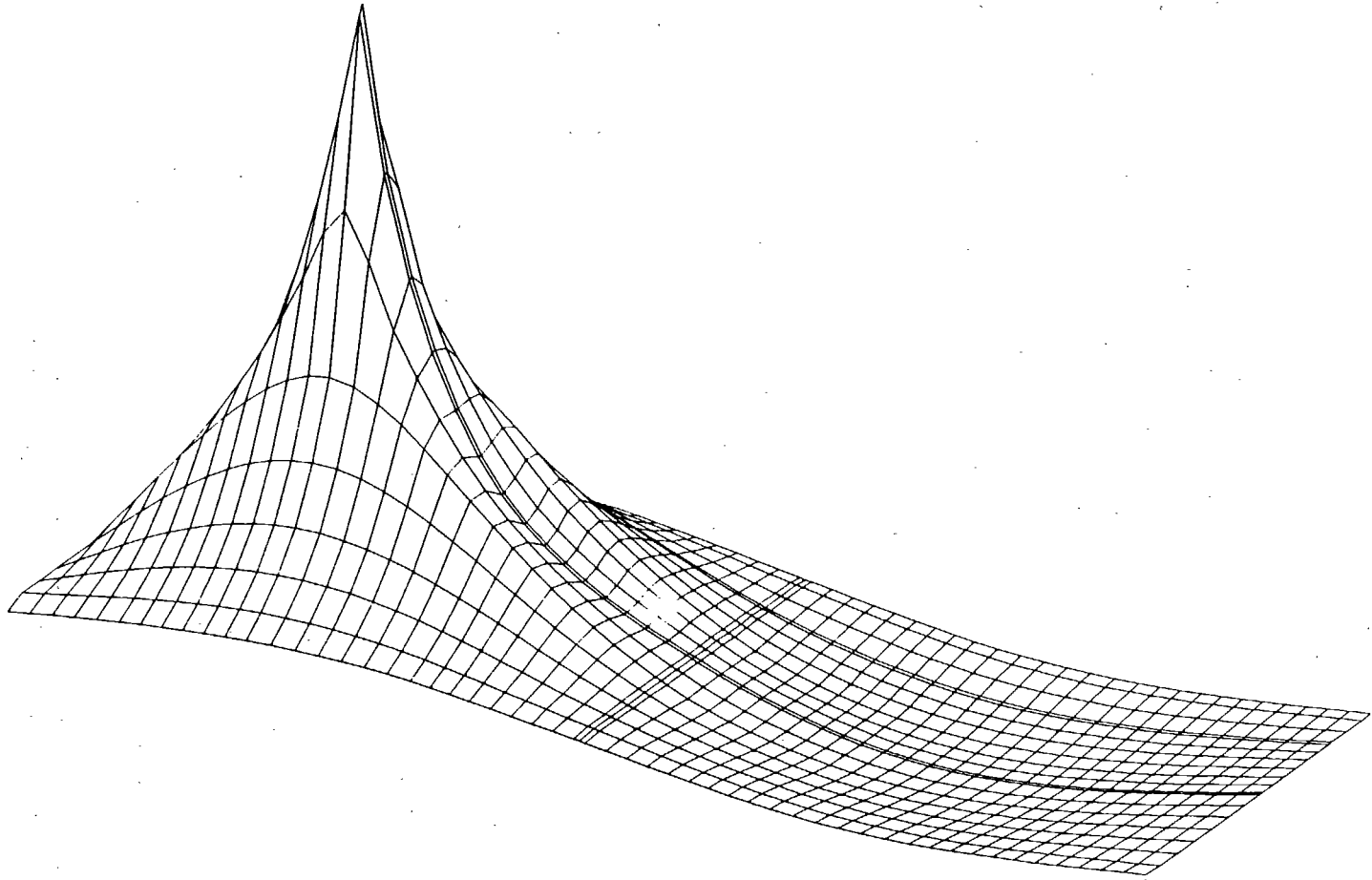
Figure 8. Influence surface for longitudinal bending moment at
0.4L on center girder of a two-span continuous bridge.
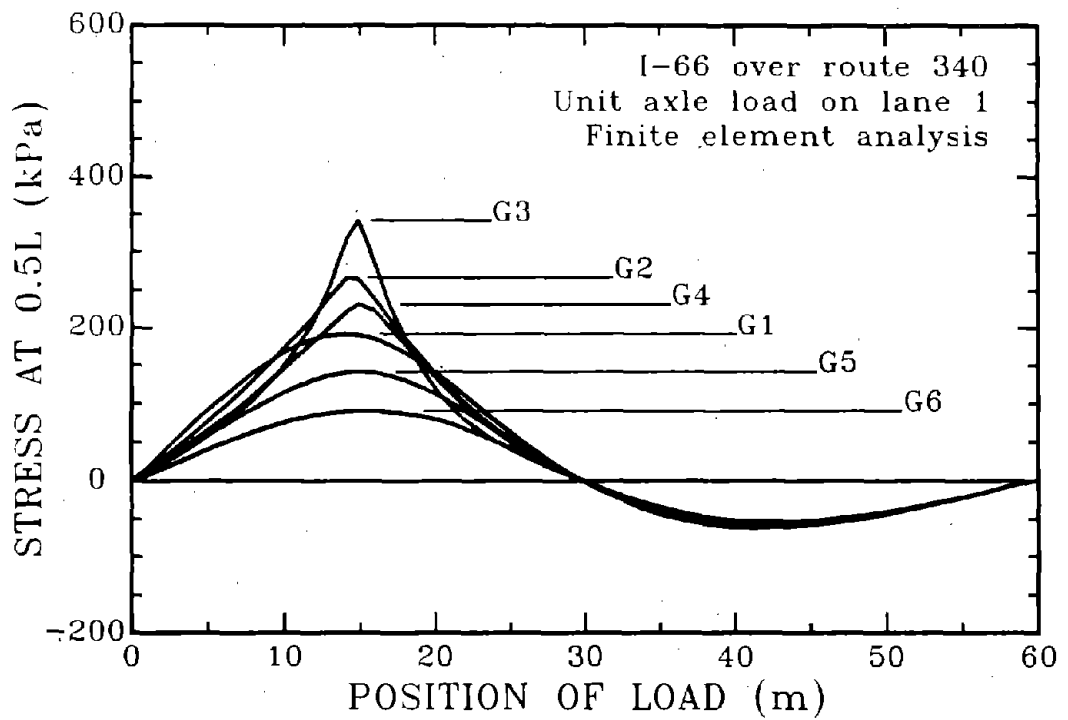
Figure 9. Influence track for longitudinal bending stress at 0.5L -- I-70
over route 340, finite element analysis, bottom flange, lane 1.
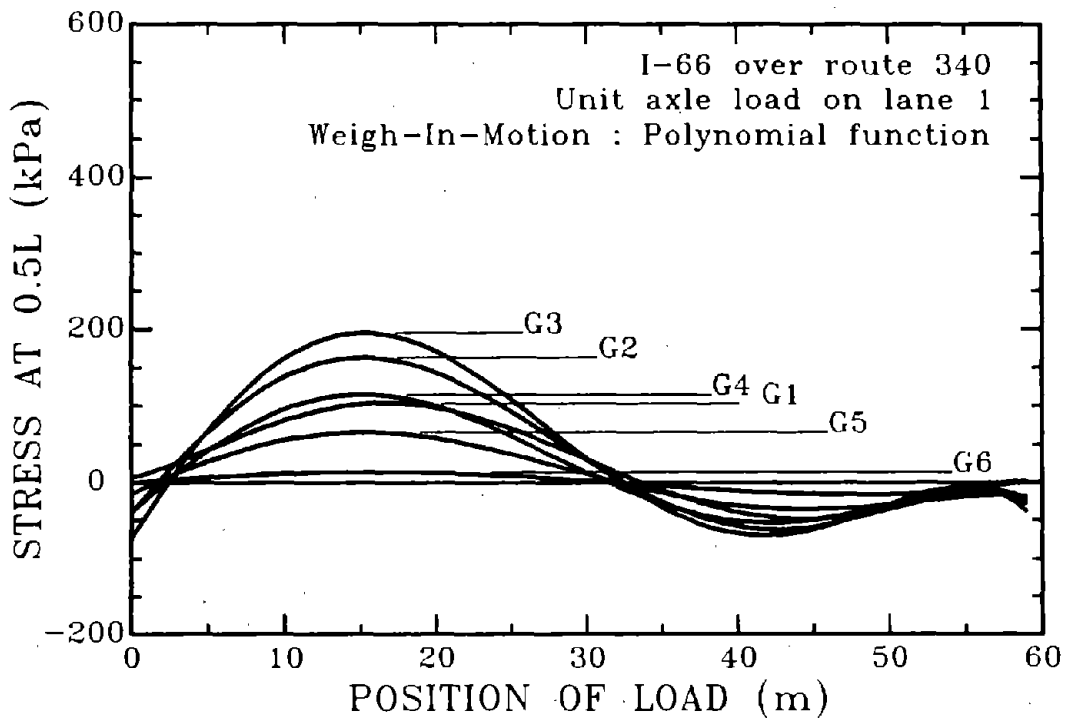
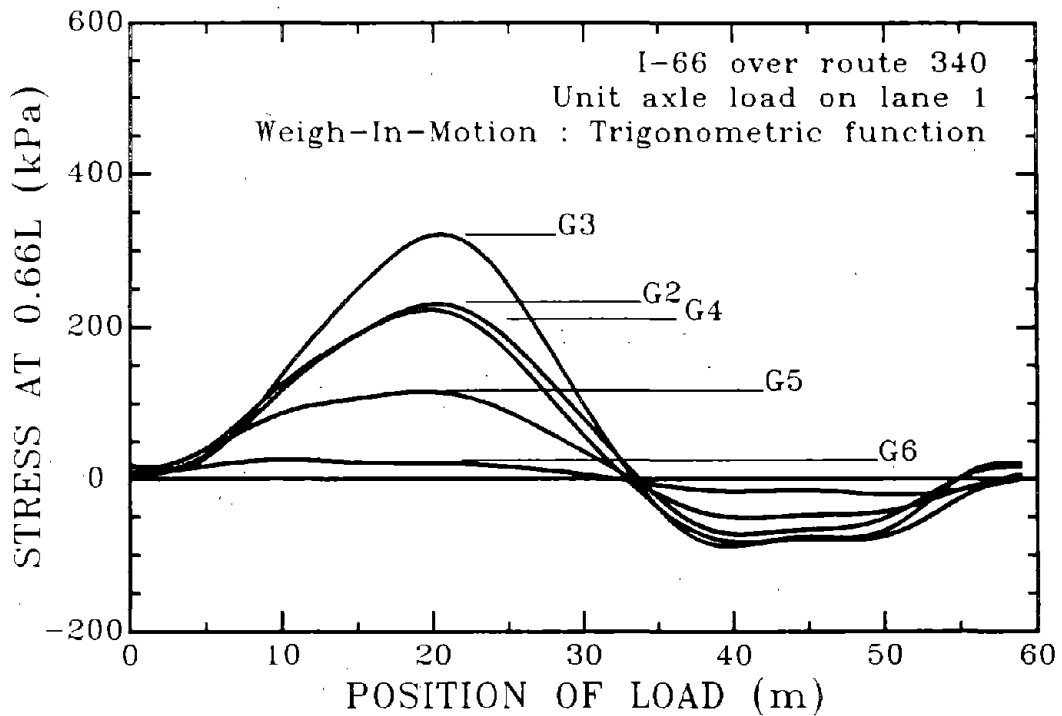Figure 10. Influence track for longitudinal bending stress at 0.5L -- I-70
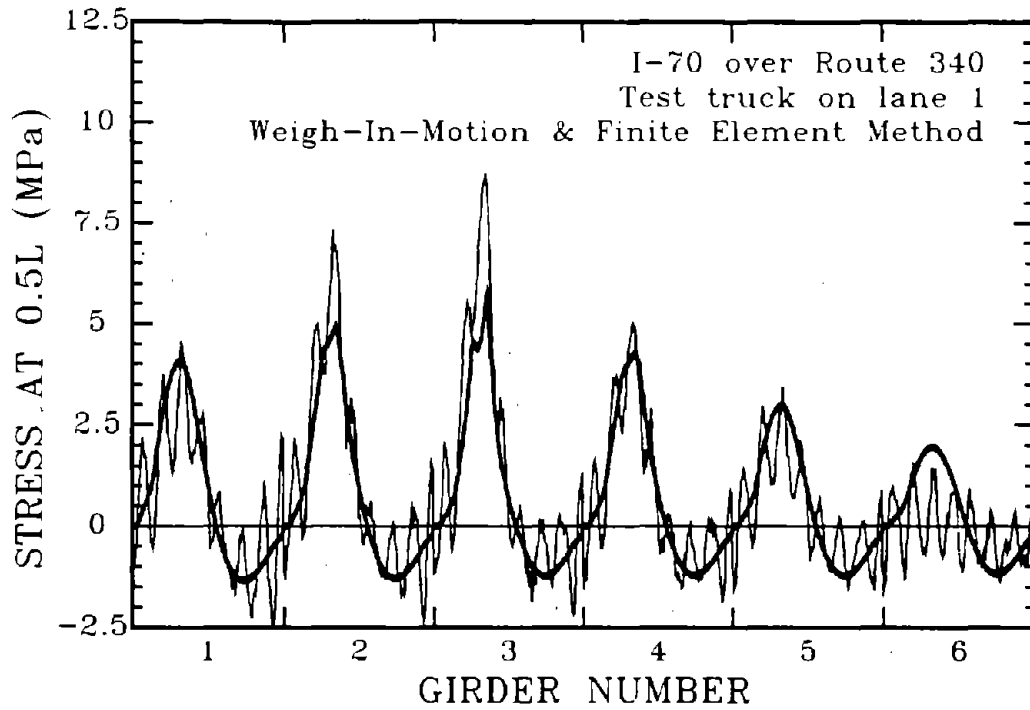over route 340, polynomial function, bottom flange, lane 1.
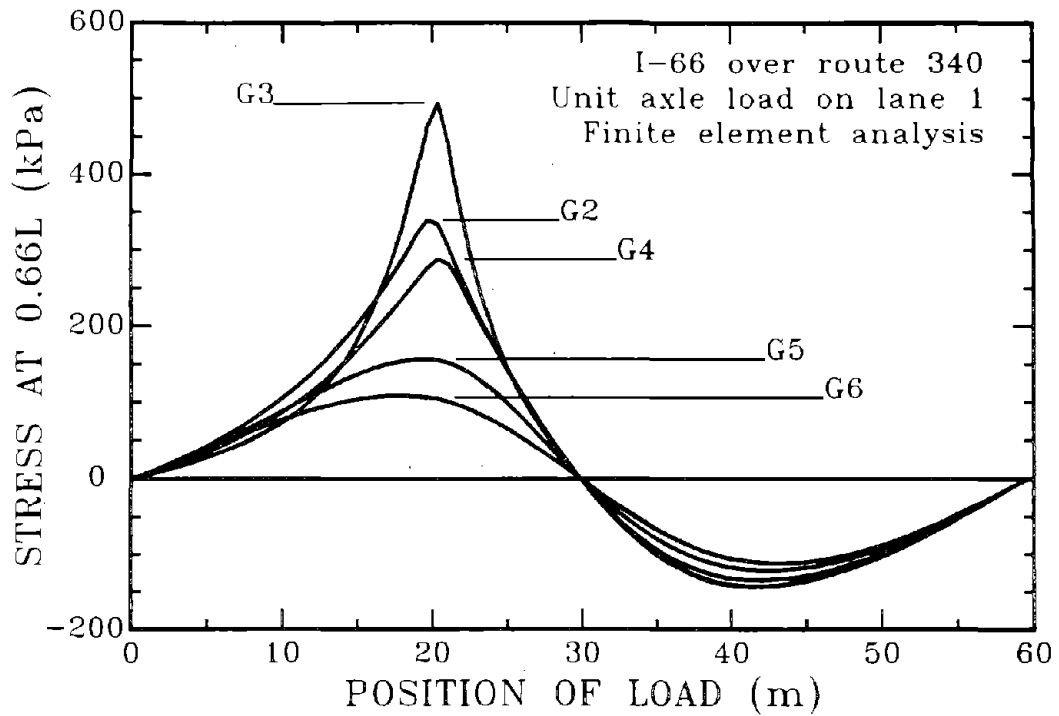
Figure 11. Influence track for longitudinal bending stress at 0.66L -- I-70
over route 340, finite element analysis, bottom flange, lane 1.

Figure 12. Influence track for longitudinal bending stress at 0.66L -- I-70
over route 340, polynomial function, bottom flange, lane 1.

Figure 13. Side-by-side plots of stress at midspan in girders 1
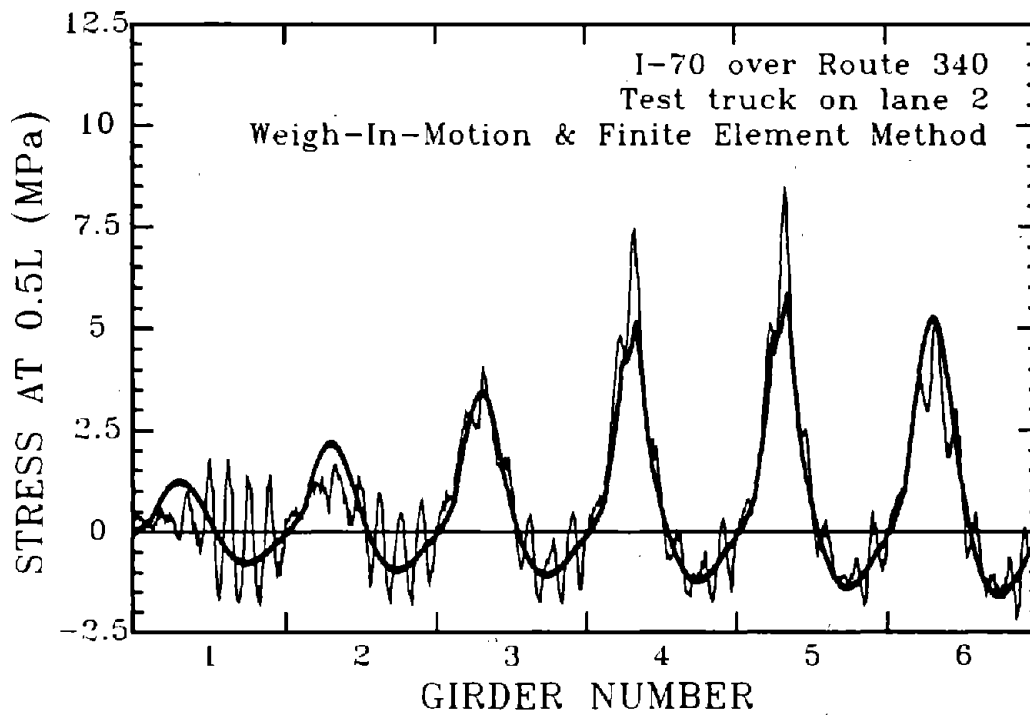through 6 -- I-70 over route 340, WIM and FEM, lane 1.

Figure 14. Side-by-side plots of stress at mid-span in girders 1
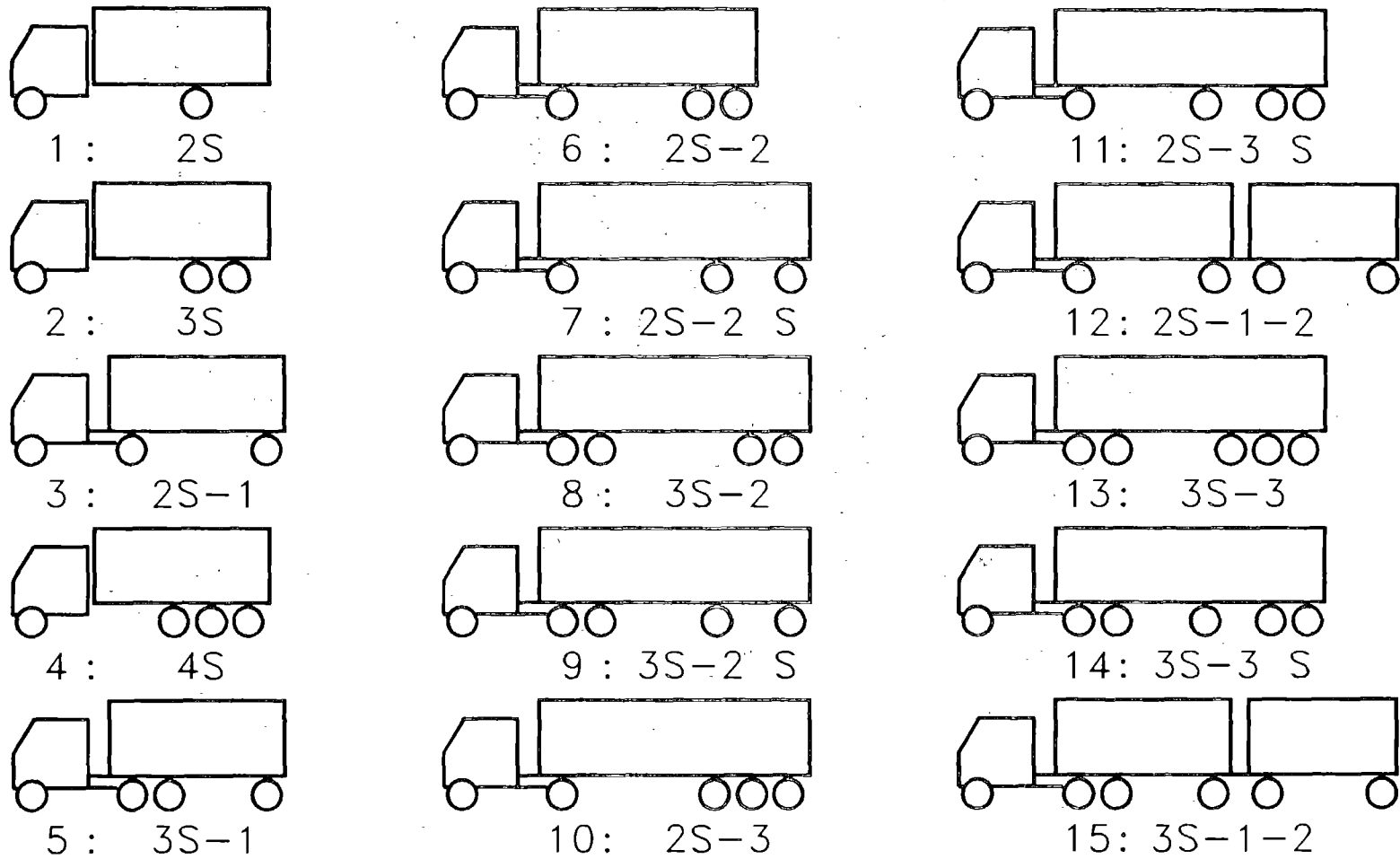through 6 -- I-70 over route 340, WIM and FEM, lane 2.

49

1 :   2S
2 :   3S
3 :   2S-1
4 :   4S
5 :   3S-1
6 :   2S-2
7 :   2S-2 S
8 :   3S-2
9 :   3S-2 S
10 :   2S-3
11:    2S-3 S
12:    2S-1-2
13:    3S-3
14:    3S-3 S
15:    3S-1-2

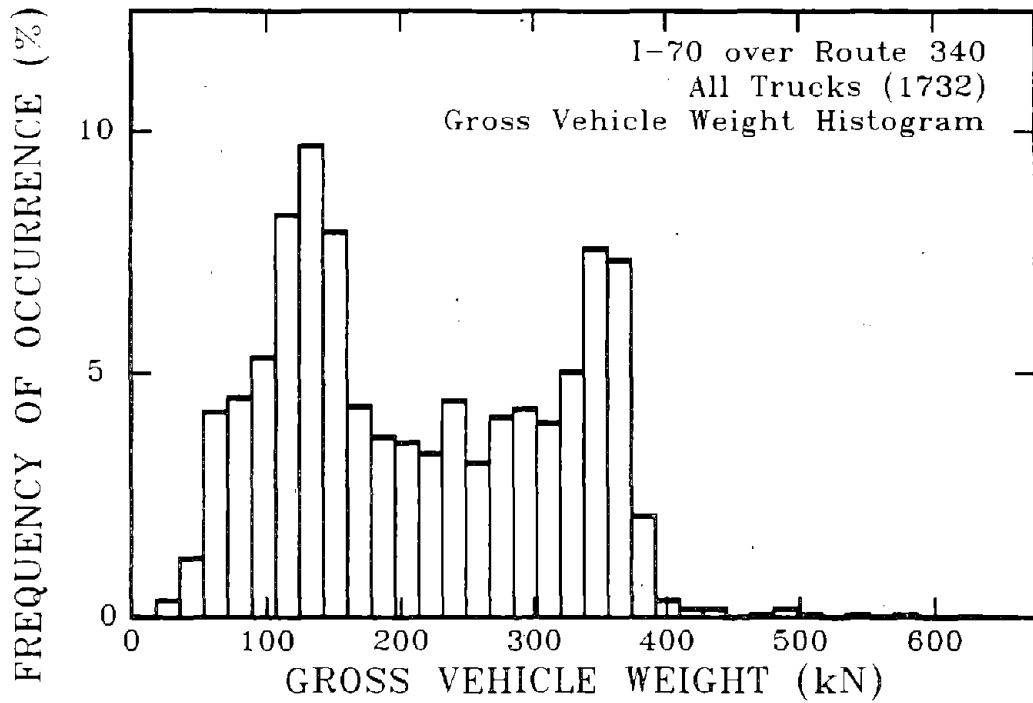Figure 15. Classification of trucks for WIM study.

Figure 16. GVW histogram for all trucks crossing
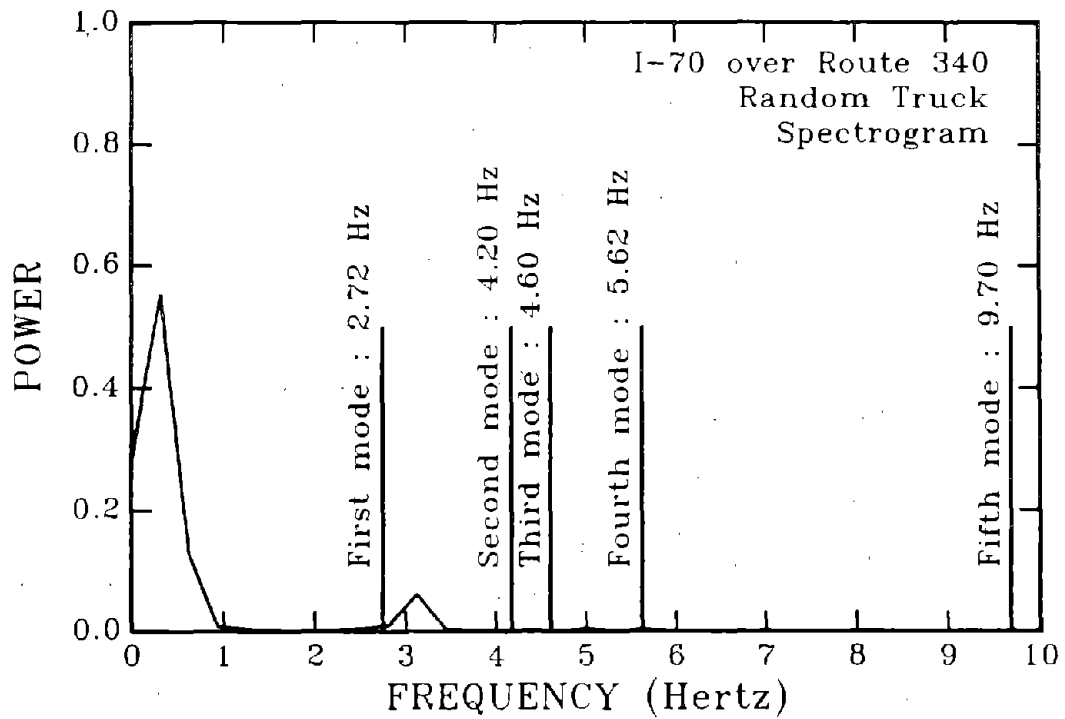I-70 over route 340 bridge.

Figure 17. Comparison of spectrogram of measured stress data for random truck event
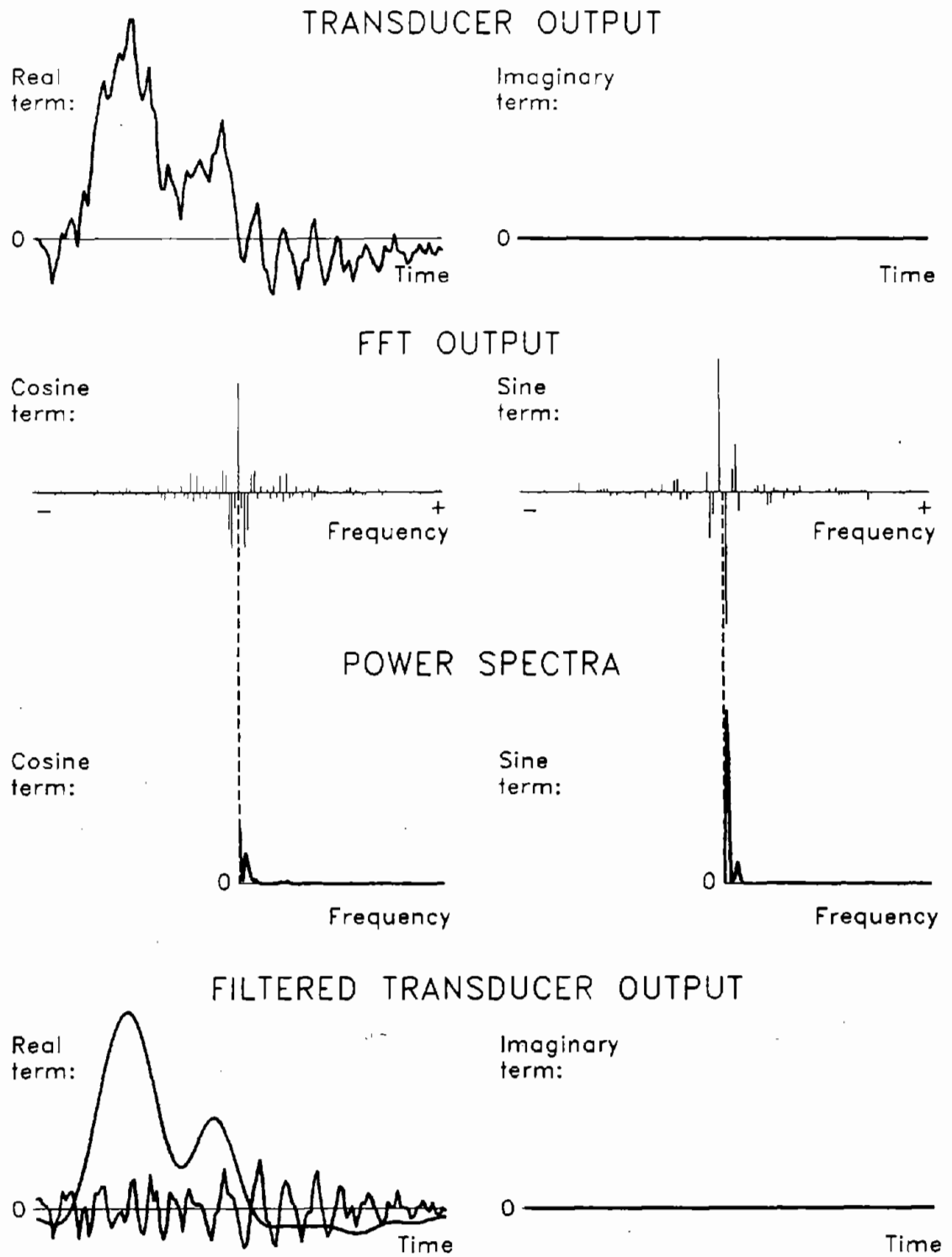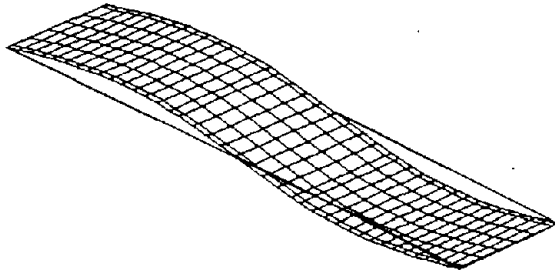with natural frequencies calculated with FEM -- I-70 over route 340 bridge.
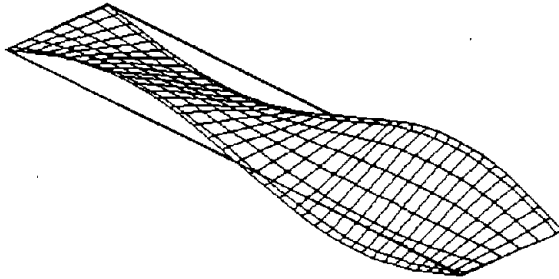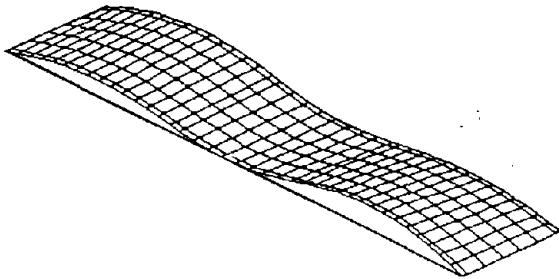
Figure 18. Low-pass filtering using discrete Fourier transforms.

First mode: f_1 = 2.72 Hz

Second mode: f_2 = 4.20 Hz

Third mode: f_3 = 4.60 Hz
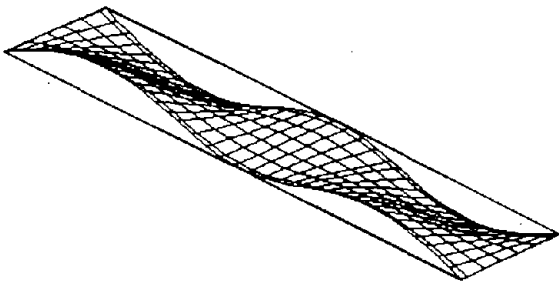
Fourth mode: f_4 = 5.62 Hz
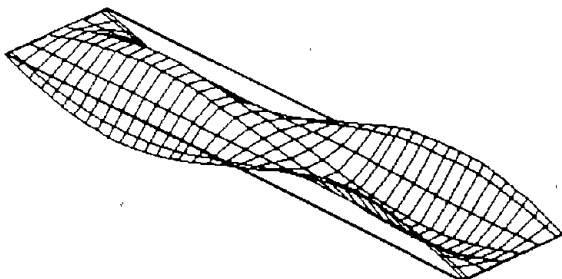
Fifth mode: f_5 = 9.70 Hz

Figure 19. Modal shapes of I-70 over route 340 bridge, five lowest natural frequencies.
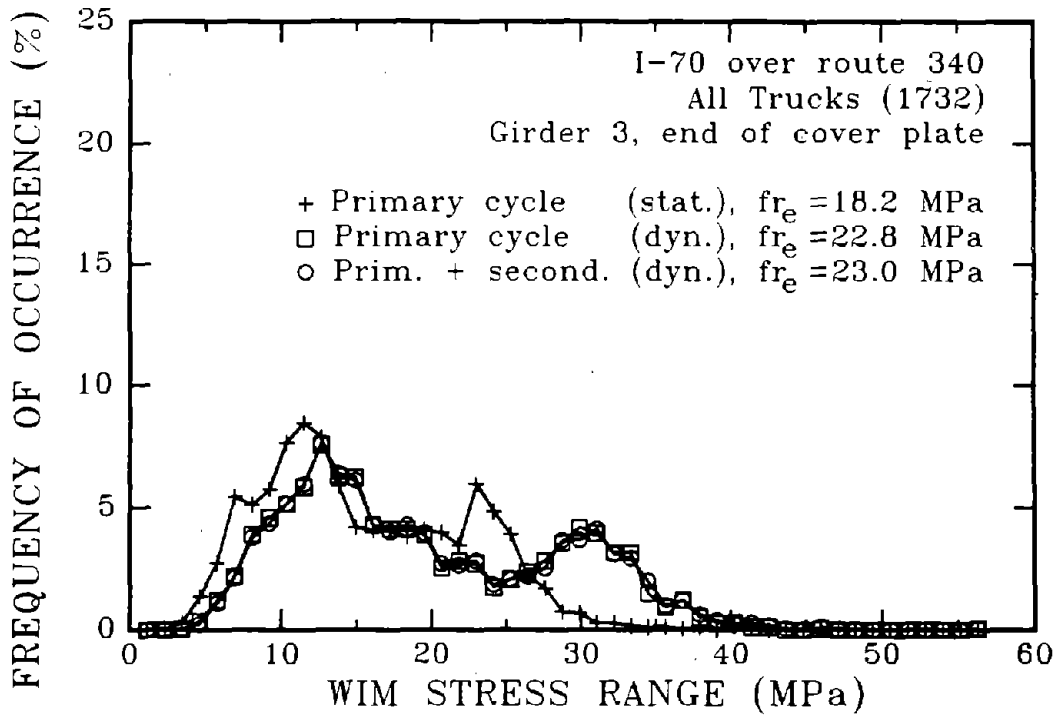
Figure 20. WIM stress range histograms, including dynamic effects and secondary cycles -- I-70 over route 340 bridge, girder 3, end of cover plate.
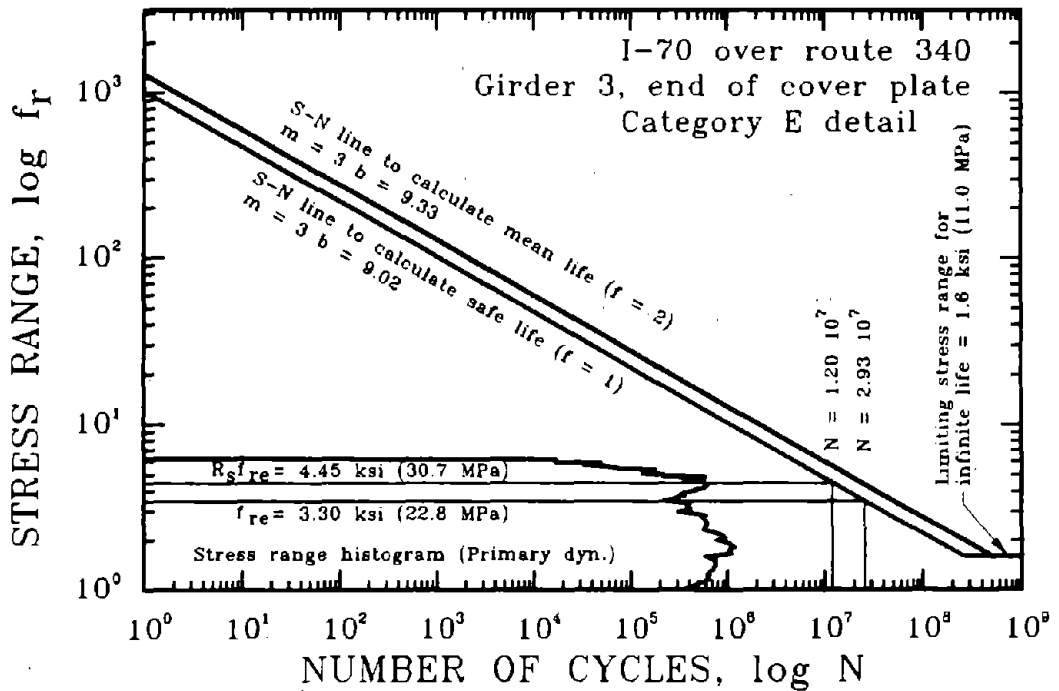
Figure 21. Illustration of fatigue calculation based on AASHTO Guide Specifications -- I-70 over route 340 bridge.
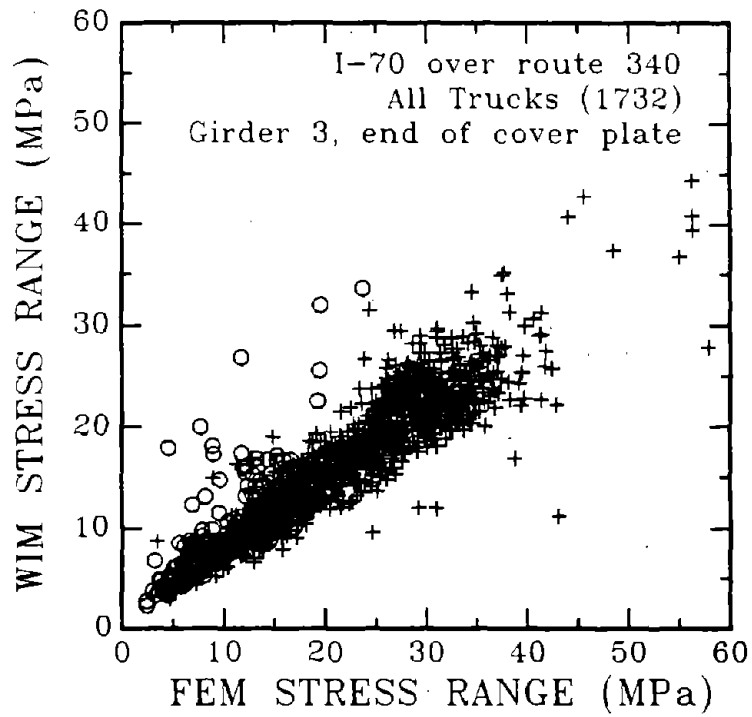
Figure 22. Comparison of stress ranges obtained from WIM data and FEM analysis -- I-70 over route 340 bridge, girder 3, end of cover plate.
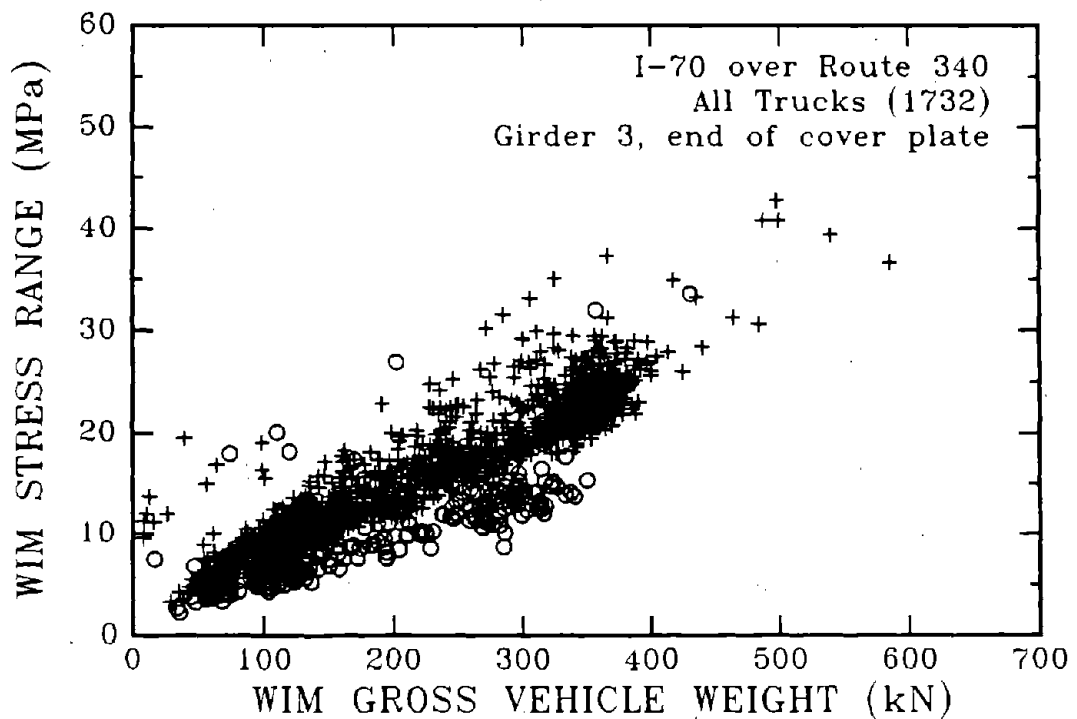
Figure 23. Comparison of GVW and stress ranges obtained from WIM data -- I-70 over route 340 bridge, girder 3, end of cover plate.
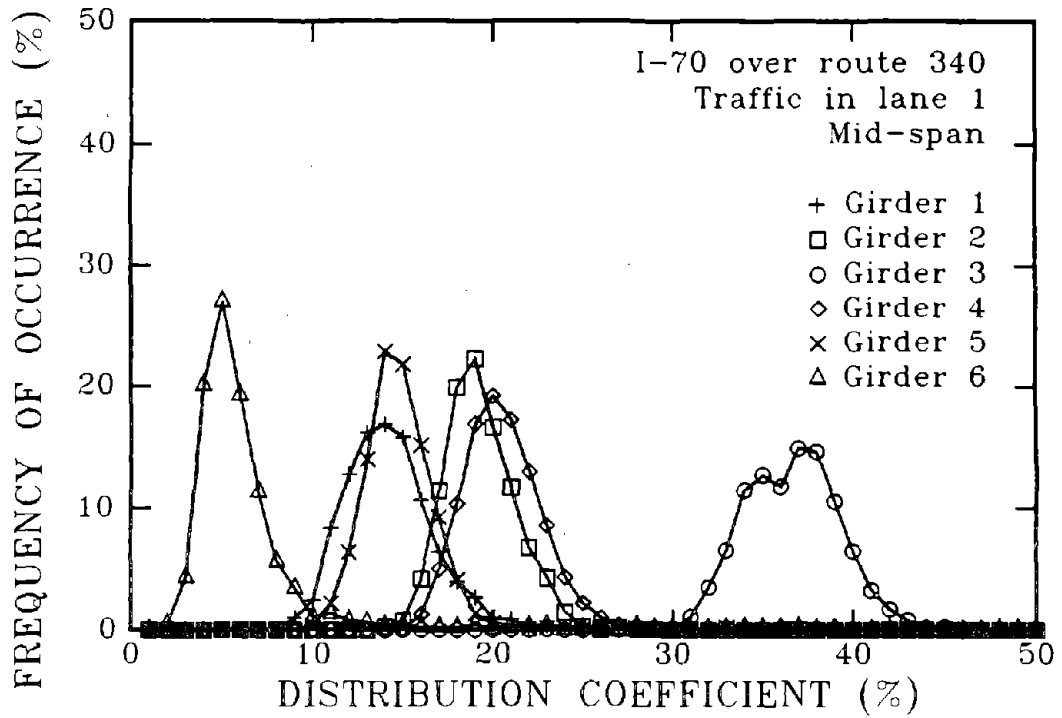
Figure 24. Distribution coefficients for traffic in lane 1 -- I-70 over route 340, mid-span.
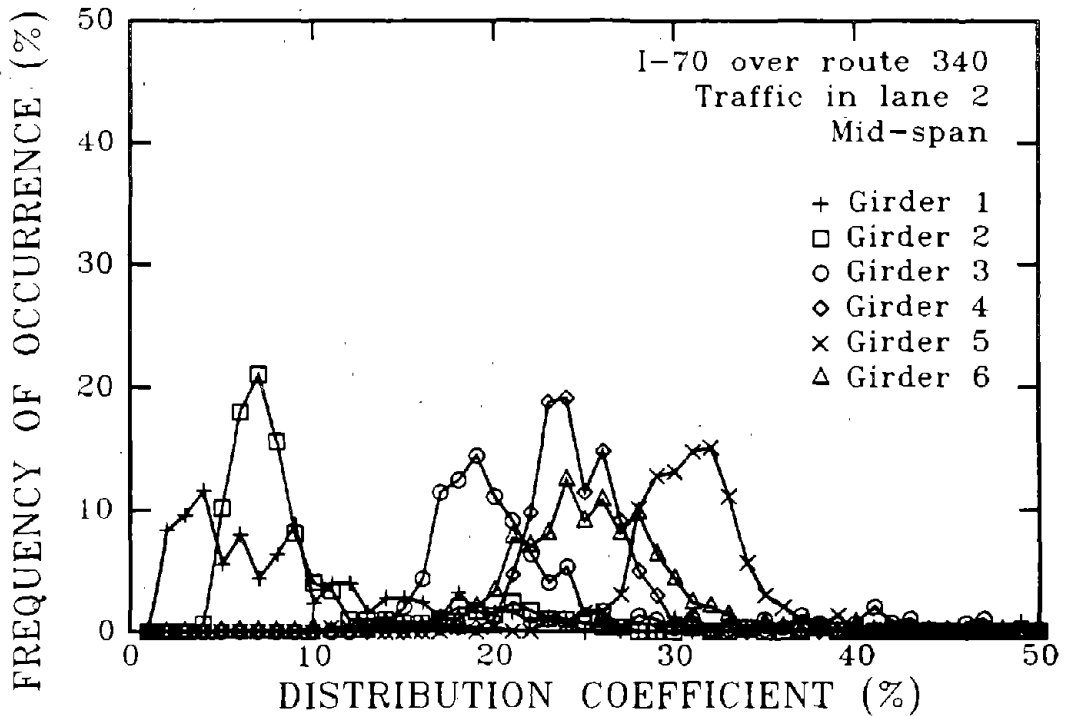
Figure 25. Distribution coefficients for traffic in lane 2 -- I-70 over route 340, mid-span.
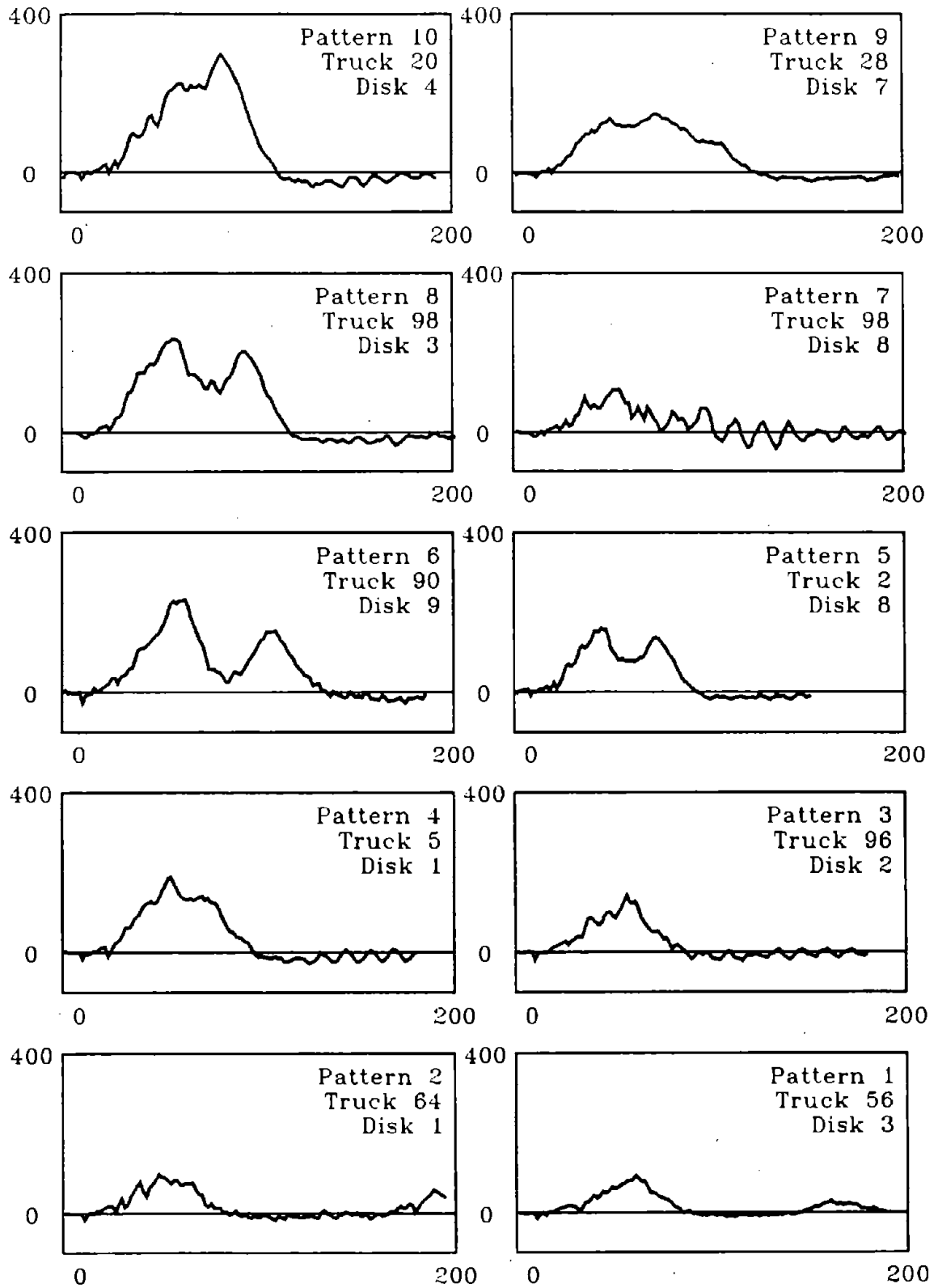
Figure 26. Stress vs. time scans for ten truck events, I-66 over
Bull Run bridge, trucks on lane 1, channel 3.

57
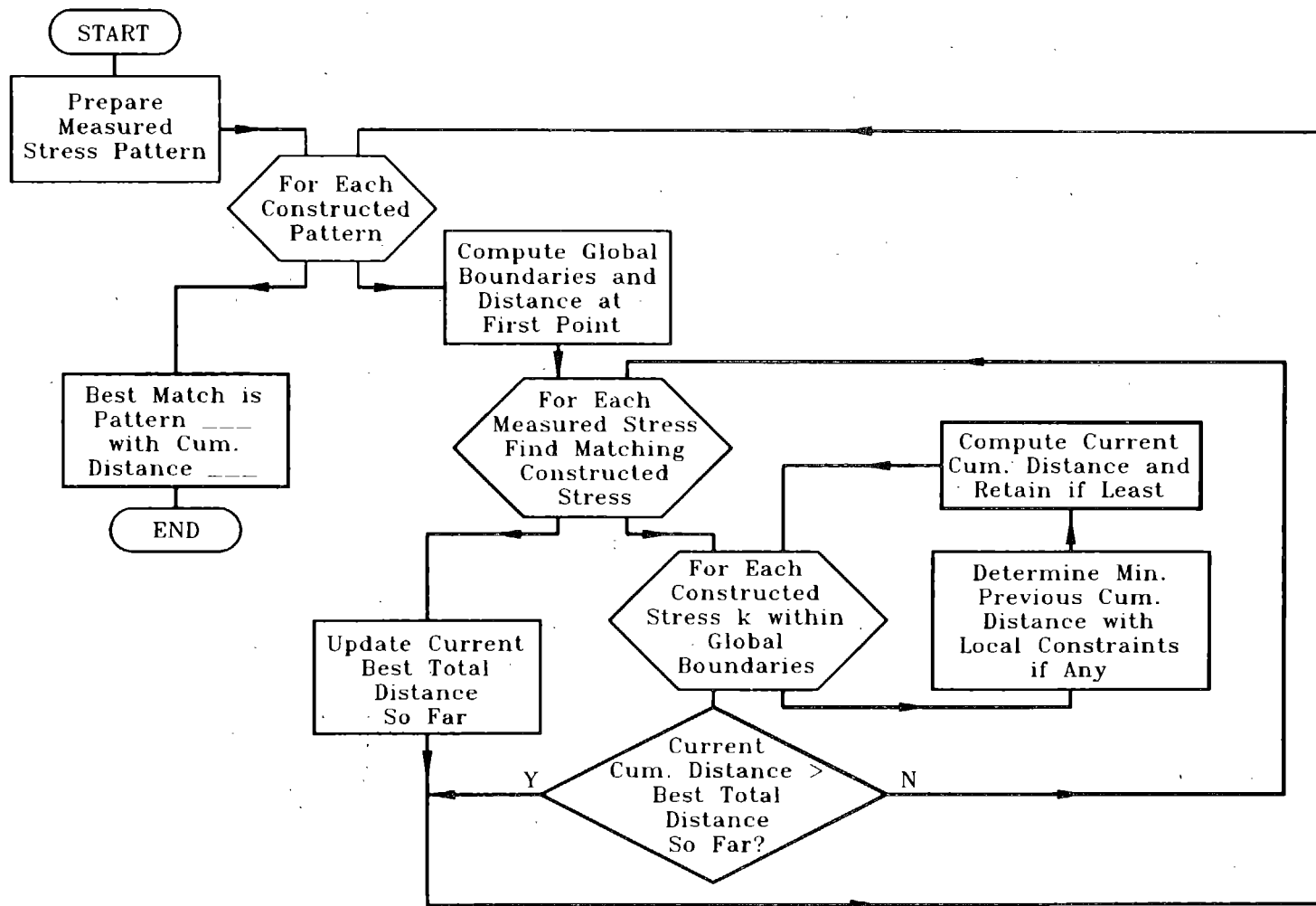
Figure 27. Flowchart for dynamic time warping analysis of WIM data.
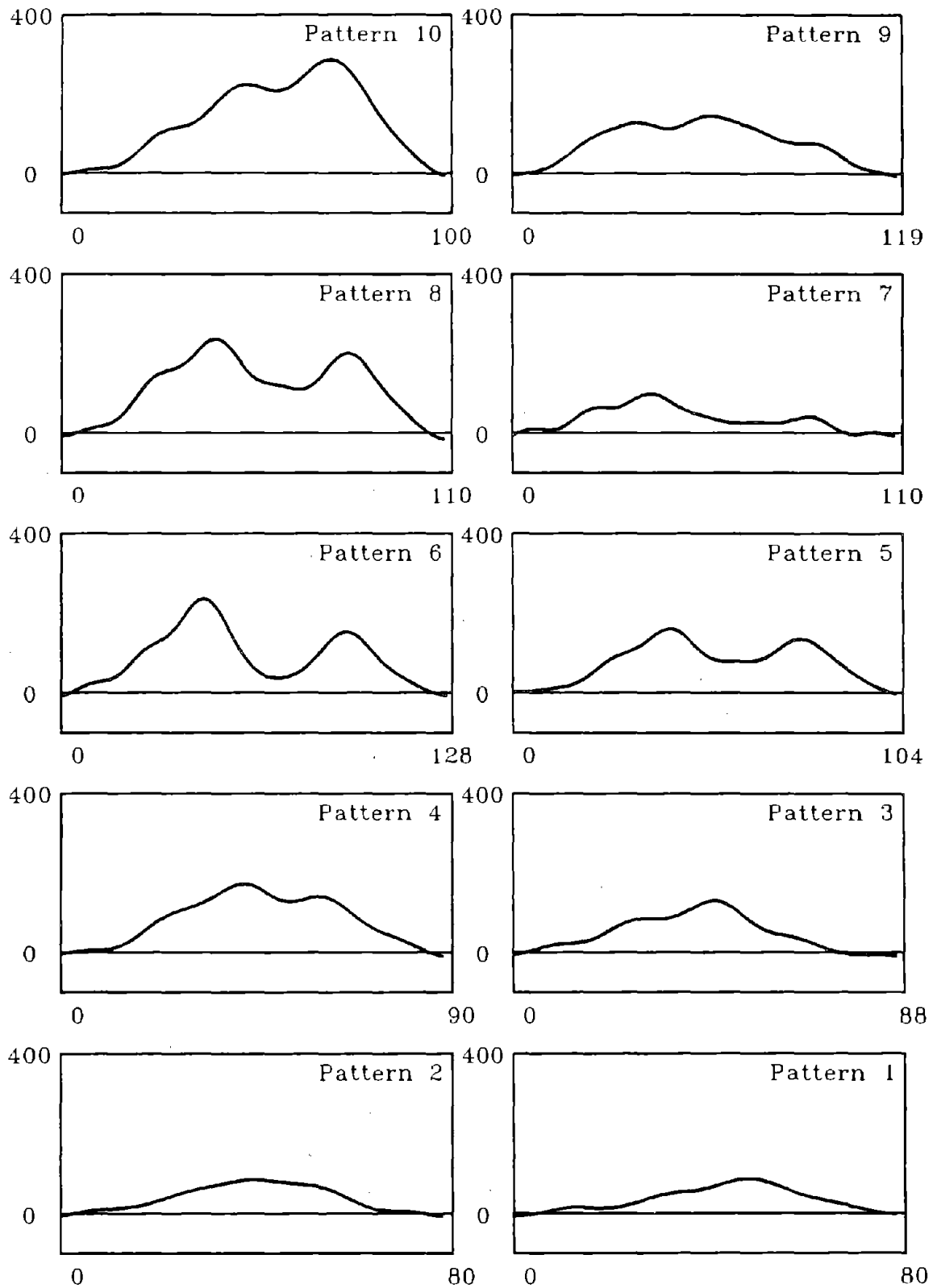
Figure 28. Measured and filtered stresses (Kip/ft^2) vs. scan number, from entry to exit of truck, channel 3.

59
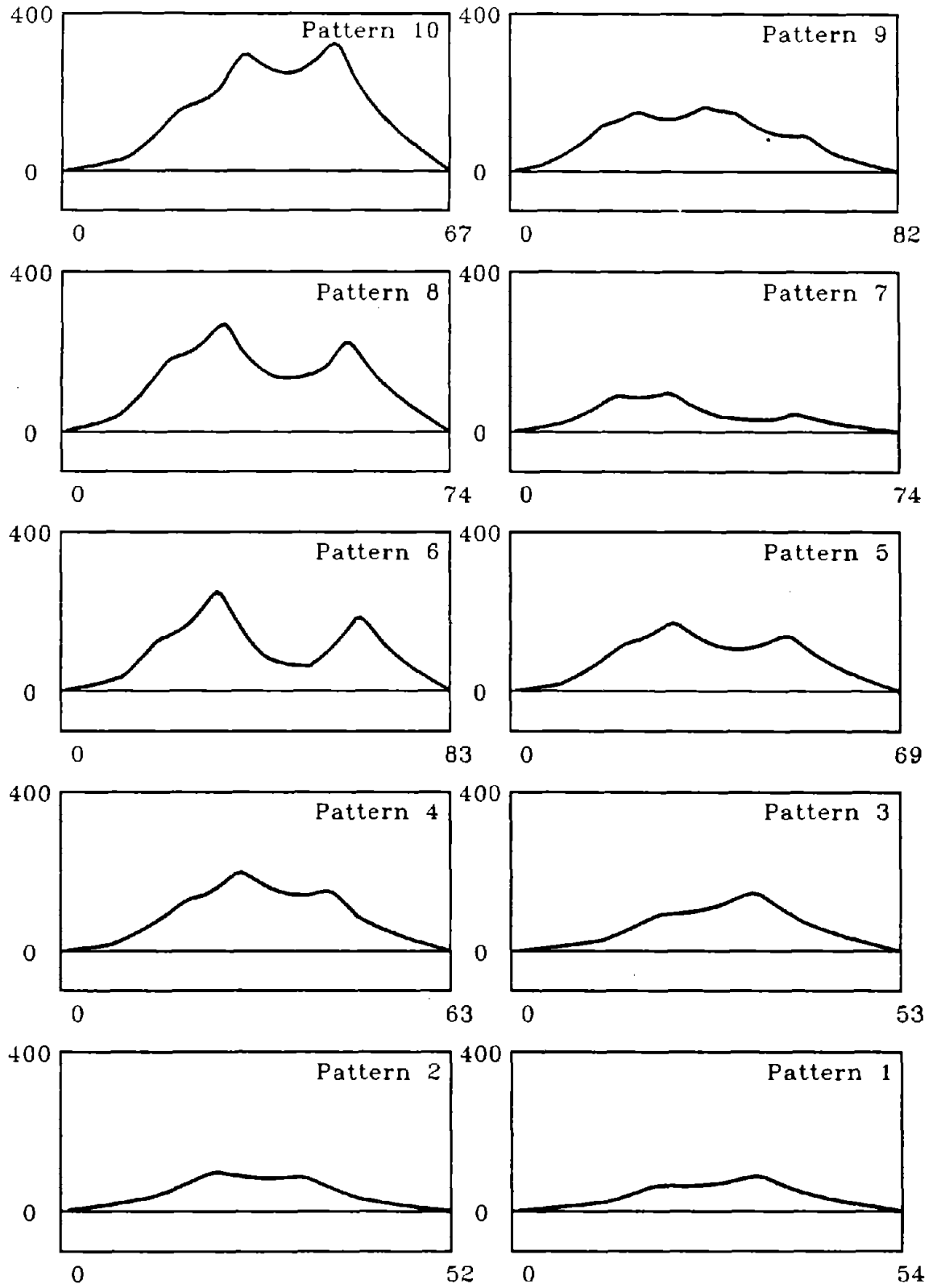
Figure 29. Stress calculated with FEM (Kip/ft^2) vs. scan number, from entry to exit of truck, channel 3.

a_{ij} = probability of transition from state i to state j

b_{jk} = probability of observation O_k at state j
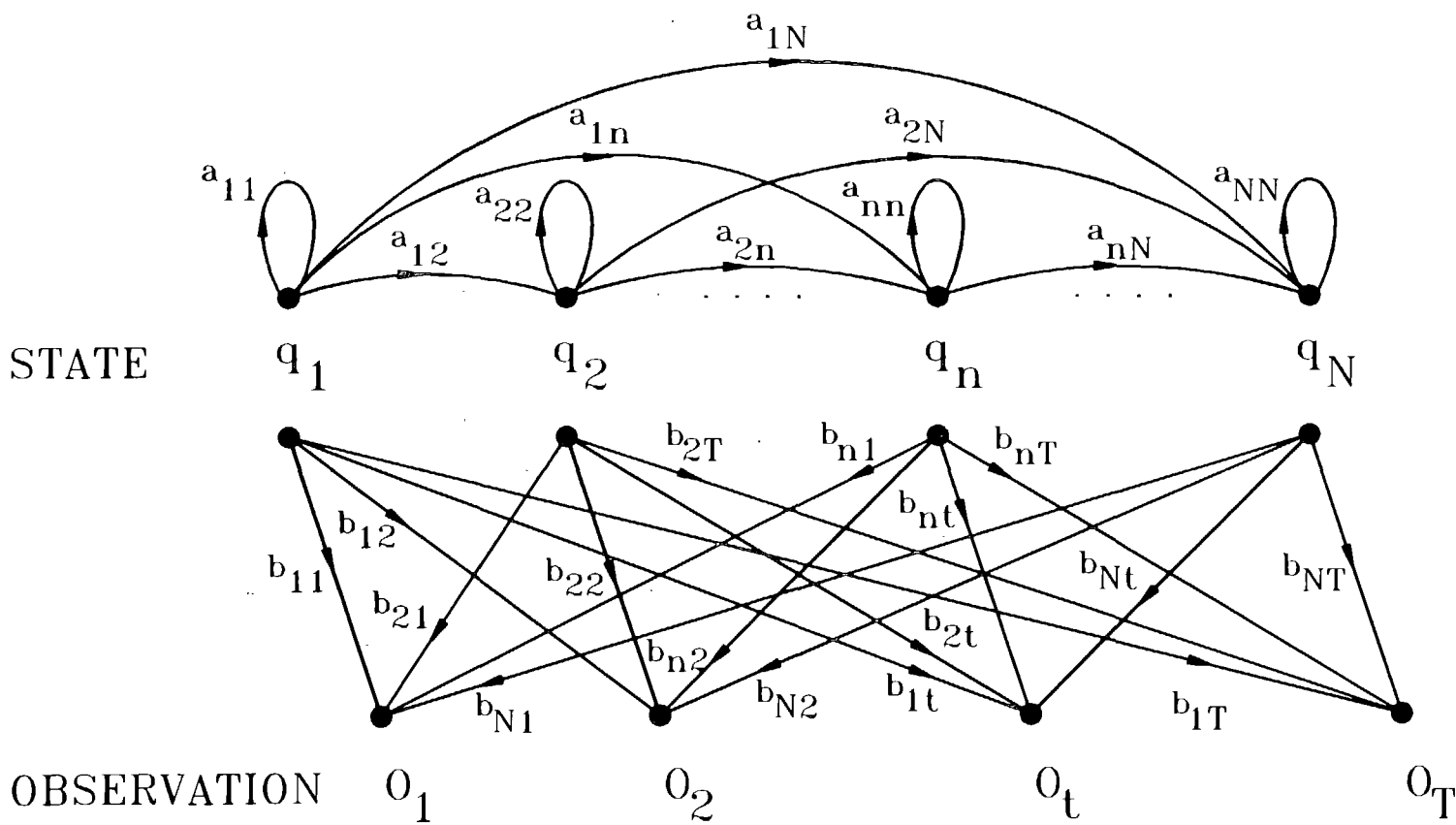
Figure 30. Illustration of left-to-right hidden Markov model.
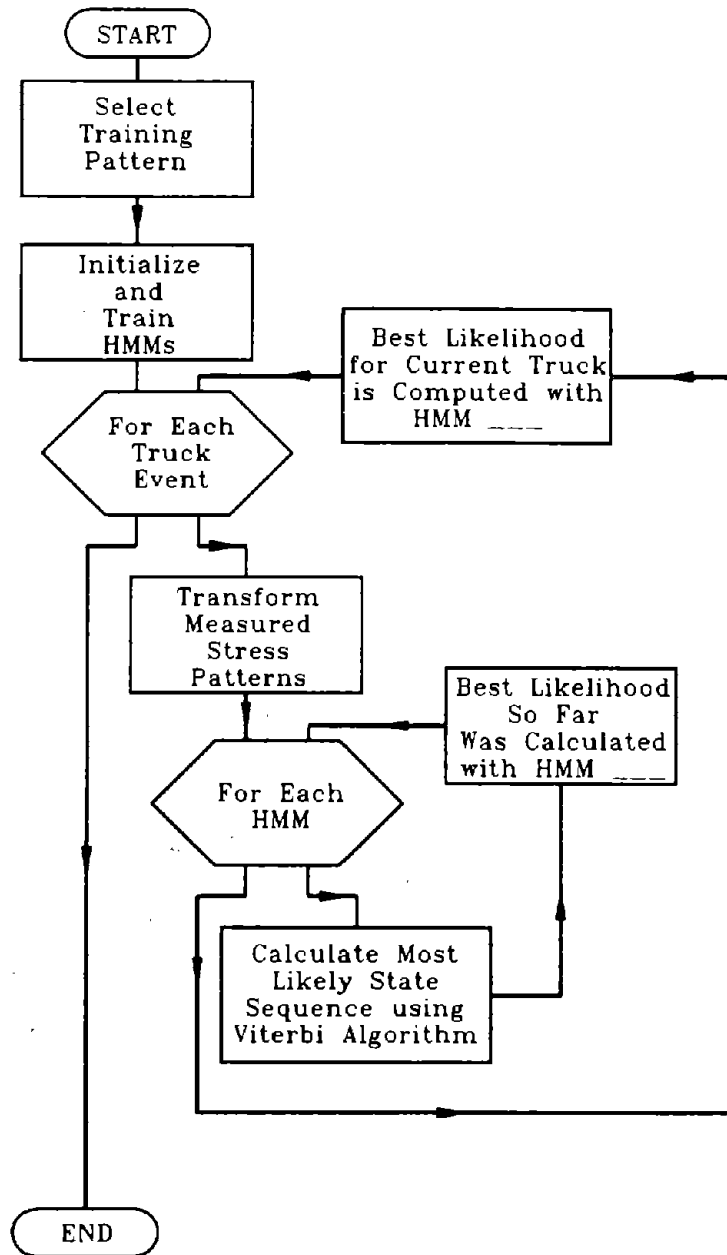
Figure 31. Flowchart for hidden Markov model analysis of WIM data.
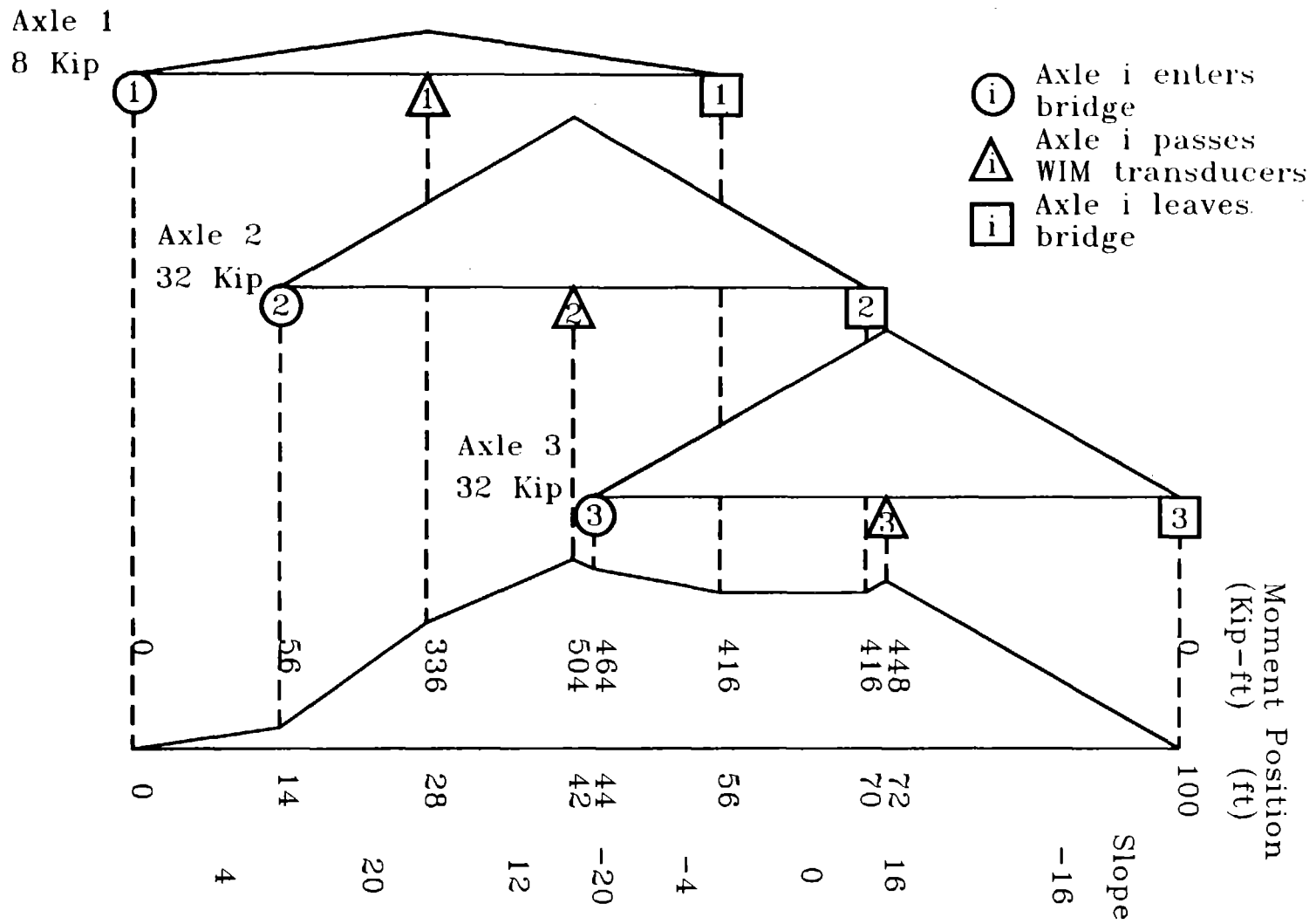
Figure 32. Illustrative example of hidden Markov model for HS20 truck on I-66 over Bull Run bridge.

$$
\text{STATES} \begin{bmatrix} q_1 & \text{No axles on bridge} \\ q_2 & \text{First axle enters bridge} \\ q_3 & \text{Second axle enters bridge} \\ q_4 & \text{First axle passes transducers} \\ q_5 & \text{Second axle passes transducers} \\ q_6 & \text{Third axle enters bridge} \\ q_7 & \text{First axle leaves bridge} \\ q_8 & \text{Second axle leaves bridge} \\ q_9 & \text{Third axle passes transducers} \\ q_{10} & \text{All axles have left bridge} \end{bmatrix}
$$

$$
\text{PRIMITIVE PATTERNS} \begin{bmatrix} \omega_1 & -20 \\ \omega_2 & -16 \\ \omega_3 & -12 \\ \omega_4 & -8 \\ \omega_5 & -4 \\ \omega_6 & 0 \\ \omega_7 & 4 \\ \omega_8 & 8 \\ \omega_9 & 12 \\ \omega_{10} & 16 \\ \omega_{11} & 20 \end{bmatrix}
$$

$$
A = \begin{bmatrix}
.5 & .5 & 0 & 0 & 0 & 0 & 0 & 0 & 0 & 0 \\
0 & .5 & .5 & 0 & 0 & 0 & 0 & 0 & 0 & 0 \\
0 & 0 & .5 & .5 & 0 & 0 & 0 & 0 & 0 & 0 \\
0 & 0 & 0 & .5 & .5 & 0 & 0 & 0 & 0 & 0 \\
0 & 0 & 0 & 0 & .5 & .5 & 0 & 0 & 0 & 0 \\
0 & 0 & 0 & 0 & 0 & .5 & .5 & 0 & 0 & 0 \\
0 & 0 & 0 & 0 & 0 & 0 & .5 & .5 & 0 & 0 \\
0 & 0 & 0 & 0 & 0 & 0 & 0 & .5 & .5 & 0 \\
0 & 0 & 0 & 0 & 0 & 0 & 0 & 0 & .5 & .5 \\
0 & 0 & 0 & 0 & 0 & 0 & 0 & 0 & 0 & 1
\end{bmatrix}
$$

$$
B = \begin{bmatrix}
0 & 0 & 0 & 0 & .2 & .6 & .2 & 0 & 0 & 0 & 0 \\
0 & 0 & 0 & 0 & 0 & .2 & .6 & .2 & 0 & 0 & 0 \\
0 & 0 & 0 & 0 & 0 & 0 & 0 & 0 & 0 & .3 & .7 \\
0 & 0 & 0 & 0 & 0 & 0 & 0 & .2 & .6 & .2 & 0 \\
.7 & .3 & 0 & 0 & 0 & 0 & 0 & 0 & 0 & 0 & 0 \\
0 & 0 & 0 & .2 & .6 & .2 & 0 & 0 & 0 & 0 & 0 \\
0 & 0 & 0 & 0 & .2 & .6 & .2 & 0 & 0 & 0 & 0 \\
0 & 0 & 0 & 0 & 0 & 0 & 0 & 0 & .2 & .6 & .2 \\
.2 & .6 & .2 & 0 & 0 & 0 & 0 & 0 & 0 & 0 & 0 \\
0 & 0 & 0 & 0 & .2 & .6 & .2 & 0 & 0 & 0 & 0
\end{bmatrix}
$$

Figure 33. Illustrative example of hidden Markov model: description of states, primitive patterns, and probability matrices.
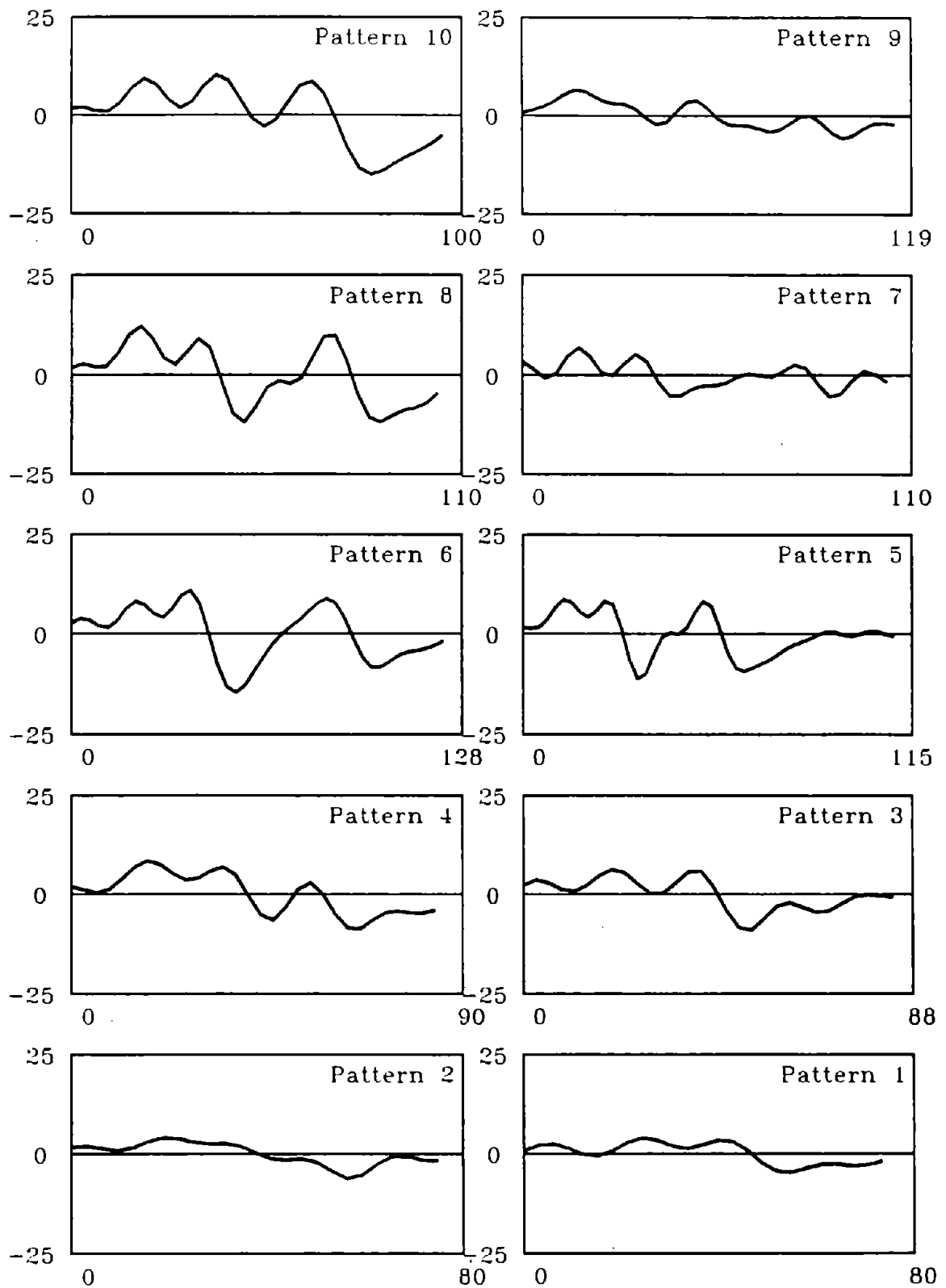
Figure 34. Slope of curve of measured and filtered stresses vs. scan number, from entry to exit of truck, channel 3.
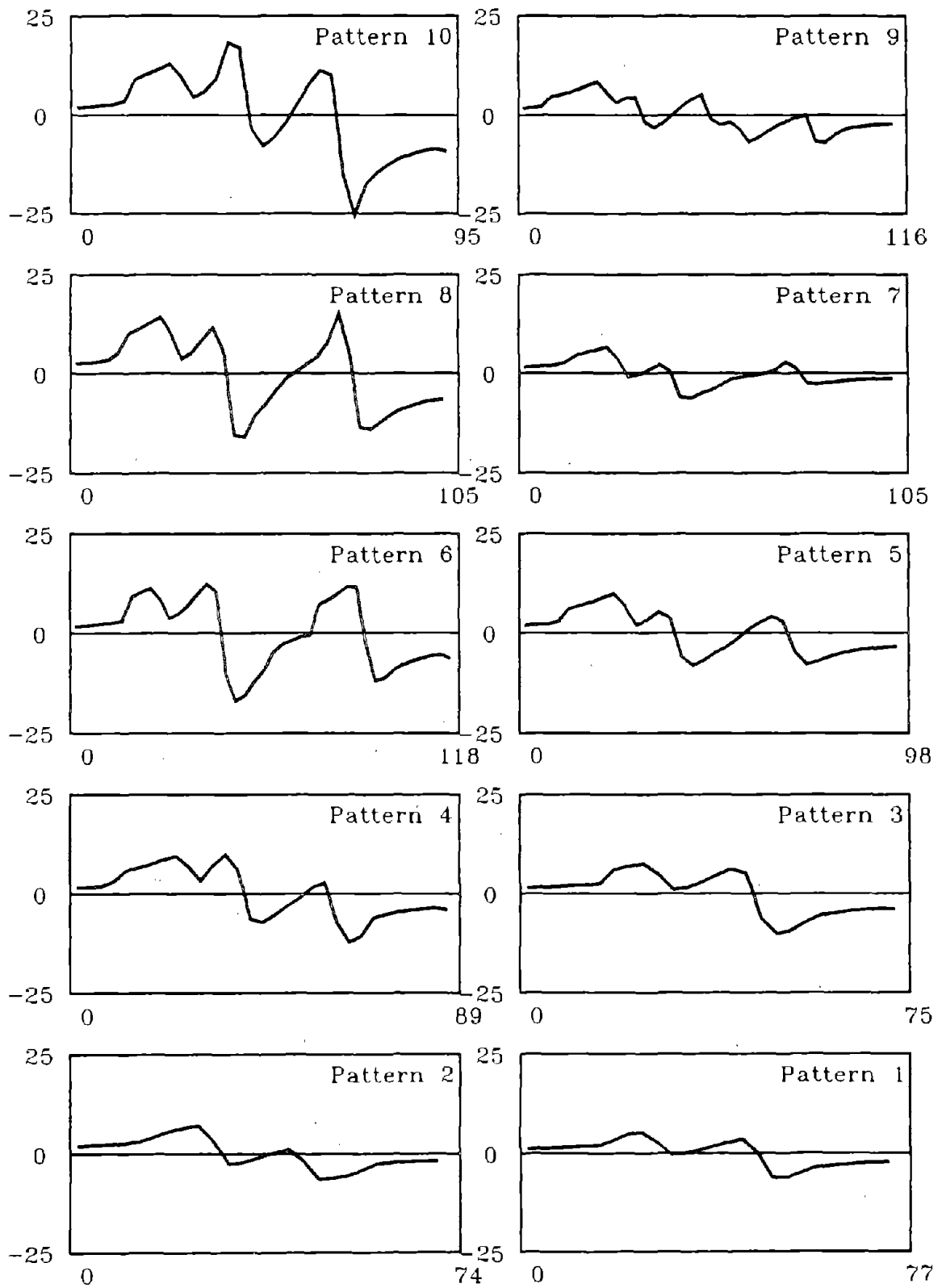
Figure 35. Slope of curve of stress calculated with FEM vs. scan number, from entry to exit of truck, channel 3.
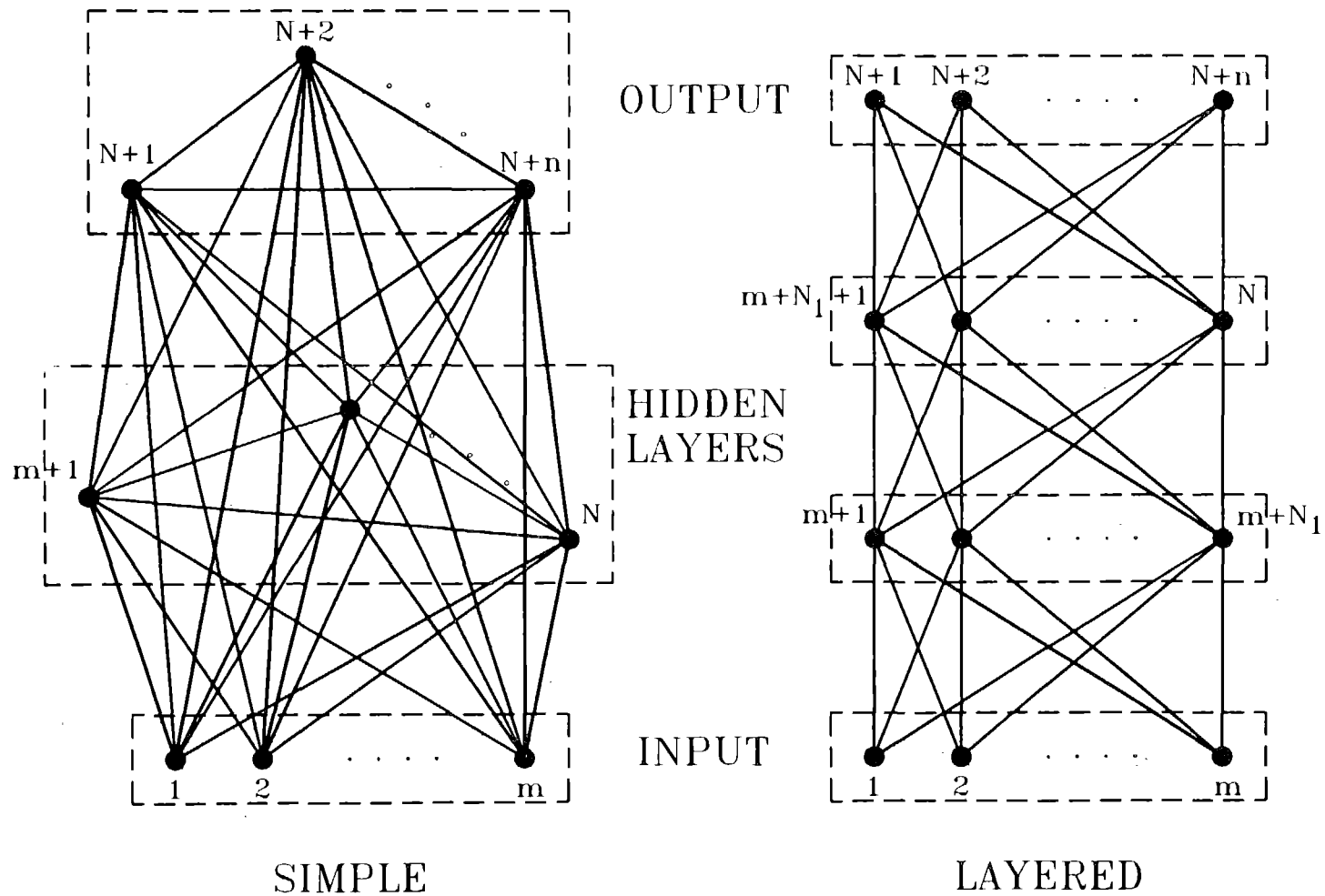
Figure 36. Simple and layered feed forward neural networks.

HARD LIMITER x_i

$s(net_i) = 0, \ net_i \leqslant 0$

$s(net_i) = 1, \ net_i > 0$

1

0 net_i

THRESHOLD LOGIC x_i

$s(net_i) = 0, \ net_i \leqslant 0$ 1

$s(net_i) = \dfrac{1}{\alpha} net_i$,

$0 < net_i \leqslant \alpha$

$s(net_i) = 1, \ net_i > \alpha$ 0

α net_i

SIGMOID x_i

1

$s(net_i) = \dfrac{1}{1 + e^{(-net_i)}}$

0 net_i
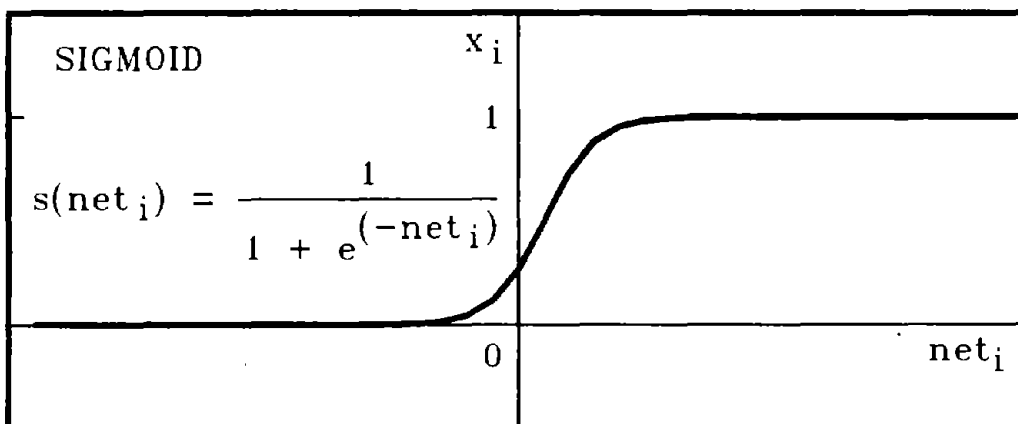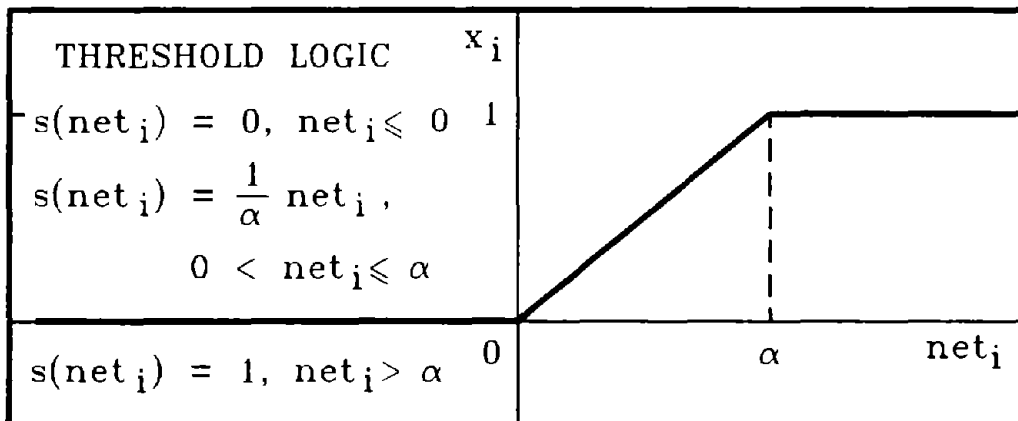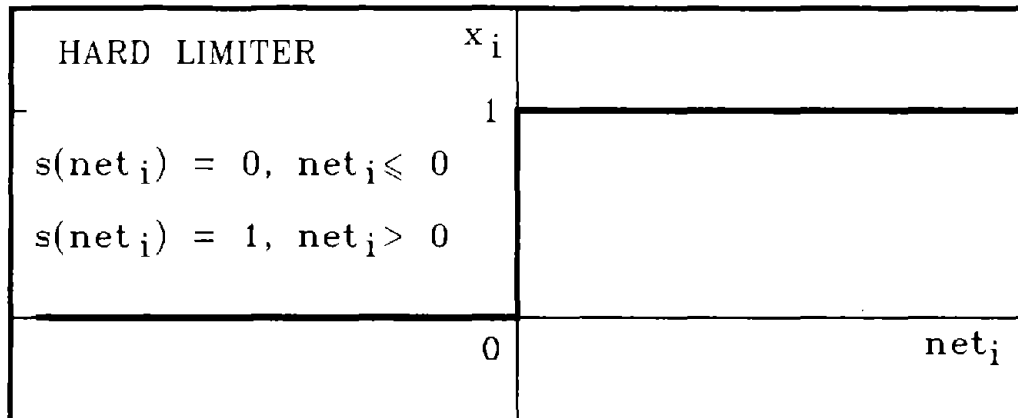
Figure 37. Types of activation functions.

68
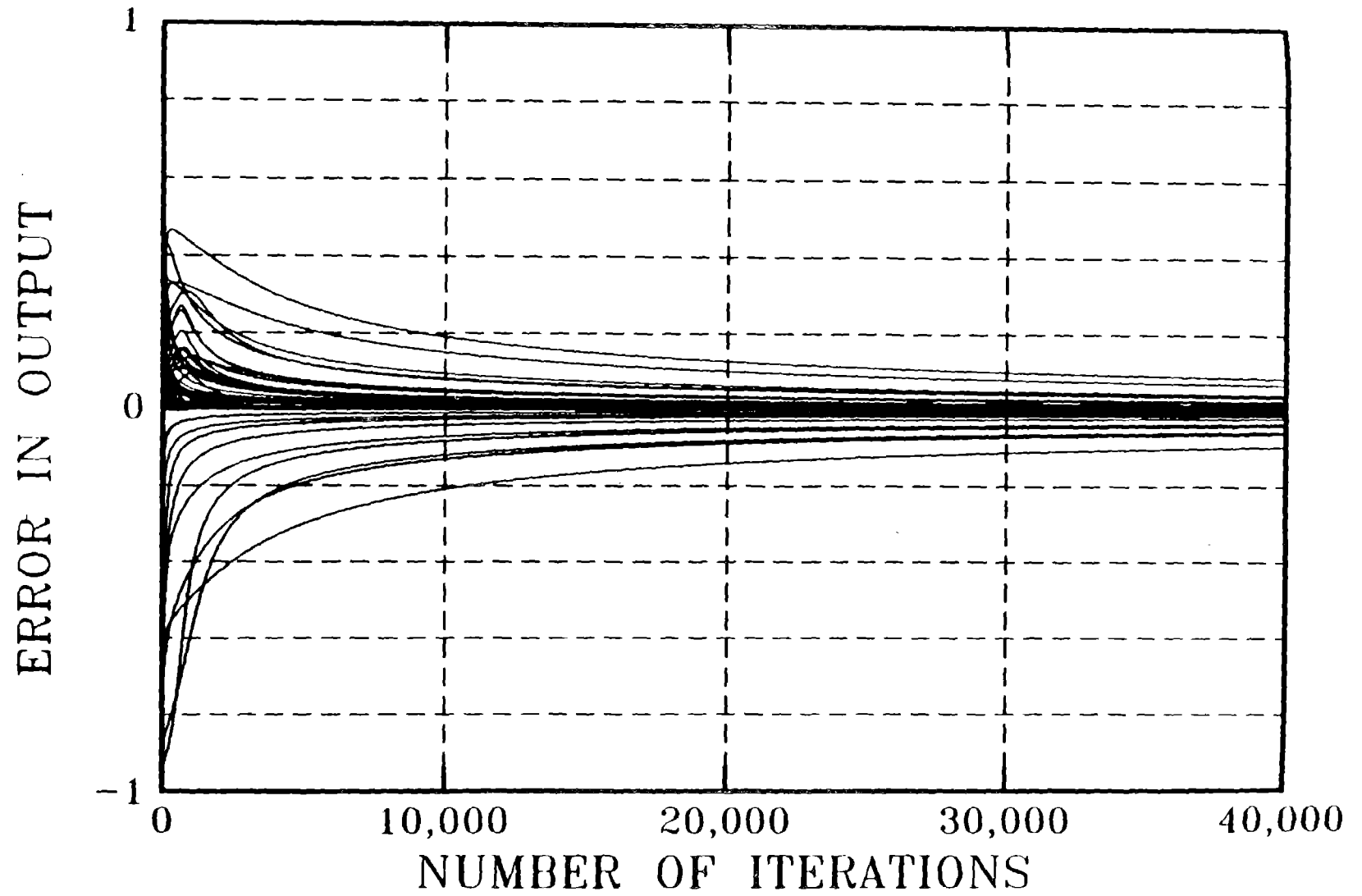
Figure 38. Error in output vs. number of learning iterations
for classification of truck with feed forward neural network.
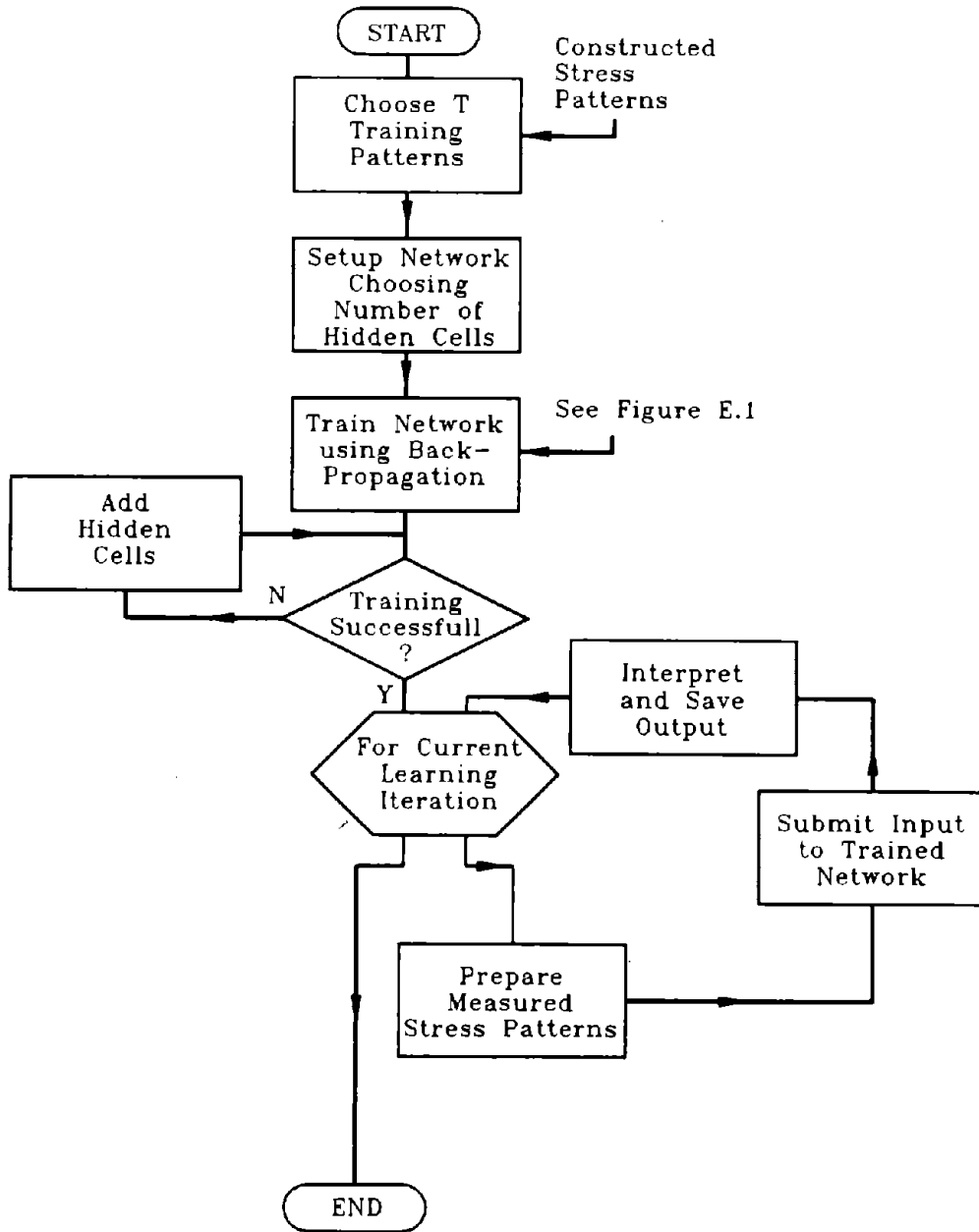
Figure 39. Flowchart for feed forward neural network analysis of WIM data.
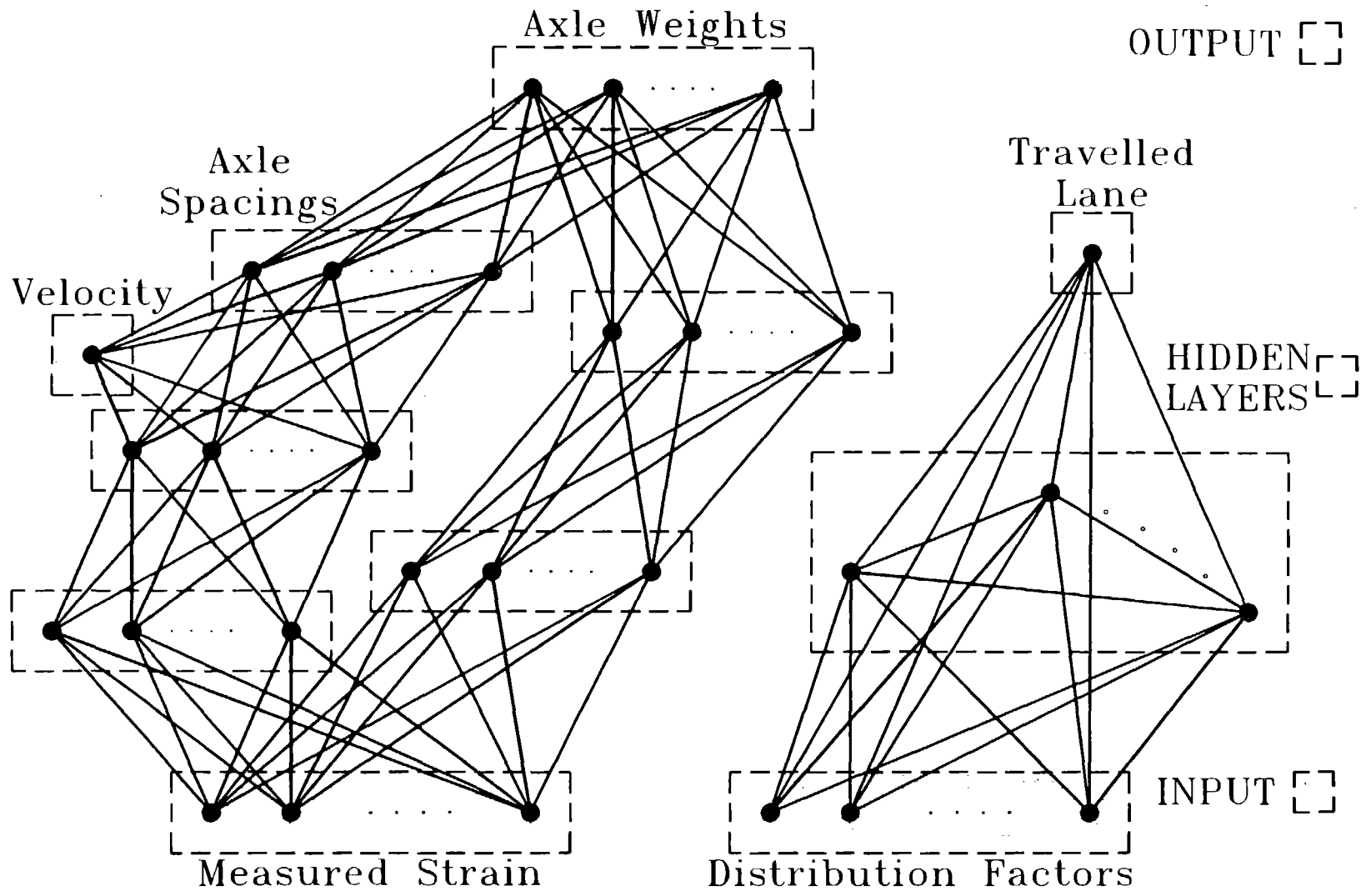
Figure 40. Sketch of feed forward neural network for WIM
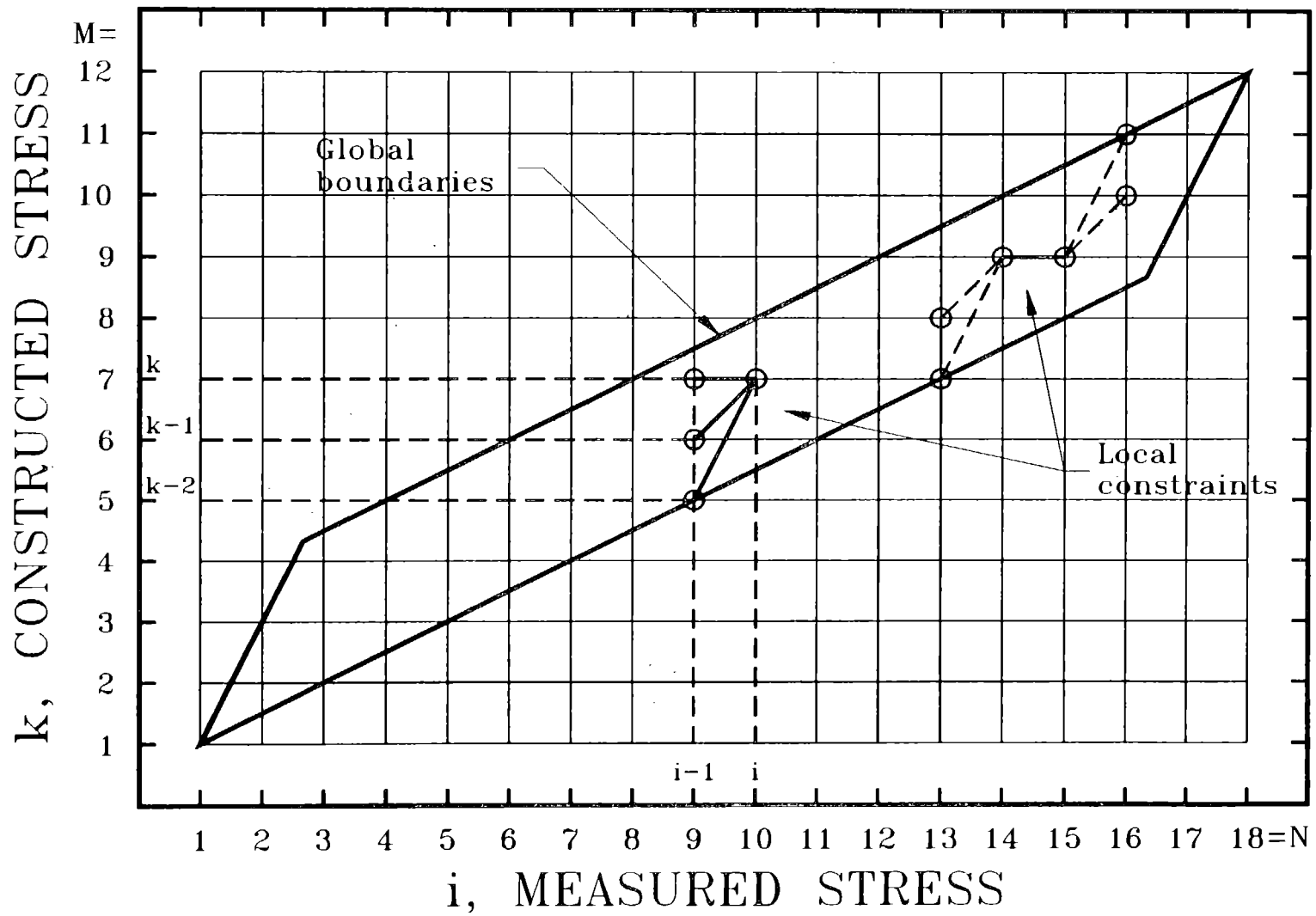
Figure 41. Global and local constraints for dynamic time warping method.
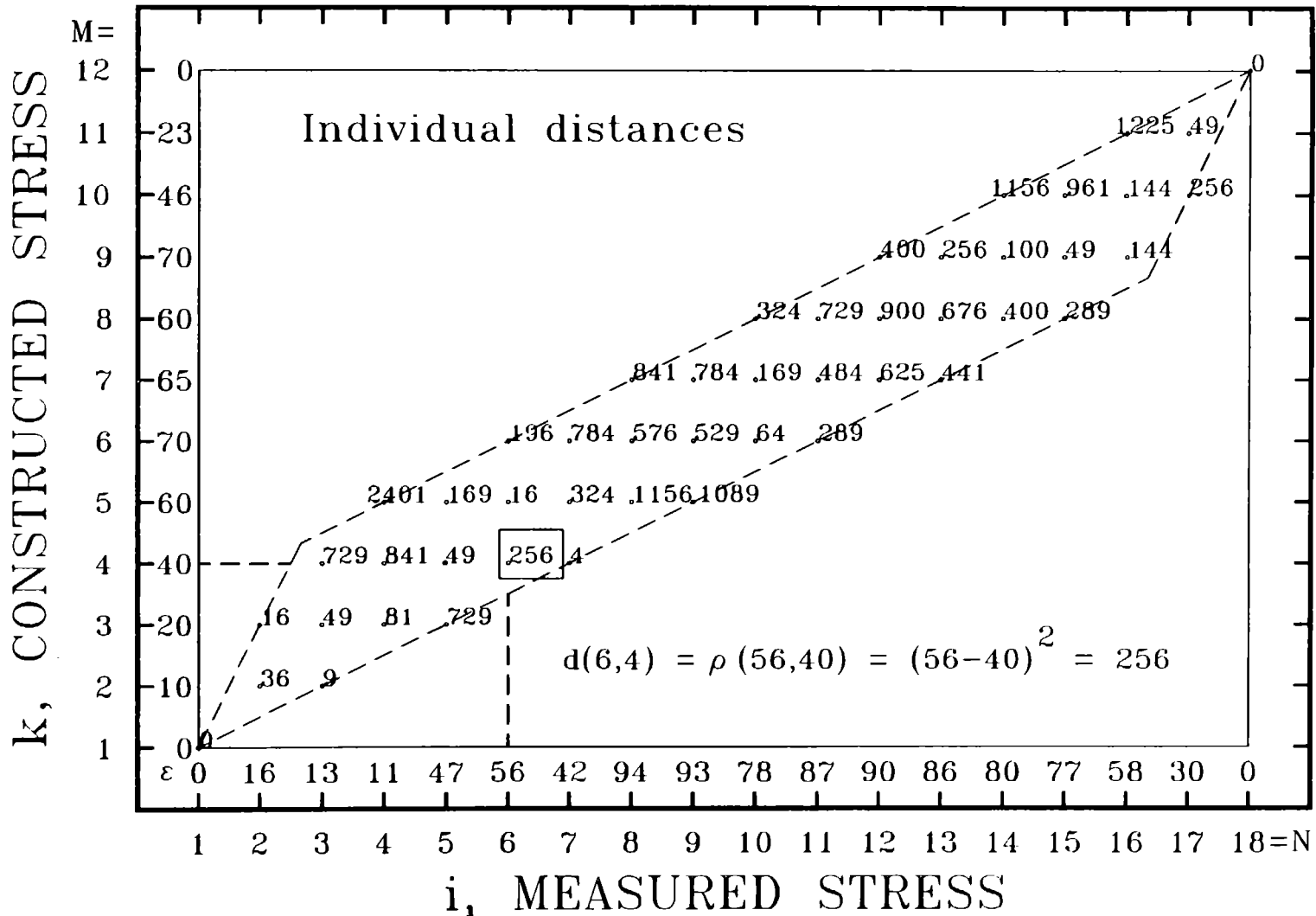
Figure 42. Illustrative example of dynamic time warping method: values of individual distances.
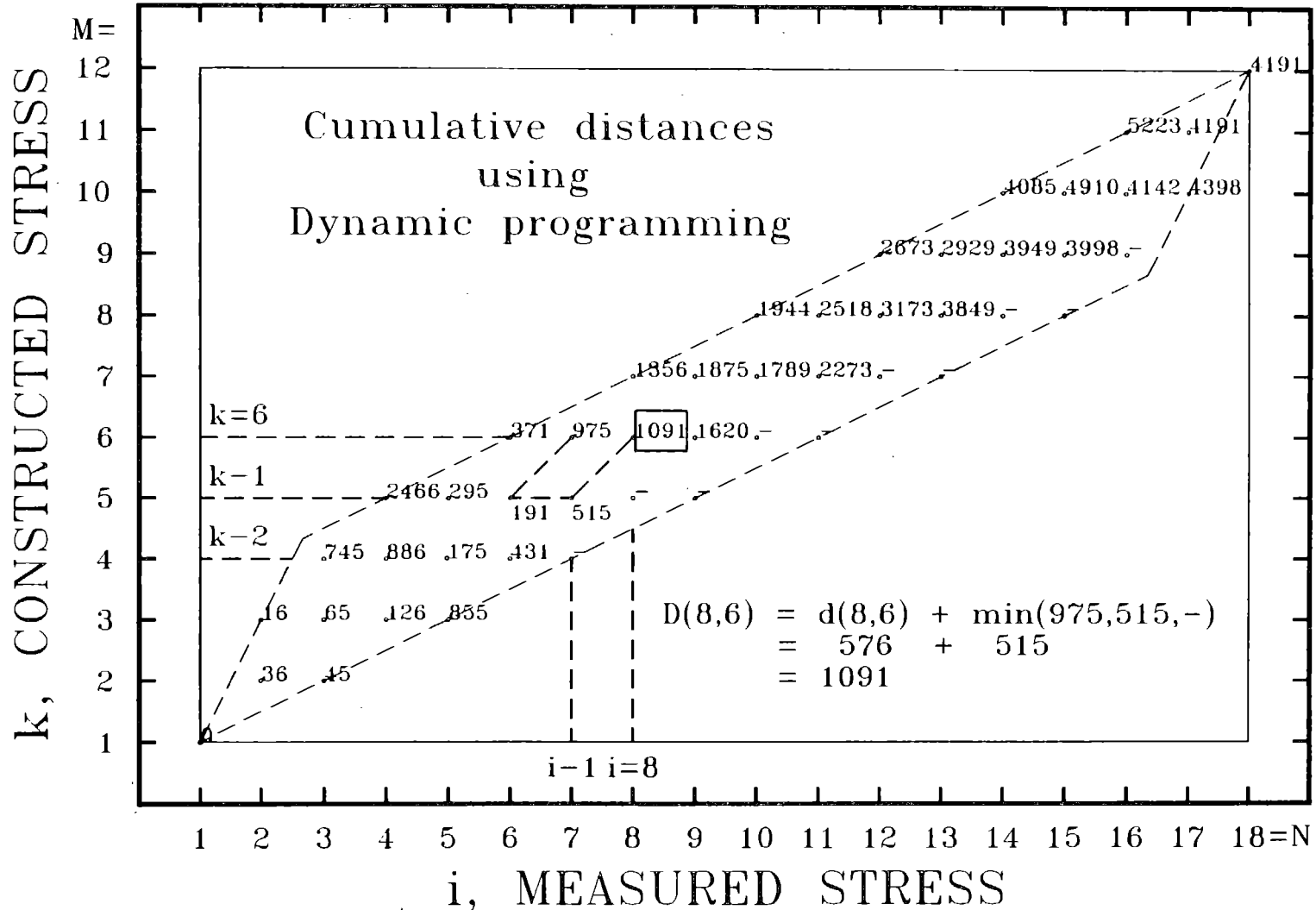
Figure 43. Illustrative example of dynamic time warping:
values of cumulative distances.
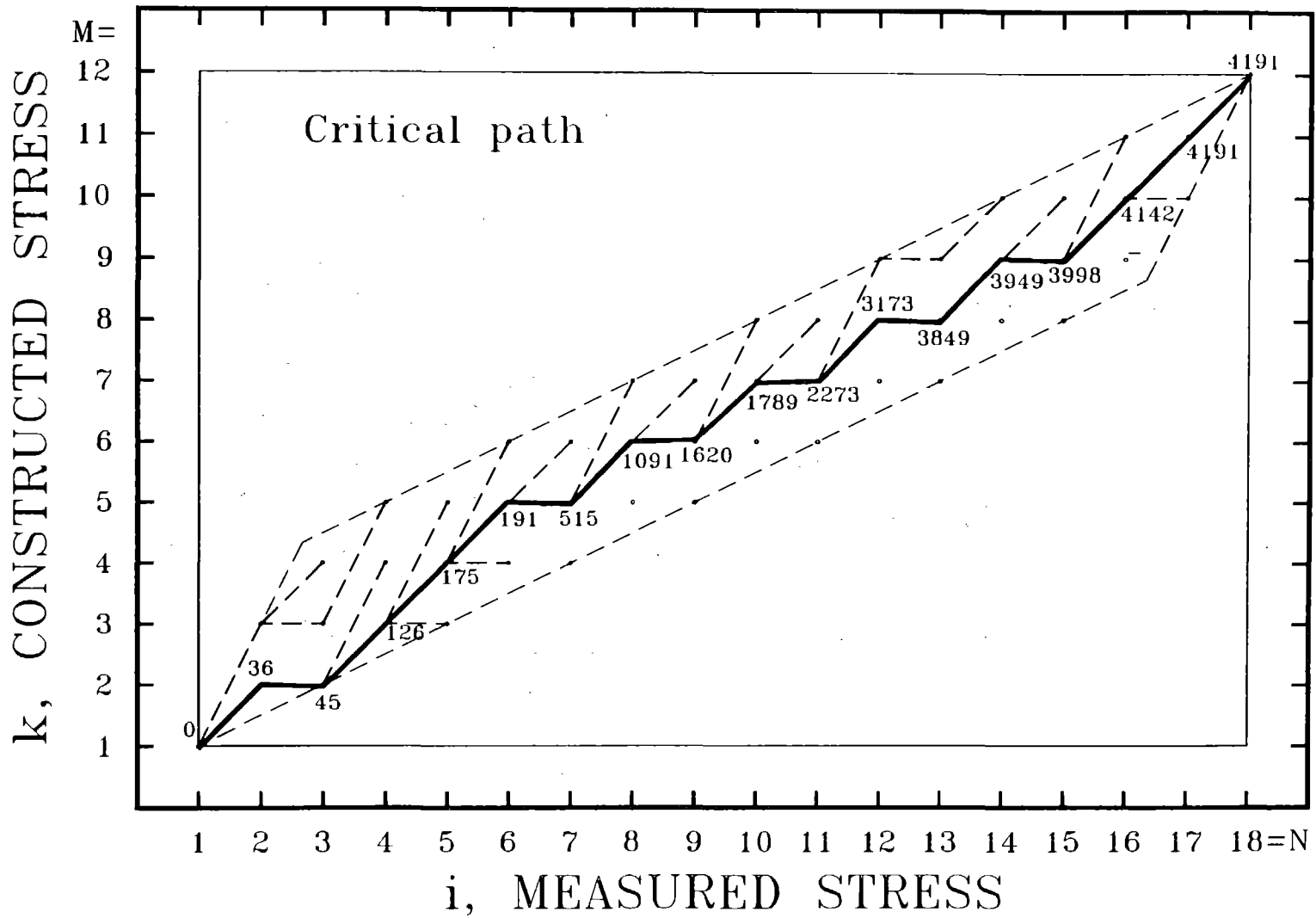
Figure 44. Illustrative example of dynamic time warping:
critical path.
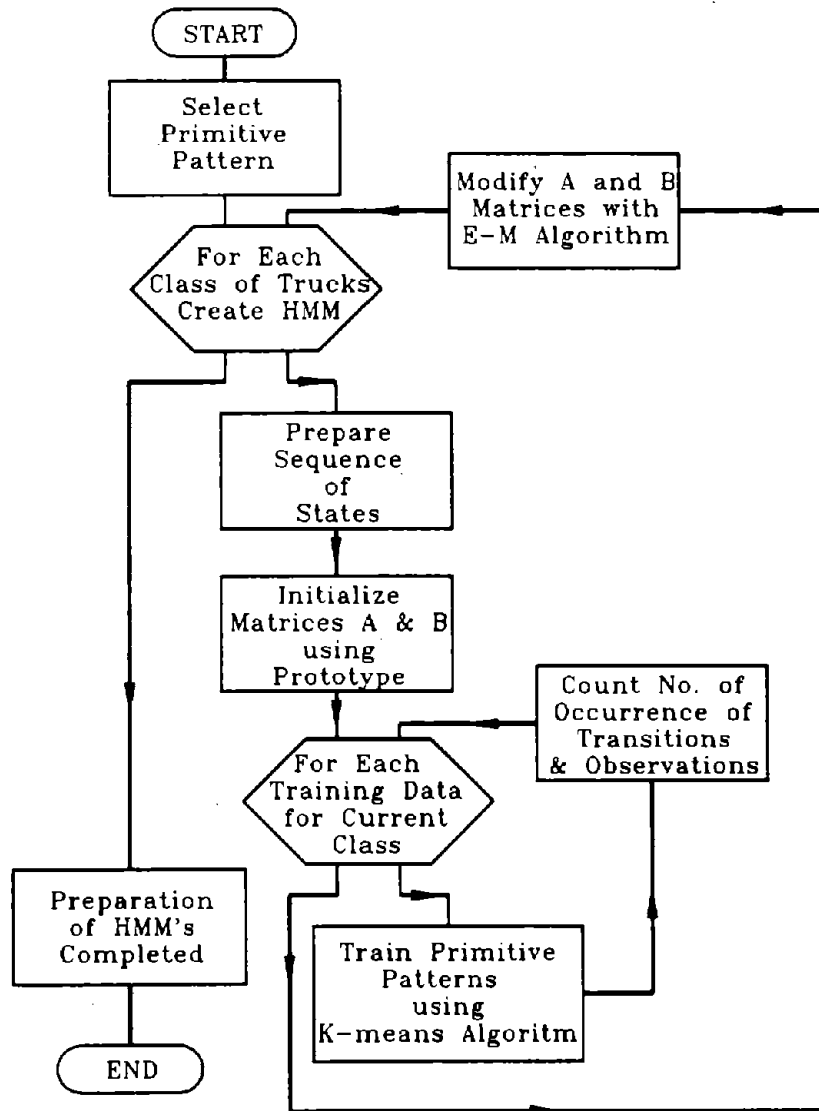
Figure 45. Creation and training of hidden Markov models.
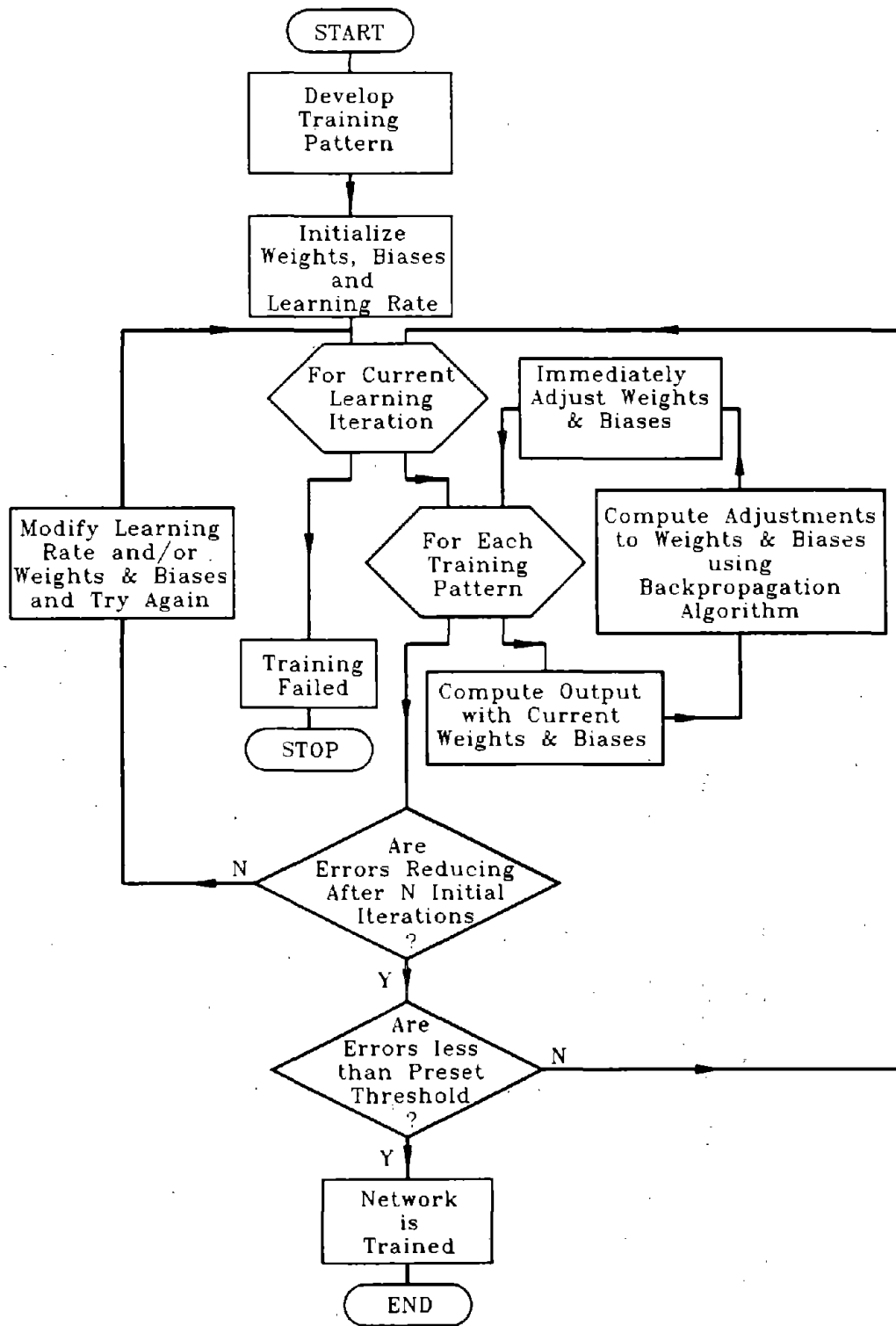
Figure 46. Flowchart of learning process with back-propagation.

Table 1. Classification of trucks according to axle spacings -- I-70 over route 340 Bridge.

Class of Truck		No of trucks travelling in lane		Average Weight of Axle (kip)								Average Axle Spacing (ft)						
#	Desc.	1	2	1	2	3	4	5	6	7	8	1	2	3	4	5	6	7
1	Car	0	0	0	0	0	0	0	0	0	0	0	0	0	0	0	0	0
2	2S	141	20	1	16	0	0	0	0	0	0	16	0	0	0	0	0	0
3	Bus	47	29	3	21	0	0	0	0	0	0	21	0	0	0	0	0	0
4	2S-1	3	0	3	11	3	0	0	0	0	0	11	11	0	0	0	0	0
5	3S	94	23	6	27	0	0	0	0	0	0	18	0	0	0	0	0	0
6	Bus	12	1	12	27	0	0	0	0	0	0	25	0	0	0	0	0	0
7	other	26	2	1	16	9	0	0	0	0	0	12	24	0	0	0	0	0
8	4S	8	1	11	54	0	0	0	0	0	0	17	0	0	0	0	0	0
9	3S-1	3	1	14	18	30	0	0	0	0	0	20	25	0	0	0	0	0
10	2S-2	88	11	1	23	18	0	0	0	0	0	11	30	0	0	0	0	0
11	5S	13	1	42	-28	0	0	0	0	0	0	13	0	0	0	0	0	0
12	3S-2	944	189	8	27	20	0	0	0	0	0	16	33	0	0	0	0	0
13	2S-3	9	0	3	16	22	0	0	0	0	0	13	31	0	0	0	0	0
14	2S-3 S	0	0	0	0	0	0	0	0	0	0	0	0	0	0	0	0	0
15	2S-1-2	26	6	-2	28	-3	22	17	0	0	0	11	20	9	21	0	0	0
16	other 5	1	0	10	-14	32	-3	14	0	0	0	20	4	31	11	0	0	0
17	3S-3	22	2	7	28	31	0	0	0	0	0	16	32	0	0	0	0	0
18	3S-3 S	0	0	0	0	0	0	0	0	0	0	0	0	0	0	0	0	0
19	3S-1-2	2	1	2	34	-14	29	22	0	0	0	13	22	10	22	0	0	0
20	other 6	0	2	4	12	-6	36	-43	65	0	0	18	4	9	17	4	0	0
21	7 axles	1	0	7	-17	38	-4	8	-23	34	0	19	4	32	5	4	4	0
22	8 axles	0	0	0	0	0	0	0	0	0	0	0	0	0	0	0	0	0
23	others	0	0	0	0	0	0	0	0	0	0	0	0	0	0	0	0	0

78

Table 2. Comparison of equivalent stress ranges obtained
with FEM and WIM for I-70 over route 340 bridge.

Location	Channel No.	FEM Prim. (Stat.) (MPa)	WIM Prim. (Stat.)		Prim. (Dyn.) (MPa)	Prim. + Second. (Dyn.) (MPa)
			Peak & Valley (MPa)	FFT Filter (MPa)		
G1, mid-span	1	11.84	7.03	7.09	9.67	9.95
G2, mid-span	2	13.64	10.06	10.22	13.15	13.25
G3, mid-span	3	15.06	12.32	11.73	15.94	16.03
G4, mid-span	4	12.90	10.14	10.03	13.14	13.23
G5, mid-span	5	10.78	8.25	8.26	10.81	10.89
G6, mid-span	6	8.89	6.13	6.37	8.16	8.34
G2, cover plate	7	19.62	13.21	13.61	17.64	17.83
G3, cover plate	8	23.29	18.24	16.03	22.77	23.00
G4, cover plate	9	18.71	16.38	14.61	19.96	20.08
G5, cover plate	10	16.26	12.98	13.25	17.05	17.17
G6, cover plate	11	12.99	3.64	3.04	4.10	4.26
G2, top fl.	12	4.38	2.15	1.24	2.57	2.62
G3, top fl.	13	6.15	2.09	1.81	3.36	3.45
G4, top fl.	14	3.55	1.83	1.48	2.13	2.14
G5, top fl.	15	2.62	1.45	1.13	2.25	2.39

Table 3. Comparison of calculated fatigue life of I-70
over route 340 bridge.

Detail: End of cover plate, category E detail

Girder: 3, Channel 8, interior girder

	Alternative 1		Alternative 3		Alternative 4	
Loading (kN)	...		GVW histogram: $GVW_c = 264$		HS15: $GVW_c = 240$	
Method of Analysis	...		2-D	3-D	2-D	3-D
Distribution Factor	...		0.33^a	...	0.33^a	...
Impact Factor	1.25^b 1.25^c		1.20^d	1.20^d	1.20^d	1.20^d
Secondary cycle Factor	1.01^c		...	...	...	...
Live load moment range (kN-m)	...		906	...	804	...
Section modulus (m^3)	...		0.0125	...	0.0125	...
Equivalent stress range, f_{re} (MPa)	22.77^e	23.00^f	28.76	27.95^g 28.49^h	26.14	25.92
Basic reliability factor, R_{so}	1.35	1.35	1.35	1.35	1.35	1.35
F_{s1}	0.85	0.85	1.00	1.00	1.00	1.00
F_{s2}	1.00	1.00	0.95	0.95	1.00	1.00
F_{s3}	1.00	1.00	1.00	0.96	1.00	0.96
R_s	1.15	1.15	1.28	1.23	1.35	1.30
R_s f_{re} (MPa)	26.19	26.45	36.81	35.04	35.29	33.70

80

Detail: End of cover plate, category E detail

Girder: 3, Channel 8, interior girder

	Alternative 1		Alternative 3		Alternative 4	
R_s f_{re} (MPa)	26.19	26.45	36.81	35.04	35.29	33.70
Limiting stress range for infinite life: 11.03 MPa (K=2.9)						
ADTT	1850[i]	1850[i]	1850[i]	1850[i]	2900[j]	2900[j]
Fatigue life (years)[k]	29	28	12	12	7	9

Note:

a. Determined using AASHTO formula for interior girders with S = 2.22 m and D = 6.71 m.

b. Determined using AASHTO empirical formula for design with 0.8L = 23.7 m.

c. Determined from measured stress ranges.

d. Selected as mean value of range suggested by AASHTO (1.1 - 1.3).

e. Corresponding to primary cycle, dynamic.

f. Corresponding to primary plus secondary cycles, dynamic.

g. Calculated with stress ranges of each truck, impact included.

h. Calculated with WIM GVW_e, impact included.

i. Estimated with test data.

j. Provided by AASHTO specifications.

k. Safe life in years, f = 1.0, C = 1.

Table 4. Classification, description, and WIM speed
of trucks for ten selected measured stress patterns.

Pattern No.	Visual Classification			Classification by Axle Spacing	Speed (fps)
	No. of Axles	Lane Travelled	Type of Truck		
1	2	1	box truck	2S	92.1
2	3	1	dump truck	3S	93.6
3	3	1	concrete mixer	3S	86.5
4	3	1	box truck	2S-1	86.5
5	5	1	box truck	3S-2	86.5
6	5	1	car carrier	3S-2	89.2
7	5	1	bulk truck	3S-2	96.8
8	5	1	tank truck	3S-2	96.8
9	5	1	double box truck	2S-1-2	95.1
10	6	1	dump truck	3S-3	92.1

Table 5. Axle weights, spacings, and GVW of trucks used for constructed stress patterns.

Pattern No.	No. of Axles	Axle		GVW (kip)
		Spacings (ft)	Weights (kip)	
1	2	20.0	6.0 10.0	16.0
2	2	17.0	10.0 8.0	18.0
3	2	18.5	7.5 17.0	24.5
4	3	12.0 21.0	8.0 19.0 16.0	43.0
5	3	12.5 28.5	9.5 18.0 16.0	43.5
6	3	18.5 43.0	9.0 30.0 24.0	63.0
7	3	15.0 33.5	8.0 9.5 5.5	23.0
8	3	15.0 33.5	12.5 30.5 29.0	72.0
9	5	10.0 20.0 9.0 21.0	9.0 12.0 13.0 10.0 10.0	54.0
10	3	15.5 23.0	10.0 30.0 38.0	78.0

Table 6. Matrix of distances computed between measured and constructed stress patterns using dynamic time warping.

	Constructed Stress Patterns										Best Match
	1	2	3	4	5	6	7	8	9	10	
1	19	33	98	292	258	495	114	589	308	739	1
2	26	16	99	272	224	466	90	556	285	722	2
3	155	126	40	167	159	391	123	453	150	608	3
4	401	324	186	32	91	225	363	201	83	426	4
5	330	255	263	263	84	171	316	349	165	636	5
6	690	629	592	411	275	65	608	338	371	834	6
7	92	89	230	311	253	443	36	606	279	858	7
8	739	663	527	197	292	150	691	56	311	459	8
9	360	312	109	130	105	262	296	309	52	514	9
10	891	836	663	410	516	542	896	298	503	142	10

Measured Stress Patterns

Table 7. Matrix of likelihoods computed between measured and constructed stress patterns using hidden Markov models.

	Constructed Stress Patterns										Best Match
	1	2	3	4	5	6	7	8	9	10	
1	0.361	0.281	0.346	0.231	0.234	0.199	0.229	0.201	0.201	0.205	1
2	0.361	0.363	0.338	0.230	0.239	0.000	0.233	0.252	0.293	0.206	2
3	0.363	0.354	0.349	0.368	0.229	0.261	0.221	0.216	0.246	0.209	4
4	0.353	0.277	0.334	0.366	0.223	0.208	0.214	0.209	0.248	0.215	4
5	0.276	0.273	0.000	0.224	0.368	0.325	0.366	0.324	0.271	0.199	5
6	0.000	0.301	0.000	0.000	0.000	0.358	0.335	0.338	0.214	0.000	6
7	0.328	0.264	0.337	0.000	0.000	0.270	0.375	0.267	0.230	0.000	7
8	0.247	0.248	0.000	0.283	0.277	0.354	0.343	0.357	0.232	0.000	8
9	0.355	0.369	0.321	0.280	0.195	0.110	0.140	0.235	0.393	0.196	9
10	0.264	0.000	0.000	0.285	0.209	0.000	0.166	0.000	0.000	0.323	10

Measured Stress Patterns

Table 8. Matrix of feed forward network outputs computed for constructed stress patterns as a result of learning iterations.

	Number of Output Neuron										Best Match
	1	2	3	4	5	6	7	8	9	10	
1	0.906	0.015	0.039	0.027	0.022	0.006	0.000	0.000	0.001	0.002	1
2	0.068	0.981	0.000	0.013	0.000	0.001	0.044	0.000	0.000	0.000	2
3	0.085	0.000	0.967	0.014	0.013	0.001	0.000	0.000	0.000	0.001	3
4	0.000	0.000	0.000	0.962	0.000	0.000	0.000	0.000	0.000	0.007	4
Const. Stress Patterns 5	0.000	0.000	0.000	0.000	0.946	0.000	0.000	0.017	0.004	0.001	5
6	0.000	0.000	0.001	0.000	0.014	0.996	0.000	0.000	0.005	0.000	6
7	0.000	0.013	0.000	0.015	0.002	0.002	0.941	0.010	0.008	0.000	7
8	0.000	0.000	0.000	0.000	0.036	0.000	0.024	0.991	0.001	0.000	8
9	0.000	0.000	0.000	0.001	0.008	0.002	0.000	0.001	0.988	0.006	9
10	0.000	0.000	0.008	0.023	0.012	0.000	0.000	0.000	0.007	0.996	10

Table 9. Matrix of feed forward network outputs computed for measured stress patterns.

	Number of Output Neuron										Best Match
	1	2	3	4	5	6	7	8	9	10	
1	0.857	0.020	0.075	0.429	0.033	0.013	0.000	0.000	0.002	0.006	1
2	0.265	0.810	0.000	0.132	0.005	0.004	0.001	0.000	0.001	0.000	2
3	0.005	0.000	0.861	0.002	0.081	0.002	0.000	0.000	0.002	0.005	3
4	0.000	0.000	0.003	0.806	0.006	0.000	0.000	0.000	0.002	0.048	4
5	0.000	0.000	0.000	0.002	1.000	0.278	0.000	0.203	0.245	0.006	5
6	0.070	0.000	0.006	0.000	0.000	0.968	0.000	0.000	0.001	0.000	6
7	0.000	0.017	0.000	0.224	0.081	0.008	0.962	0.036	0.053	0.001	7
8	0.000	0.000	0.000	0.000	0.980	0.000	0.699	0.999	0.054	0.000	8
9	0.000	0.000	0.000	0.001	0.023	0.020	0.000	0.013	0.987	0.020	9
10	0.000	0.000	0.001	0.037	0.031	0.000	0.000	0.317	0.683	0.995	10

Measured Stress Patterns (row labels 1–10)

Table 10. Illustrative example for dynamic time warping
method: summary of results.

Measured Strain		Mapping	Construct. Strain		Distance Ind.	Distance Cum.
i	ε	j	k	ε^*	$d(i,k)$	$D(i,k)$
1	0	1			0	0
2	16	2			36	36
3	13	2			9	45
4	11	3	1	0	81	126
5	47	4	2	10	49	175
6	56	5	3	20	16	191
7	42	5	4	40	324	515
8	94	6	5	60	576	1091
9	93	6	6	70	529	1620
10	78	7	7	65	169	1789
11	87	7	8	60	484	2273
12	90	8	9	70	900	3173
13	86	8	10	46	676	3849
14	80	9	11	23	100	3949
15	77	9	12	0	49	3998
16	58	10			144	4142
17	30	11			49	4191
18	0	12			0	4191